Topics in Quantum Physics: Quantum Transport and Quantum Metrology

An Abstract
Submitted On The Eleventh Day Of August, 2017
To The Department Of Physics
Of The Graduate School Of
Tulane University
In Partial Fulfillment Of The Requirements
For The Degree Of
Doctor Of Philosophy
By

Yang Zhang

Approved:

Lev Kaplan, Ph.D.
Chairman

Dmitry Uskov, Ph.D.

Ryan Glasser, Ph.D.

Abstract

I review my three papers on two topics in quantum physics. The first two papers are about quantum transport in open systems. In the first paper, we study quantum enhancement of transport in open systems in the presence of disorder and dephasing. Quantum coherence effects may significantly enhance transport in open systems even in the semiclassical regime (where the decoherence rate is greater than the inter-site hopping amplitude), as long as the disorder is sufficiently strong. Analytic results are obtained in the linear chain and fully connected network. The physical behavior is also reflected in the FMO photosynthetic complex.

In the second paper, we specifically study the effects of dephasing on transport in chains with opening. At very weak disorder strength, dephasing always hinders transport, but for disorder strength W above a small critical value W^{cr}, optimal transport always occurs at a nonzero value of dephasing. The critical disorder strength W^{cr} grows linearly with the strength of opening for small opening, and inversely with the opening strength for large opening; furthermore W^{cr} behaves as $1/N^2$ for large chain length N. For $W > W^{\mathrm{cr}}$, we obtain three distinct regimes for the optimal dephasing. Notably, dephasing is shown to aid transport even for weak or moderate disorder, where motion is ballistic and quantum states are delocalized.

Finally, the third paper is about quantum metrology. Here, we conduct numerical optimization for a lossy Mach-Zehnder interferometer with varying prior phase information, using an entangled multi-photon input state and photon-counting detection techniques. Assuming a flat prior phase probability distribution and no photon

loss, quasi-Gaussian states and N00N states are shown to be optimal when the prior phase interval Δ is large and small, respectively, for a single measurement. A third class of optimal input states exists for intermediate values of Δ. The effects of photon loss on the optimal states and the measurement precision are also studied. Optimal states are shown to be stable when other symmetric prior phase distributions are used, which suggests a possible method to determine optimal input states for a sequence of measurements.

Topics in Quantum Physics: Quantum Transport and Quantum Metrology

A Dissertation
Submitted On The Eleventh Day Of August, 2017
To The Department Of Physics
Of The Graduate School Of
Tulane University
In Partial Fulfillment Of The Requirements
For The Degree Of
Doctor Of Philosophy
By

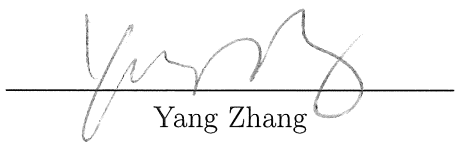

Yang Zhang

Approved: 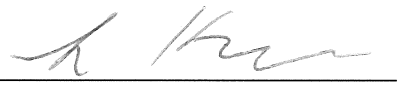

Lev Kaplan, Ph.D.
Chairman

Dmitry Uskov, Ph.D.

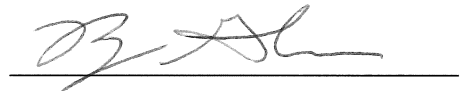

Ryan Glasser, Ph.D.

Acknowledgments

First of all, I would like to express my sincere appreciation to my advisor, Prof. Lev Kaplan. Through all these years, his constant and patient guidance kept me moving on. His brilliant insights on physics and priceless advices on research made me grow so much as a Ph.D. student. I will benefit from what I learned from him for the rest of my life. Also, I would like to give my special thanks to my advisor's wife, Rachel, and his new-born daughter, Liora. Rachel has been really warm and caring to me and Liora brought endless joy to me and everyone around her.

I would also like to thank all my collaborators: Dr. Giuseppe Luca Celardo, Dr. Fausto Borgonovi, and Dr. Dmitry Uskov. I thank Dr. Ryan Glasser for serving on the dissertation committee. I also have to thank all my friends that I met at Tulane. Their friendship is a very important part of my life.

I thank Tulane's Center for Computational Science for their computational facilities. I also thank the National Science Foundation and the Louisiana Board of Regents for their financial support.

Last but not least, I have to thank my family. My parents are always supportive of me pursuing my dreams. My wife, Shasha, has always been standing by my side and encouraging me. She is also currently nurturing our soon-to-be-born daughter. I truly appreciate everything I have now.

Contents

List of Figures

Chapter 1

Introduction

Electronic transport in the quantum regime can be considered as one of the central topics in modern solid state physics [1, 2]. Another important subject in quantum transport is the energy transfer in molecular systems [3], such as the photosynthetic light-harvesting complexes [4, 5]. Light-harvesting complexes are natural systems that can absorb and convert photon energy to excitation energy, and subsequently transfer excitons to the reaction center. They are disordered open quantum systems subject to dephasing due to interactions with the surrounding protein environment.

In Chapter 2 and Chapter 3 of this thesis, I discuss quantum transport in disordered open networks in the presence of dephasing. More specifically, Chapter 2 presents quantum enhancement of the transport in the linear chain, the fully-connected network, and the Fenna-Matthews-Olson (FMO) complex. In all of above models, we show that the opening can enhance the transport in the presence of large dephasing, as long as the disorder is sufficiently strong. In Chapter 3, we focus on the linear chain and the beneficial effects of dephasing. In this introduction, I present general phenomena associated with the three important ingredients, namely disorder, dephasing, and opening, important in the discussion of quantum transport. As for quantum metrology, this topic will be discussed in Chapter 4.

1.1 Closed homogeneous systems without dephasing

In the closed homogenous systems of N sites where disorder strength W is zero, the transport is ballistic if there is no dephasing. Here we define the mean-squared displacement (MSD) $\langle R^2(t)\rangle$ as

$$\left\langle R^2(t)\right\rangle = \sum_n n^2 \rho_{nn}(t), \tag{1.1}$$

where $\rho_{nn}(t)$ are the time-dependent populations at site n and the origin is chosen to make the first moment zero. Then for ballistic motion we have $\langle R^2(t)\rangle \propto t^2$.

However, coherent transport is generally suppressed in the presence of disorder. In 1957, P. W. Anderson suggested that randomness associated with impurities or defects in a medium can destroy electron diffusion, thus making the medium an insulator [6]. Here, the absence of diffusion of electron waves in a disordered medium is called Anderson localization. The wave function decays exponentially outside of the delocalized regime with width ξ, $\phi(r) \propto e^{-|r-r_0|/\xi}$. For an infinitely long tight-binding chain in the presence of disorder, the eigenstates will always be localized, no matter how small the disorder is. Specially, the localization length ξ in a one-dimensional chain scales as $\xi \propto \Omega^2/W^2$, where Ω is the inter-site coupling strength.

1.2 Closed homogeneous systems with dephasing

With the introduction of dephasing, localized states can be freed up and the transport becomes diffusive at long times [7]

$$\lim_{t\to\infty} \left\langle R^2(t)\right\rangle_W = 2Dt, \tag{1.2}$$

where D is the diffusion constant. Specifically in the strong dephasing case ($\gamma \gg \Omega$), the transport is described as an incoherent exciton hopping between sites in a classical random walk [8], and the diffusion constant becomes $D_{hop} = 2\gamma\Omega^2/(\gamma^2 + \Delta^2)$, where Δ is the detuning between neighboring sites.

1.3 Open systems

Now we open up the system by allowing the exciton to escape into a continuum. In the case of a single decay channel, the effects of the opening can be conveniently included by augmenting the term $\frac{i}{2}\Gamma_{\text{trap}} |N\rangle \langle N|$ to the original system Hamiltonian, and Γ_{trap} denotes the opening strength. So now the transport contains two stages. The first stage is the spreading of the wave function of the exciton, while the second stage is the decay to the continuum at site N. The average transfer time τ, defined in Eq (2.10) as a measure of the transport efficiency, starts with infinity when $\Gamma_{\text{trap}} = 0$ and decreases as Γ_{trap} increases. However, if Γ_{trap} becomes too large, τ starts to increase. This process is called the superradiance transition [9]. More details will be explained in Chapter 2.

Chapter 2

Opening-Assisted Coherent Transport in the Semiclassical Regime

2.1 Introduction

Since the discovery that quantum coherence may have a functional role in biological systems even at room temperature [5, 10, 11, 12, 13], there has been great interest in understanding how coherence can be maintained and used under the influence of different environments with competing effects. In particular, much recent research has focused on quantum networks, due to their relevance to molecular aggregates, such as the J-aggregates [14, 15], natural photosynthetic systems [7], bio-engineered devices for photon sensing [16], and light-harvesting systems [17].

Many photosynthetic organisms contain networks of chlorophyll molecular aggregates in their light-harvesting complexes, *e.g.* LHI and LHII [4, 18]. These complexes absorb light and then transfer the excitations to other structures or to a central core absorber, the reaction center, where charge separation, necessary in the next steps of photosynthesis, occurs. Exciton transport in biological systems can be inter-

preted as an energy transfer between chromophores described as two-level systems. When chromophores are very close, which for chlorophylls is often less than 10 Å, the interaction between them is manifested in a manner known as exciton coupling. Under low light intensity, in many natural photosynthetic systems or in ultra-precise photon sensors, the single-excitation approximation is usually valid. In this case the system is equivalent to a tight binding model where one excitation can hop from site to site [7, 16, 17, 19, 20, 21].

Light-harvesting complexes are subject to the effects of different environments: *i*) dissipative, where the excitation can be lost; and *ii*) proteic, which induce static or dynamical disorder. The efficiency of excitation transfer can be determined only through a comprehensive analysis of the effects due to the interplay of all those environments.

Here we consider systems subject to the influence of a single decay channel, in the presence of both static and dynamical disorder. The decay channel represents coupling to a central core absorber (loss of excitation by trapping). For many molecular aggregates, the single-channel approximation is appropriate to describe this coupling, modeled for instance by a semi-infinite one-dimensional lead [9, 22, 23, 24, 25, 26]. The disorder is due to a protein scaffold, in which photosynthetic complexes are embedded, that induces fluctuations in the site energies. Fluctuations that are slow or fast on the time scale of the dynamics are described as static or dynamic disorder, respectively.

Several works in the literature aim to understand the parameter regime in which transport efficiency is maximized. Some general principles that might be used as a guide to understand how optimal transport can be achieved have been proposed: Enhanced noise assisted transport [27, 28, 29], the Goldilocks principle [30], and superradiance in transport [31]. Even though none of these principles alone can solve

the problem of optimal efficiency, here we will focus on the role of the opening and the associated superradiance effect, which has been less investigated in the literature.

Though originally discovered in the context of atomic clouds interacting with an electromagnetic field [32], and in the presence of many excitations, superradiance was soon recognized to be a general phenomenon in open quantum systems [33, 34, 35, 36] under the conditions of coherent coupling with a common decay channel. In the case of many excitations, superradiance allows N excited states to radiate with an intensity proportional to N^2. On the other hand, in exciton transport, usually only one excitation is present in the system. Crucially, superradiance can occur also in the presence of a single excitation [9, 22, 31], entailing a purely quantum effect (the "super" of superradiance [37]). Since here we address the single-excitation regime, superradiance in the following refers exclusively to single-excitation superradiance. Single-excitation superradiance implies the existence of some states with a cooperatively enhanced decay rate, and is always accompanied by subradiance, the existence of states with a cooperatively suppressed decay rate. Most importantly for the present work, single-excitation superradiance can have profound effects on transport efficiency in open systems: for example, in a linear chain, the integrated transmission from one end to the other is peaked precisely at the superradiance transition [9, 22].

The functional role that superradiance might have in natural photosynthetic systems has been discussed in many publications [13, 16, 38, 39], and experimentally observed in molecular aggregates [14, 15, 40]. Superradiance (or supertransfer) is also thought to play an important role in the transfer of excitation to the central core absorber [13], and its effects on the efficiency of energy transport in photosynthetic molecular aggregates have recently been analyzed [31, 41].

While superradiance may enhance transport, static disorder is often expected to hinder it, since it induces localization [6]. The relation between superradiance

and localization has been already analyzed in the literature in different contexts [21, 42, 43, 44, 45]. Additionally, dynamical disorder (or dephasing) will generally destroy cooperativity [46], and hence counteract quantum coherence effects, including superradiance. On the other hand, dynamical disorder may also enhance efficiency, through the so-called noise assisted transport [27, 28, 29].

In the semiclassical regime where dephasing is stronger than the coupling between the chromophores, transport in quantum networks can be described by incoherent master equations with an appropriate choice of transition rates. However, the presence of an opening (trapping) introduces a new time scale to the system. When the opening strength is large, coherent effects may be revived even in the semiclassical regime. Here we want to address the following questions: *i*) For which values of the opening strength are coherent effects relevant? *ii*) Can we enhance transport by increasing the opening, which induces coherent effects not present in the incoherent model? *iii*) Under what generic conditions can coherent effects enhance transport in open quantum systems?

The remainder of the chapter is organized as follows. In Sec. 2.2, we present the basic mathematical formalism for analyzing the dynamics of open quantum networks in the presence of both static disorder and dephasing, and define the average transfer time, which measures the transport efficiency in these systems. Then in Sec. 2.3, we first focus on the two-site model, where all results may be obtained analytically, and determine the regime of dephasing, detuning, and opening strength in which quantum coherent effects enhance quantum transport. Specifically, we show that if the strengths of static and dynamical disorder (detuning and dephasing, respectively) are fixed, there is an optimal opening strength at which the coherent transport enhancement is optimized. In Secs. 2.4 and 2.5, respectively, we extend our analysis to two paradigmatic models of transport: the linear chain and the fully connected

network. The linear chain in particular has been widely considered in the literature [7, 29, 47, 48], and the fully connected network has been explored in Ref. [48]. Finally, in Sec. 2.6 we consider the Fenna-Matthews-Olson (FMO) light-harvesting complex, and demonstrate that the opening-assisted coherent transport obtained analytically in the earlier models is also present in this naturally occurring system. In Sec. 2.7 we present our conclusions.

2.2 Quantum networks

Here we present the quantum network models that we will consider. A quantum network is a tight binding model where an excitation can hop from site to site in a specified geometry.

The first example is the linear chain, see Fig. 2.1 a). This model has been widely analyzed in the literature due to its relevance in natural and artificial energy transport devices, and is characterized by the following system Hamiltonian ($\hbar = 1$ here and in the following):

$$\mathrm{H}_{\mathrm{lin}} = \sum_{i=1}^{N} \omega_i \left|i\right\rangle \left\langle i\right| + \Omega \sum_{j=1}^{N-1} \left(\left|j\right\rangle \left\langle j+1\right| + \left|j+1\right\rangle \left\langle j\right|\right) , \tag{2.1}$$

where ω_i are the site energies and Ω is the coupling between neighboring sites. Here, $|j\rangle$ represents a state in which the excitation is at the site j, when all the other sites are unoccupied. In terms of two-level states, $|0\rangle, |1\rangle$, it can be written as $|j\rangle = |0\rangle_1|0\rangle_2 \ldots |1\rangle_j \ldots |0\rangle_N$. It is common to introduce static noise by letting the energies ω_i fluctuate randomly in the interval $[-W/2, W/2]$ with a uniform distribution, and variance $\sigma^2 = W^2/12$.

This model can be "opened" by allowing the excitation to escape the system from one or more sites into continuum channels describing the reaction center where the excitation is lost. This situation of "coherent dissipation" is applicable to many

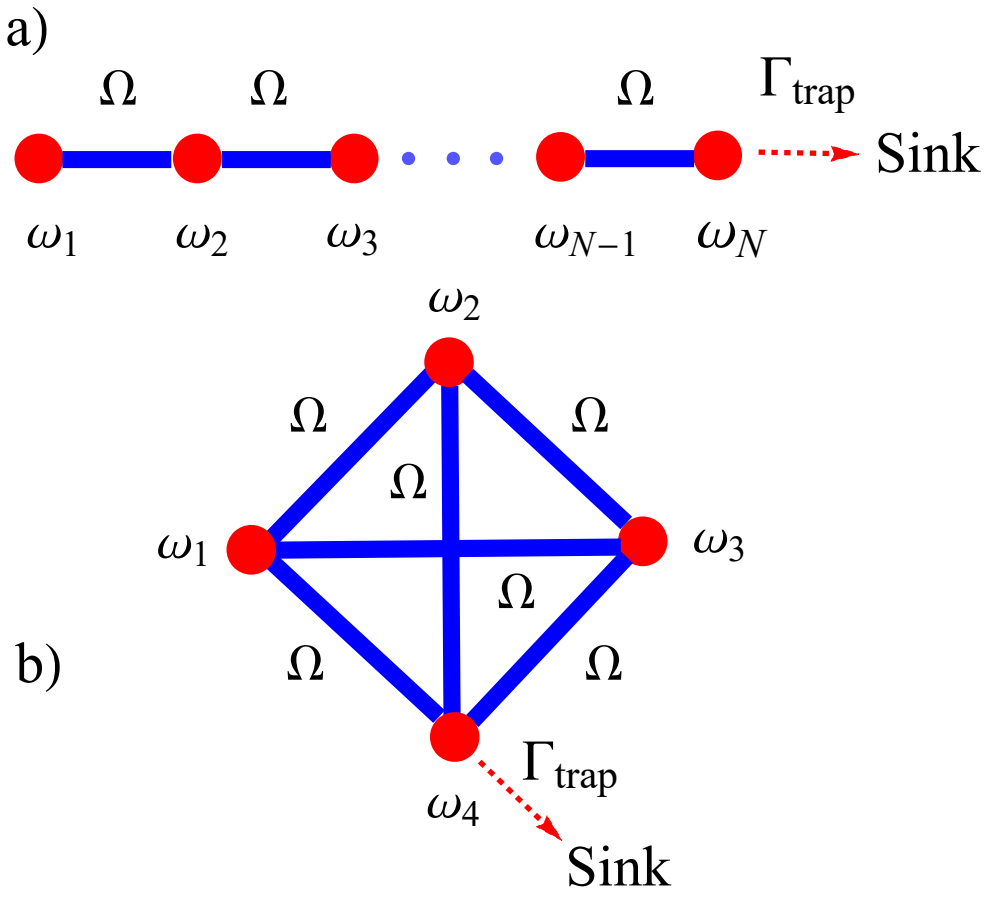

Figure 2.1: a) The linear chain. One excitation can hop between N sites, with on-site energies ω_i and with nearest neighbors connected by tunneling transition amplitude Ω. Site N is connected to a decay channel, where the excitation can escape, with coupling strength $\Gamma_{\rm trap}$. b) The analogous fully connected model with $N = 4$ sites.

systems and has been recently considered in Ref. [43, 44], where it has been shown to give rise to the following effective non-Hermitian Hamiltonian (see also [26]):

$$(H_{\rm eff})_{jk} = ({\rm H}_{\rm sys})_{jk} - \frac{i}{2}\sum_c A_j^c (A_k^c)^* \equiv ({\rm H}_{\rm sys})_{jk} - \frac{i}{2} Q_{jk}\,, \tag{2.2}$$

where $\rm H_{sys}$ is the closed system Hamiltonian, e.g. $\rm H_{sys} = H_{lin}$, and A_i^c are the transition amplitudes from the discrete states i to the continuum channels c. If we consider a single decay channel, $c = 1$, coupled to site N with decay rate $\Gamma_{\rm trap}$, we have

$A_N^1 = \sqrt{\Gamma_{\rm trap}/2}$, and $Q_{jk} = \Gamma_{\rm trap}\delta_{jN}\delta_{kN}$. Including fluorescence effects, where the excitation may be lost from any site with rate $\Gamma_{\rm fl}$, we have $Q_{jk} = (\Gamma_{\rm trap}\delta_{jN} + \Gamma_{\rm fl})\,\delta_{jk}$.

The quantum evolution (given by the operator $\mathcal{U} = e^{-iH_{\rm eff}t}$) is non-unitary, since there is a loss of probability due to the decay channel and fluorescence. The complex eigenvalues of $H_{\rm eff}$ can be written as $E_r - i\Gamma_r/2$, where Γ_r represent the decay widths of the resonances. Superradiance, as discussed in the literature [33, 34, 35, 36, 49, 50, 51, 52], is usually reached only above a critical coupling strength with the continuum (in the overlapping resonance regime):

$$\langle\Gamma\rangle/D \geq 1\,, \tag{2.3}$$

where $\langle\Gamma\rangle$ is the average decay width and D is the mean level spacing of the closed system described by $\mathrm{H_{sys}}$.

As a further effect of the environment we consider the dephasing caused by dynamic disorder. To include dephasing, we need to switch to a master equation for the reduced density matrix ρ [53],

$$\dot{\rho}(t) = -\mathcal{L}_{\rm tot}\rho(t), \tag{2.4}$$

where the Liouville superoperator is given by $\mathcal{L}_{\rm tot} = \mathcal{L}_{\rm sys} + \mathcal{L}_{\rm trap} + \mathcal{L}_{\rm fl} + \mathcal{L}_{\rm deph}$ and the four terms respectively describe the dynamics of the closed system,

$$\mathcal{L}_{\rm sys}\rho = i\left[\mathrm{H_{sys}}, \rho\right]\,, \tag{2.5}$$

exciton trapping to the reaction center,

$$\mathcal{L}_{\rm trap}\rho = \frac{\Gamma_{\rm trap}}{2}\left\{|N\rangle\langle N|\,, \rho\right\}\,, \tag{2.6}$$

decay due to fluorescence,

$$\mathcal{L}_{\text{fl}}\rho = \Gamma_{\text{fl}}\rho\,, \tag{2.7}$$

and the dephasing effect as described in the simplest approximation by the Haken-Strobl-Reineker (HSR) model [53] with dephasing rate γ,

$$(\mathcal{L}_{\text{deph}}\rho)_{jk} = \gamma\rho_{jk}\,(1-\delta_{jk})\ . \tag{2.8}$$

The efficiency of exciton transport can be measured by the total population trapped by the sink [29, 48],

$$\eta = \Gamma_{\text{trap}}\int_0^\infty \rho_{NN}(t)\,dt\,, \tag{2.9}$$

or by the average transfer time to reach the sink [27],

$$\tau = \frac{\Gamma_{\text{trap}}}{\eta}\int_0^\infty t\,\rho_{NN}(t)\,dt\,. \tag{2.10}$$

The system is initiated with one exciton at site 1, i.e., $\rho(0) = |1\rangle\langle 1|$. Formally the solutions for η and τ can be written as,

$$\eta = \Gamma_{\text{trap}}(\mathcal{L}_{\text{tot}}^{-1}\rho(0))_{\text{NN}} \tag{2.11}$$

and

$$\tau = \frac{\Gamma_{\text{trap}}}{\eta}(\mathcal{L}_{\text{tot}}^{-2}\rho(0))_{\text{NN}}\,. \tag{2.12}$$

In physical applications, we are typically interested in the parameter regime of high efficiency η, which can occur only when fluorescence is weak, i.e., when the fluorescence rate Γ_{fl} is smaller than both the trapping rate Γ_{trap} and the energy scales in the closed-system Hamiltonian H_{sys}. The FMO complex discussed in Sec. 2.6 is a typical

example: here the exciton recombination time $1/\Gamma_{\rm fl}$ is estimated to be around 1 ns, whereas the other times scales in the problem are of the order of picoseconds or tens of picoseconds [27, 28, 29, 48]. In this regime, the effect of $\Gamma_{\rm fl}$ on the efficiency η and transfer time τ may be treated perturbatively (see e.g. Ref. [54]): Specifically, τ is independent of $\Gamma_{\rm fl}$ to leading order, and η is related to τ by

$$\eta = \frac{1}{1+\Gamma_{\rm fl}\tau} \tag{2.13}$$

when higher-order corrections are omitted. Thus, for a given fluorescence rate, maximizing efficiency η is entirely equivalent to minimizing the transfer time τ. In the following, we will assume for simplicity of presentation that $\Gamma_{\rm fl}$ is indeed small, and will present results for τ only; analogous expressions for the efficiency η may be easily obtained by inserting these results into Eq. (2.13).

In the following, we will be interested in the disorder-ensemble averaged transfer time, defined as

$$\langle\tau\rangle_W = \frac{1}{W^N}\int_{-W/2}^{W/2}..\int_{-W/2}^{W/2}\tau(\omega_1,\omega_2,..\omega_N)\,d\omega_1 d\omega_2\ldots d\omega_N\,. \tag{2.14}$$

2.3 Two-site model

2.3.1 Förster approximation

In the 1940s, Förster [8] proposed an incoherent non-radiative resonance theory of the energy transfer process in weakly coupled pigments. This mechanism was based on the assumption that, due to large dephasing, the motion of an excitation between chromophores is a classical random walk, which can be described by an incoherent master equation.

Let us first consider a dimer of interacting chromophores and the transmission of the excitation from one molecule to the other. The Hamiltonian of the system is

$$H = \begin{pmatrix} \omega_1 & \Omega \\ \Omega & \omega_2 \end{pmatrix} , \tag{2.15}$$

where Ω and $\omega_1 - \omega_2 = \Delta$ are respectively the coupling and the excitation energy difference between the two molecules. Note that $|1\rangle$ represents a state where molecule 1 is excited and molecule 2 is in its ground state.

The energy difference or detuning Δ is entirely due to the interaction with the environment, if we assume the molecules of the dimer to be identical. The exciton-coupled dimer is most productively viewed as a supermolecule with two delocalized electronic transitions, rather than a pair of individual molecules, which means switching to the basis that diagonalizes H.

For this Hamiltonian, the probability for an initial excitation in the first molecule to move to the second one is given by

$$P_{1\to 2}(t) = \frac{4\Omega^2}{4\Omega^2 + \Delta^2} \sin^2\left(\sqrt{4\Omega^2 + \Delta^2}\, t/2\right) , \tag{2.16}$$

to which we can associate a typical hopping time $\tau_{\text{hop}} = \pi/\sqrt{4\Omega^2 + \Delta^2}$, a very important parameter for understanding the propagation.

In the Förster theory, dephasing is assumed to be large. If $\gamma \gg 1/\tau_{\text{hop}}$, the dephasing time is much smaller than the hopping time, $\tau_d = 1/\gamma \ll \tau_{\text{hop}}$. In this regime, coherence is suppressed and exciton dynamics becomes diffusive. The transfer rate from one molecule to the other is given by:

$$T_{1\to 2} \sim \frac{dP_{1\to 2}(\tau_d)}{d\tau_d} \approx \frac{2\Omega^2}{\gamma} . \tag{2.17}$$

This transfer rate also gives the diffusion coefficient for a linear chain of chromophores coupled by a nearest-neighbor interaction, as considered in Refs. [7, 30] for $\Omega \gg \Delta$. Indeed, the mean squared number of steps that an excitation can move is proportional to the time measured in units of the average transfer time $\tau = 1/T_{1\to 2}$, i.e., $r^2(t) \propto t/\tau = T_{1\to 2}t$. The diffusion coefficient in this regime is thus given by Eq. (2.17) and it agrees with previous results [7, 30] in the same regime.

If dephasing is still large compared to the coupling Ω, but small compared to the detuning Δ, $\Delta \gg \gamma \gg \Omega$, we must average $P_{1\to 2}(t)$ over time and obtain

$$T_{1\to 2} = \frac{\overline{P_{1\to 2}}}{\tau_d} \approx \frac{2\Omega^2\gamma}{\Delta^2} \tag{2.18}$$

This expression also agrees with the diffusion coefficient given in [30, 7] in the same regime.

In general, as long as $\gamma \gg \Omega$ holds, we have the Förster transition rate

$$T_{\mathrm{F}} = \frac{2\Omega^2\gamma}{\gamma^2 + \Delta^2}\,, \tag{2.19}$$

with the scalings given by Eqs. (2.17) and (2.18) as special cases.

Here we will not discuss the weak dephasing regime $\gamma < \Omega$ in which Förster theory does not apply. This regime has been investigated in [7, 30], where it was shown that the excitation dynamics is still diffusive, but with mean free path of order the localization length, so that the diffusion coefficient is enhanced by the localization length squared.

2.3.2 Two-site model with opening

The same two-site system can be considered in the most general context in which the interaction with a sink is explicitly taken into account. For this purpose we add to the two-site Hamiltonian described in the previous section a term repre-

senting the possibility of escaping from state $|2\rangle$ to an external continuum with decay rate $\Gamma_{\rm trap}$, see Fig. 2.2 (left panel). Moreover the system is in contact with another environment that induces fast time-dependent fluctuations of the site energies with variance proportional to γ. The presence of detuning strongly suppresses the probability of the excitation leaving the system. On the other hand, dephasing produces an energy broadening, which facilitates transport. For very large dephasing, the probability for the two site energies to match becomes small and thus transport is again suppressed. Optimal transport thus occurs at some intermediate dephasing value: $\gamma \approx \Delta$ [27, 28, 29]. This is the noise assisted transport: Noise can help in a situation where transport is suppressed in presence of only coherent motion.

Another general principle that is essential for understanding transport efficiency in open systems is superradiance. Indeed, due to the coupling with a continuum of states, the state $|2\rangle$ has an energy broadening $\Gamma_{\rm trap}$, even in absence of dephasing, which can also facilitate transport. The system in the absence of dephasing is described by the following 2×2 effective non-Hermitian Hamiltonian:

$$H_{\rm eff} = \begin{pmatrix} \omega_1 & \Omega \\ \Omega & \omega_2 - i\Gamma_{\rm trap}/2 \end{pmatrix} . \tag{2.20}$$

The complex eigenvalues (taking $\omega_1 = 0$ and $\omega_2 = \Delta$) are:

$$\mathcal{E}_\pm = \frac{\Delta}{2} - i\frac{\Gamma_{\rm trap}}{4} \pm \frac{1}{2}\sqrt{(\Delta - i\frac{\Gamma_{\rm trap}}{2})^2 + 4\Omega^2}\,, \tag{2.21}$$

and their imaginary parts represent the decay widths of the system. As a function of $\Gamma_{\rm trap}$, one of the decay widths has a non-monotonic behavior which signals the superradiance transition (ST), see Fig. 2.2 b). For $\Delta \gg \Omega$, this transition, corresponding to the maximum of the smaller width, occurs at $\Gamma_{\rm trap} \approx 2\Delta$, see the dashed

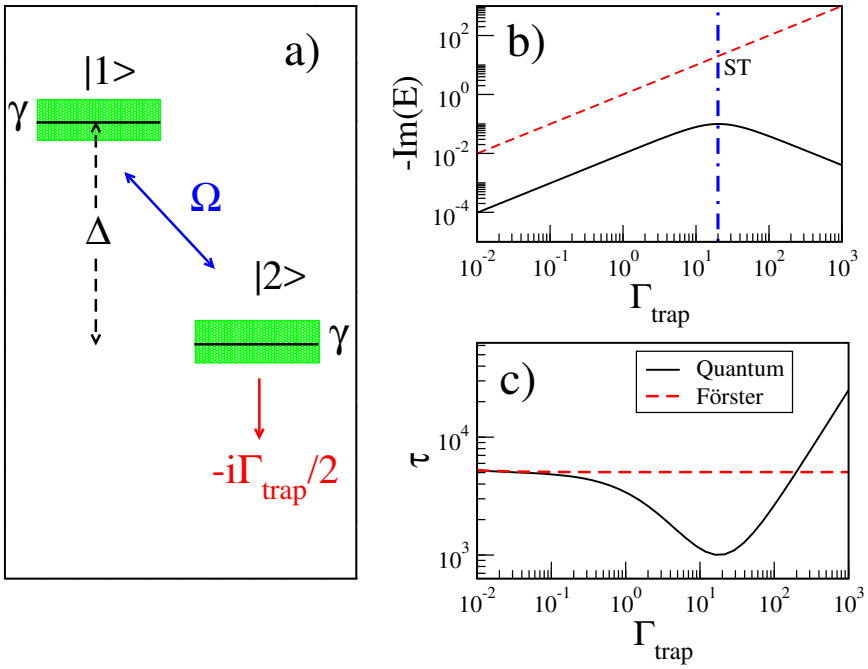

Figure 2.2: a) Schematic view of the two-site model in the presence of dephasing and coupling to the sink. b) The imaginary part of the eigenvalues of the non-Hermitian Hamiltonian given in Eq. (2.20). Here $\Omega = 1, \Delta = 10, \gamma = 0$. c) Transfer time as a function of decay width to the sink for the quantum model (solid curve) and for the Förster model (dashed curve). The vertical dashed line represents the superradiance transition (ST). Here $\Omega = 0.1$, $\gamma = 1, \Delta = 10$.

vertical line in Fig. 2.2 b). Transport efficiency is optimized around the ST, where the transfer time has a minimum as shown in Fig. 2.2 c). Indeed for small Γ_{trap}, the transport becomes more efficient with increasing Γ_{trap}, since the decay width of both states increases. On the other side, above the ST, only one of the two decay widths continues to increase with Γ_{trap}, while the other decreases. At the same time, the state with the larger decay width becomes localized on site $|2\rangle$, thus suppressing transport.

Note that while noise-assisted transport occurs only in presence of a detuning Δ, superradiance-assisted transport (SAT) occurs even with $\Delta = 0$ and in the absence of dephasing.

The non-monotonic behavior of the transfer time as a function of Γ_{trap} is a purely quantum coherent effect. To see this effect analytically, we consider the master equation (2.4), which for the two-site model can be written explicitly as

$$\begin{pmatrix} \dot{\rho}_{11} \\ \dot{\rho}_{12} \\ \dot{\rho}_{21} \\ \dot{\rho}_{22} \end{pmatrix} = \begin{pmatrix} 0 & i\Omega & -i\Omega & 0 \\ i\Omega & i\Delta - \frac{\Gamma_{\text{trap}}}{2} - \gamma & 0 & -i\Omega \\ -i\Omega & 0 & -i\Delta - \frac{\Gamma_{\text{trap}}}{2} - \gamma & i\Omega \\ 0 & -i\Omega & i\Omega & -\Gamma_{\text{trap}} \end{pmatrix} \begin{pmatrix} \rho_{11} \\ \rho_{12} \\ \rho_{21} \\ \rho_{22} \end{pmatrix} . \quad (2.22)$$

Following [54] we may insert the stationary solution ($\dot{\rho}_{12} = \dot{\rho}_{21} = 0$) for the off-diagonal matrix elements into Eq. (2.22) and obtain a rate equation for the populations ρ_{11} and ρ_{22} only:

$$\begin{pmatrix} \dot{\rho}_{11} \\ \dot{\rho}_{22} \end{pmatrix} = \begin{pmatrix} -T_{1\to 2} & T_{2\to 1} \\ T_{1\to 2} & -T_{2\to 1} - \Gamma_{\text{trap}} \end{pmatrix} \begin{pmatrix} \rho_{11} \\ \rho_{22} \end{pmatrix} . \quad (2.23)$$

These transition rates have been derived by Leegwater in [55]. In our case we have $T_{1\to 2} = T_{2\to 1} = T_{\text{L}}$ with

$$T_{\text{L}} = \frac{2\Omega^2(\gamma + \Gamma_{\text{trap}}/2)}{(\gamma + \Gamma_{\text{trap}}/2)^2 + \Delta^2} . \quad (2.24)$$

The incoherent master equation given in Eq. (2.23) represents a good approximation of the exact quantum dynamics, Eq. (2.22), when the off-diagonal matrix elements reach a stationary solution very fast. This is valid when the dephasing is sufficiently fast:

$$\gamma \gg \Omega , \quad (2.25)$$

which is the same condition as the one that ensures validity of the Förster transition rate approximation (2.19) in the closed system. We observe that the Leegwater rate given by Eq. (2.24) reduces to the Förster rate given by Eq. (2.19) in the limit where

the system is closed, $\Gamma_{\rm trap} \to 0$.

Here we would like to stress an important point: in a classical model of diffusion the transition rates from site to site are completely independent of the escape rates associated with individual sites. For this reason the transition rates given in Eq. (2.24) cannot correspond to any classical diffusion model due to their dependence on $\Gamma_{\rm trap}$. So the transition probability given in Eq. (2.24) includes also coherent effects due to the opening. This point of view is slightly different from the one in [54] where the master equation Eq. (2.23) is viewed as "classical." From now on we will refer to the master equation (2.22) with transition rates given in Eq. (2.24) as the Leegwater model, while the Förster model will denote the master equation (2.22) with the Förster transition rates (2.19), independent of $\Gamma_{\rm trap}$. Needless to say, $T_{\rm L}(\Gamma_{\rm trap} = 0) = T_{\rm F}$.

Now two questions present themselves. First, we would like to understand which values of the opening strength $\Gamma_{\rm trap}$ cause the Förster model to fail due to the coherent effects induced by the opening. Comparing Eqs. (2.19) and (2.24), it is clear that the Förster model applies when Eq. (2.25) holds and $\Gamma_{\rm trap}/2 \ll \gamma$. Even in the presence of large dephasing, when $\Gamma_{\rm trap}$ is also large (and becomes of the order of γ), coherent effects cannot be neglected and quantum transport differs significantly from that predicted by the Förster theory (compare the red dashed curve with the solid black curve in Fig. 2.2 c)).

Second, we would like to address whether quantum effects can provide enhancement over the transport predicted by Förster theory. A clear example showing that this can happen appears in Fig. 2.2 c), where, for a large region of values of $\Gamma_{\rm trap}$, the quantum transfer time is significantly less than that predicted by Förster theory. So the idea is the following: Even in presence of large dephasing, for which a Förster model of incoherent transport is expected to apply, as we increase the coupling $\Gamma_{\rm trap}$ to a sink, coherent effects can be revived and enhance transport. Finding overall

conditions for optimal transport in open quantum systems will be a key focus of the following analysis.

Below we will derive analytical expressions for the transfer times and address the above questions quantitatively.

2.3.3 Transfer time, optimal opening, and quantum enhancement

In the two-site case, one can obtain a simple yet exact analytic form for the transport time τ, Eq. (2.10), using Eq. (2.12) and substituting the exact Liouville operator $\mathcal{L}$ given by Eq. (2.22) [54]:

$$\tau = \frac{1}{2\Omega^2}\left(\frac{4\Omega^2}{\Gamma_{\text{trap}}} + \gamma + \frac{\Gamma_{\text{trap}}}{2} + \frac{\Delta^2}{\gamma + \frac{\Gamma_{\text{trap}}}{2}}\right). \tag{2.26}$$

Eq. (2.26) shows explicitly the non-monotonic behavior of the transfer time with the opening Γ_{trap}, which is a signature of quantum coherence and is clearly visible in Fig. 2.2 c).

The expression for the average transfer time can be aso computed using the incoherent master equation (2.22), with either the Förster or Leegwater transition rate. While for the two-site case the Leegwater average transfer time is exactly the same as the full quantum result (2.26), for the Förster theory we have:

$$\tau_{\text{F}} = \frac{1}{2\Omega^2}\left(\frac{4\Omega^2}{\Gamma_{\text{trap}}} + \gamma + \frac{\Delta^2}{\gamma}\right). \tag{2.27}$$

We note that τ_{F} decays monotonically with increasing opening Γ_{trap}, as it must in a classical calculation. Clearly for $\Gamma_{\text{trap}} \ll \gamma$, Förster theory coincides with the full quantum result. On the other hand for $\Gamma_{\text{trap}} \gtrsim \gamma$, coherent effects become important and they can be incorporated using the Leegwater model (at least for the two-site

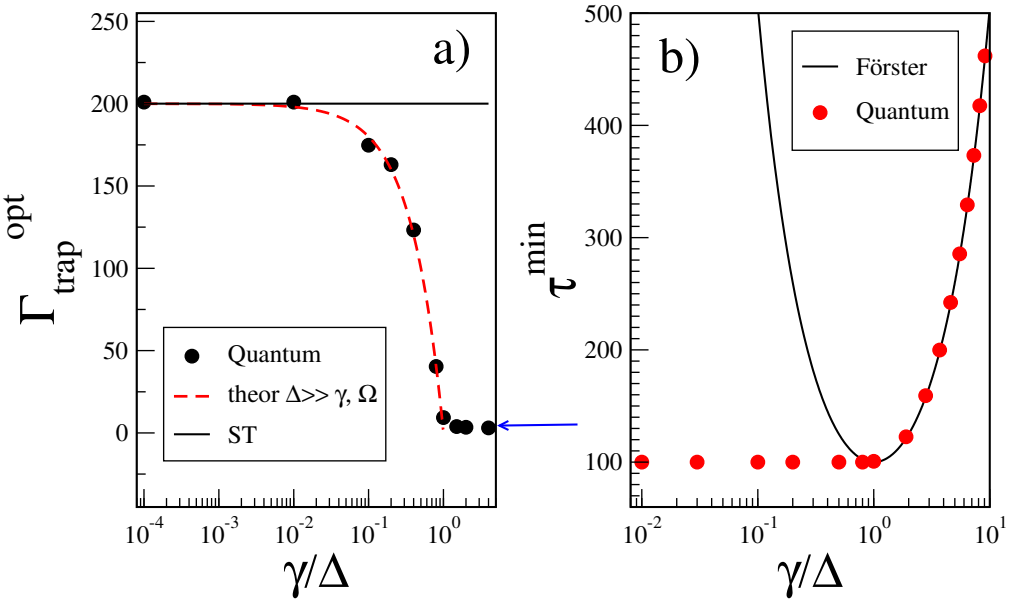

Figure 2.3: a) Optimal coupling to the sink, $\Gamma_{\rm trap}^{\rm opt}$, in a two-site system, as a function of the rescaled dephasing strength γ/Δ in the regime $\Delta \gg \Omega$. Data refer to the case $\Delta = 100, \Omega = 1$. Symbols represent numerical simulations of the full quantum model, the dashed red curve shows the analytical result given by Eq. (2.30), and the blue arrow shows the asymptotic value given by Eq. (2.34). The solid horizontal line indicates the value at which the superradiance transition (ST) occurs for zero dephasing. b) Minimal transfer times for the Förster model (solid curve) and for the full quantum calculation (symbols) are shown as functions of the rescaled dephasing strength γ/Δ.

case).

Since $\tau_{\rm F}$ is a monotonic function of $\Gamma_{\rm trap}$, it assumes its minimum value

$$\tau_{\rm F}^{\rm min} = \frac{1}{2\Omega^2}\left(\gamma + \frac{\Delta^2}{\gamma}\right) \tag{2.28}$$

for $\Gamma_{\rm trap} \to \infty$. On the other hand, the quantum transfer time is minimized at a finite value of $\Gamma_{\rm trap}$. Unfortunately the optimal value of $\Gamma_{\rm trap}$ is given in general by the solution to a quartic equation. Nevertheless it is easy to obtain simple expressions in several physically relevant regimes. In particular, of greatest physical interest is the

situation where the quantum minimum associated with optimal value of the opening is deep, which is only possible where a large difference exists in the first place between quantum and incoherent transport, i.e., $\Gamma_{\rm trap} \gg \gamma$, as discussed above in Sec. 2.3. In that regime, the optimal opening is given by

$$\Gamma_{\rm trap}^{\rm opt} \approx 2\sqrt{\Delta^2 + 2\Omega^2} - \frac{2\gamma\Delta^2}{\Delta^2 + 2\Omega^2} + O(\gamma^2)\,. \tag{2.29}$$

If in addition to dephasing being weak, detuning is strong ($\Delta \gg \Omega$), Eq. (2.29) simplifies to

$$\Gamma_{\rm trap}^{\rm opt} \approx 2\Delta - 2\gamma\,. \tag{2.30}$$

In Fig. 2.3 a) the simple analytical expression (2.30) is shown to agree very well with exact numerical calculations for the quantum model. This result is particularly interesting since it shows the effect of dephasing on the ST: While for small dephasing the optimal opening strength is given by the ST criterion $\Gamma_{\rm ST} \approx 2\Delta$, for larger dephasing the optimal $\Gamma_{\rm trap} = \Gamma_{\rm ST} - 2\gamma$ decreases with the dephasing γ.

The condition for optimal transport given in Eq. (2.30), can be re-written as $\Delta = \gamma + \Gamma_{\rm trap}^{\rm opt}/2$. This can be interpreted by saying that dephasing and opening together induce a cumulative energy broadening, which optimize transport when it matches the detuning Δ. Also striking is the symmetrical role that γ and $\Gamma_{\rm trap}$ play in controlling transport efficiency even if their origin and underlying physics are completely different. For instance γ induces dephasing in the system, whereas $\Gamma_{\rm trap}$ increases the coherent effects.

The optimal dephasing, fixing all other variables, is given exactly by

$$\gamma^{\rm opt} = \Delta - \Gamma_{\rm trap}/2\,, \tag{2.31}$$

in any regime. This shows that also the criterion for noise assisted transport, $\gamma \approx \Delta$,

is modified by the presence of a strong opening.

For the value of $\Gamma_{\rm trap}$ given in Eq. (2.30), the minimal transfer time assumes the value:

$$\tau^{\rm min} \approx \frac{\Delta}{\Omega^2}\,, \tag{2.32}$$

which should be compared with the Förster expression (2.28) in the same regime,

$$\tau_{\rm F}^{\rm min} \approx \frac{\Delta^2}{2\gamma\Omega^2} = \tau^{\rm min}\frac{\Delta}{2\gamma} \gg \tau^{\rm min}\,, \tag{2.33}$$

showing that in this regime ($\Delta \gg \gamma \gg \Omega$) quantum coherence, induced by the coupling to the sink, can always enhance transport.

In the opposite limit $\Omega \gg \Delta \gg \gamma$ one obtains:

$$\Gamma_{\rm trap}^{\rm opt} = 2\sqrt{2}\Omega\,. \tag{2.34}$$

We summarize our results so far in the following way: For very small opening, $\Gamma_{\rm trap} \ll \gamma$, the Förster model reproduces the quantum results. In the opposite limit $\Gamma_{\rm trap} \to \infty$, quantum transport is always fully suppressed while the Förster model prediction for the average transfer time approaches a non-zero asymptotic value, thus showing the non-applicability of this model. In general, we expect the Förster model to fail when $\Gamma_{\rm trap} \gtrsim \gamma$, so that coherent effects that occur on a time scale $1/\Gamma_{\rm trap}$, can be relevant before dephasing destroys them on a time scale $1/\gamma$.

What is the regime in which quantum transport is better than the incoherent transport described by the Förster model? In order to find this regime, let us write the difference between the two transfer times:

$$\tau_{\rm F} - \tau = \frac{\Gamma_{\rm trap}}{4\Omega^2}\left[\frac{\Delta^2}{\gamma(\gamma+\Gamma_{\rm trap}/2)} - 1\right]\,. \tag{2.35}$$

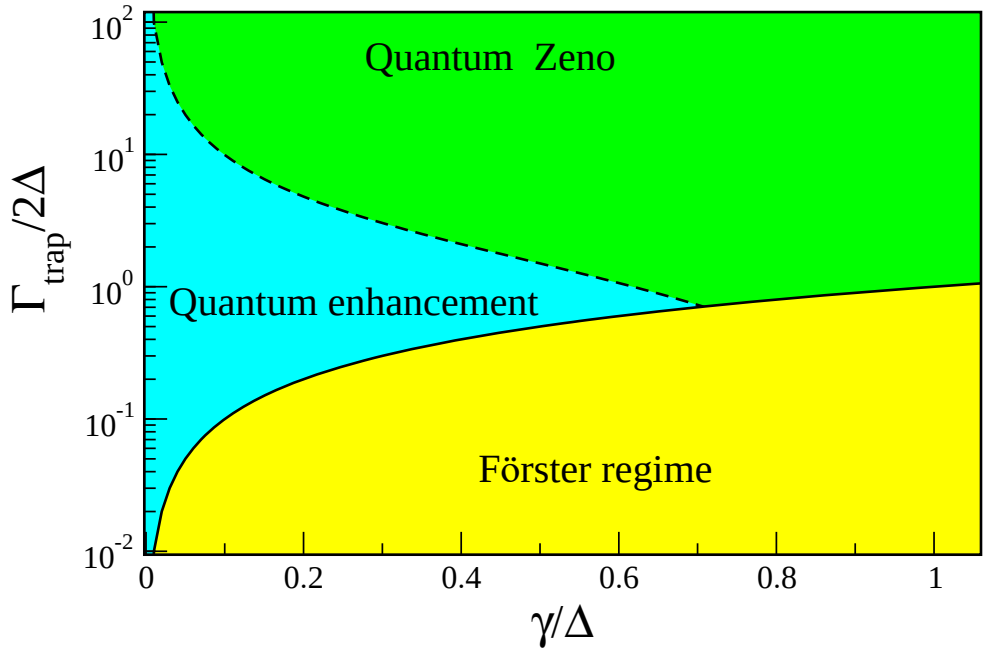

Figure 2.4: The parameter regime of significant quantum enhancement of transport in the two-site model, Eq. (2.36), and the Förster regime, $\gamma < \Gamma_{\rm trap}/2$, where quantum effects are negligible. In the third regime, corresponding to very large opening $\Gamma_{\rm trap}$, quantum mechanics suppresses transport due to the quantum Zeno effect. Generalization to a disordered linear chain of arbitrary length is obtained by replacing the detuning Δ in the two-site model with $W/\sqrt{6}$, where W is the disorder strength.

Clearly, quantum transfer is enhanced over the Förster prediction ($\tau < \tau_{\rm F}$) if and only if $\gamma + \Gamma_{\rm trap}/2 < \Delta^2/\gamma$. On the other hand, as noted earlier, the relative difference is small, i.e., the Förster model is a good approximation, when $\Gamma_{\rm trap}/2 \ll \gamma$. So the regime where quantum coherent effects produce a significant enhancement of transfer efficiency in the two-site model is given by

$$\gamma \lesssim \frac{\Gamma_{\rm trap}}{2} < \frac{\Delta^2}{\gamma} - \gamma \,. \tag{2.36}$$

This result is consistent with the illustration in Fig. 2.2 c): when the opening is very small, the Förster approximation holds, whereas for very large opening, coherent

effects cause trapping (a quantum Zeno effect). It is only for the range of openings given in Eq. (2.36) that quantum coherence aids transport.

The quantum transport enhancement regime given by Eq. (2.36) is illustrated graphically in Fig. 2.4. As the dephasing decreases, quantum enhancement of transport occurs for an ever wider range of openings $\Gamma_{\rm trap}$. We also observe that near the superradiance transition, $\Gamma_{\rm trap} \sim 2\Delta$, quantum transport enhancement obtains for the widest range of dephasing strengths γ.

Note that in the case of static disorder, the disorder-averaged transfer time can be computed as stated in Eq. (2.14). The results of this section remain valid if we substitute Δ^2 with $\langle(\omega_1 - \omega_2)^2\rangle = W^2/6$.

2.4 Long chains with static disorder

2.4.1 Linear chain: analytic results

For a linear chain with N sites, see Fig. 2.1 a), in the presence of static disorder, it is not possible to get an analytical expression for the full quantum model. Nevertheless under the strong dephasing condition given in Eq. (2.25) the dynamics of the system can be described by the incoherent master equation,

$$\frac{dP_j}{dt} = \sum_k (T_{k\to j} P_k - T_{j\to k} P_j) - \delta_{j,n}\Gamma_{\rm trap} P_j \,, \tag{2.37}$$

where P_j is the probability to be at site j. The nearest-neighbor transfer rates in Eq. (2.37), $T_{k\to j}$, are given by $T_{\rm F}$, Eq. (2.19), with the exception of the transfer rate along the bond adjacent to the sink, $T_{n-1\to n} = T_{n\to n-1}$, which is given by the Leegwater expression $T_{\rm L}$, Eq. (2.24). The Förster model is also given by Eq. (2.37) but with all the transfer rates given by $T_{\rm F}$, Eq. (2.19).

Proceeding in the same way as for the case $N = 2$, we obtain analytical

expressions for the ensemble-averaged Förster and Leegwater transfer times:

$$\langle \tau_{\mathrm{F}} \rangle_W = \frac{N}{\Gamma_{\mathrm{trap}}} + \frac{N\,(N-1)}{4\Omega^2}\left(\gamma + \frac{W^2}{6\gamma}\right) \tag{2.38}$$

and

$$\langle \tau_{\mathrm{L}} \rangle_W = \frac{N}{\Gamma_{\mathrm{trap}}} + \frac{N\,(N-1)}{4\Omega^2}\left[\gamma + \frac{\Gamma_{\mathrm{trap}}}{N} + \frac{W^2}{6\gamma}\left(1 - \frac{2\Gamma_{\mathrm{trap}}}{N(2\gamma + \Gamma_{\mathrm{trap}})}\right)\right]. \tag{2.39}$$

The effect of quantum coherence is given by the difference in transfer times,

$$\langle \tau_{\mathrm{F}} \rangle_W - \langle \tau_{\mathrm{L}} \rangle_W = \frac{(N-1)\Gamma_{\mathrm{trap}}}{4\Omega^2}\left(\frac{W^2}{3\gamma\,(2\gamma + \Gamma_{\mathrm{trap}})} - 1\right). \tag{2.40}$$

In general, increasing the ratio W/γ (i.e., increasing the strength of static as compared to dynamical disorder) will make the difference in Eq. (2.40) more positive, i.e., quantum transport becomes more favored relative to incoherent transport, just as has been seen already in the two-site case. To be precise, from Eq. (2.40),

$$\frac{W^2}{3\gamma\,(2\gamma + \Gamma_{\mathrm{trap}})} > 1 \Rightarrow W > \sqrt{6}\gamma$$

must hold in order to have $\langle \tau_{\mathrm{F}} \rangle_W > \langle \tau_{\mathrm{L}} \rangle_W$, and the regime where quantum effects are both helpful and significant is then identical to the one identified in Eq. (2.36) and Fig. 2.4 for the two-site model, with the simple replacement $\Delta^2 \to W^2/6$:

$$\gamma \lesssim \frac{\Gamma_{\mathrm{trap}}}{2} < \frac{W^2}{6\gamma} - \gamma\,. \tag{2.41}$$

We notice that $W > \sqrt{6}\gamma$ is a necessary condition for significant quantum transport enhancement to occur, i.e., static disorder must be stronger than dynamic disorder.

Given $W > \sqrt{6}\gamma$, $\langle \tau_{\rm F} \rangle_W - \langle \tau_L \rangle_W$ is maximized when $\Gamma_{\rm trap} = \Gamma_{\rm trap}^{\rm opt}$, where

$$\Gamma_{\rm trap}^{\rm opt} = 2\left(W/\sqrt{6} - \gamma\right) . \tag{2.42}$$

To be precise, we should note that the value of $\Gamma_{\rm trap}$ that maximizes the transport enhancement $\langle \tau_{\rm F} \rangle_W - \langle \tau_L \rangle_W$ is not exactly the same as the value at which the quantum transport time $\langle \tau_L \rangle_W$ is minimized, but in the limit of small Ω where the Förster approximation is meaningful, the difference is negligible. In the limiting case $W \sim \Gamma_{\rm trap} \gg \gamma \gg \Omega$ and $N \gg 1$, $\langle \tau_{\rm F} \rangle_W \approx \langle \tau_{\rm L} \rangle_W \approx N^2 W^2/24\gamma\Omega^2$, so both types of transport are diffusive, while the difference in transfer times $\langle \tau_{\rm F} \rangle_W - \langle \tau_L \rangle_W$ is $NW^2/12\gamma\Omega^2$. In relative terms, quantum enhancement is therefore most important in short chains, which is a case relevant in realistic photosynthetic complexes where the number of chromophores is small, e.g. the FMO complex which will be the focus of Sec. 2.6.

2.4.2 Linear chain: numerical results

Eqs. (2.38) and (2.39) provide, respectively, the analytical results for the average transfer time in the Förster model, which is purely incoherent, and in the Leegwater approximation, which incorporates quantum coherence effects. Unfortunately no analytic result is available for the exact quantum calculation in a chain of general length N and for this reason we will present results obtained by means of numerical simulations. In particular we will show that:

- The Leegwater expression, Eq. (2.39), provides a good approximation for the exact quantum transfer time in the regime of interest given by Eq. (2.41), as long as the semiclassical condition, $\gamma \gg \Omega$, holds;

- Equation (2.42), obtained from the analytic Leegwater calculation, accurately describes the opening at which the exact quantum transport enhancement

$\langle \tau_{\rm F} \rangle_W - \langle \tau \rangle_W$ is maximized;

- Quantum corrections beyond the Leegwater approximation give rise to even stronger quantum transport enhancement when the semiclassical condition $\gamma \gg \Omega$ is no longer satisfied.

First, results for $N = 3$ sites are reported in Fig. 2.5. We see that in the case $W \gg \gamma \gg \Omega$ ($W = 100$, $\gamma = 10$), the exact quantum results agree very well with the Leegwater approximation, and the maximal quantum enhancement occurs at $\Gamma_{\rm trap} \approx \Gamma_{\rm trap}^{\rm opt}$, as predicted. For $W \sim \gamma$ (see $W = 3, \gamma = 1$), quantum transport enhancement becomes negligible, and the enhancement effect disappears entirely for $W \lesssim \gamma$ (see $W = 0.3, \gamma = 0.3$). Where a noticeable difference is observed between the Leegwater approximation and the exact quantum results, the exact quantum corrections favor somewhat greater coherent transport enhancement, i.e., the true enhancement is slightly stronger than that predicted by the Leegwater model (see for example $W = 10, \gamma = 1$ in Fig. 2.5). This correction is addressed at a quantitative level below.

Next, we confirm that these results continue to hold for long chains ($N \gg 1$). In Fig. 2.6. The results of the Förster model (2.38) and of the Leegwater approximation (2.39) are compared with the exact quantum calculation for $N = 10$ and 20 with a fixed set of parameters such that $W \gg \gamma \gg \Omega$. It is clear from Fig. 2.6 that the above picture continues to hold at large N: The difference between incoherent and quantum transfer times is still maximized for $\Gamma_{\rm trap} \simeq \Gamma_{\rm trap}^{\rm opt}$, the minimal quantum transfer time also occurs near $\Gamma_{\rm trap}^{\rm opt}$, and the Leegwater approximation underpredicts the true quantum enhancement by a slight margin.

We now briefly return to the observation in Figs. 2.5 and 2.6 of a slight discrepancy between the exact quantum calculation and the Leegwater expressions. Although no analytic expression is available for the quantum chain with $N > 2$, a

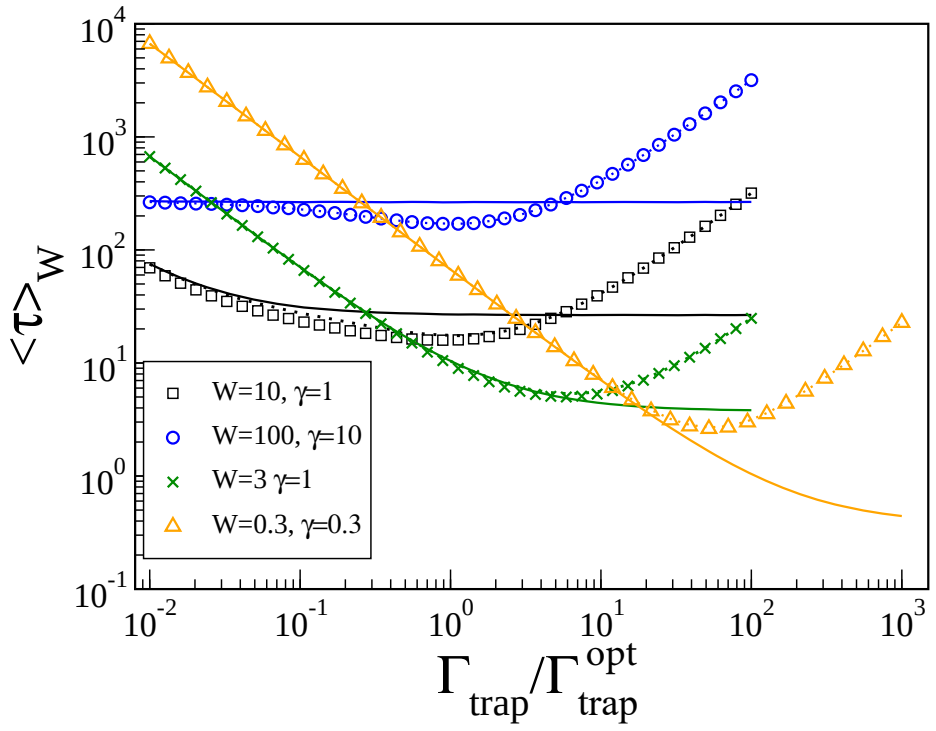

Figure 2.5: Förster (solid), Leegwater (dotted), and quantum (symbols) average transfer times for the $N = 3$ linear chain. Here we fix $\Omega = 1$. On the horizontal axis we normalize the trapping by $\Gamma^{\rm opt}_{\rm trap}$ as given by Eq. (2.42).

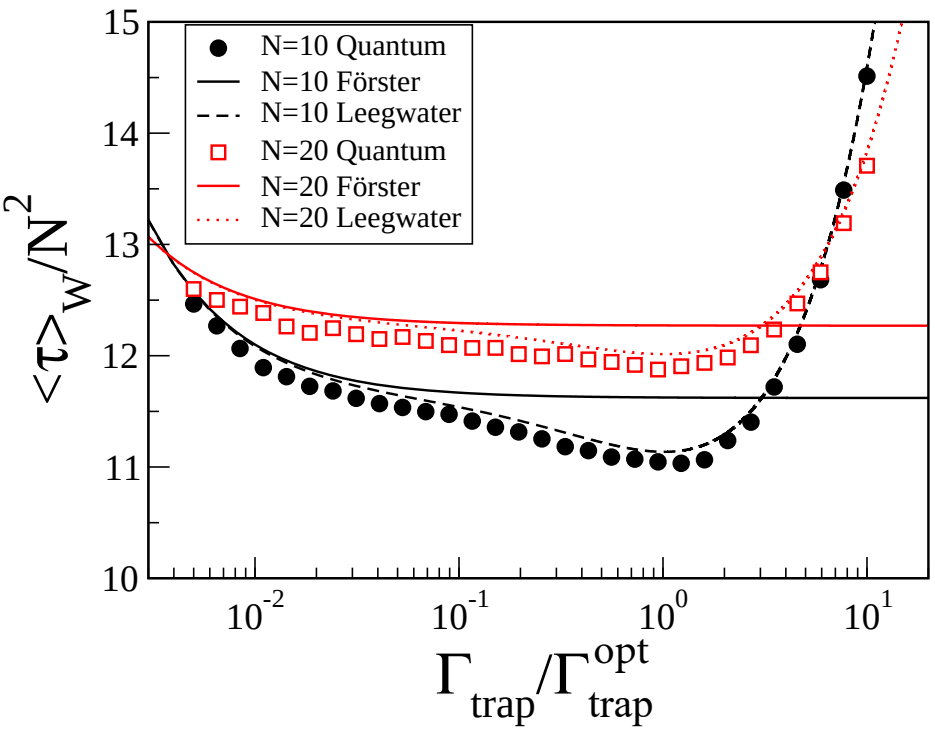

Figure 2.6: Comparison among Förster (solid cures), Leegwater (dotted and dashed curves), and quantum (symbols) average transfer times (rescaled by a factor N^2) for a linear chain with $N = 10$ and $N = 20$ sites. Here we fix $\Omega = 1$, $\gamma = 10$, and $W = 50$. On the horizontal axis we renormalize the trapping by $\Gamma_{\rm trap}^{\rm opt}$ (Eq. (2.42)).

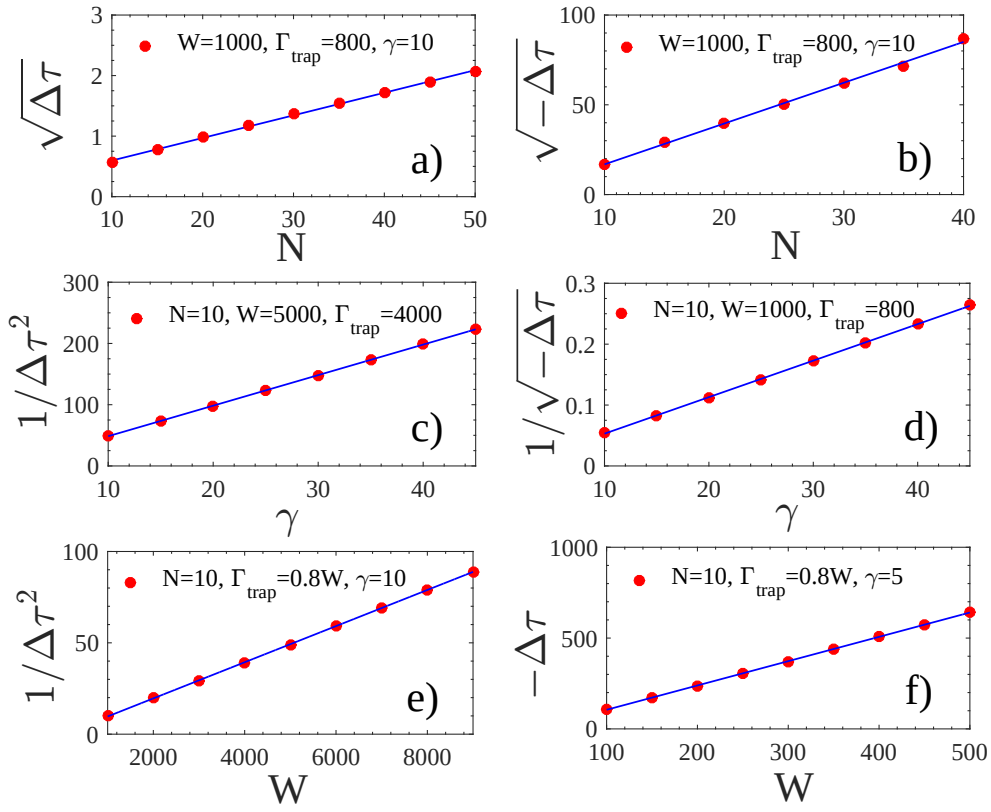

Figure 2.7: The error in the Leegwater approximation, $\Delta\tau = \langle\tau\rangle - \langle\tau_L\rangle$, is shown as a function of system size N, dephasing strength γ, and disorder strength W, in the parameter regime of interest. Panels a), c), and e) are for the fully-connected network and b), d), and f) are for the linear chain. The solid blue lines in panels a) and b) are fits to $(a' + b'N)^2/\sqrt{\gamma W}$ for the fully-connected network (with $a' = 2.33$, $b' = 0.37$) and to $-(a + bN)^2 W/\gamma^2$ for the chain (with $a = 1.82$, $b = 0.72$), which converge to Eqs. (2.56) and (2.43), respectively in the large-N limit. We fix $\Omega = 1$, and the other parameters are shown in the legend of each panel. Specially we fix $\Gamma_{\text{trap}} = 0.8W$, which is close to the optimal opening $\Gamma_{\text{trap}}^{\text{opt}} = \sqrt{6}W/3$ for both systems.

systematic numerical scaling analysis in the regime of interest, $N \gg 1$, $W \gg \gamma \gg \Omega$, shows that the leading quantum correction to the Leegwater formula scales as

$$\langle \tau \rangle_W - \langle \tau_L \rangle_W = -bN^2 W/\gamma^2 \,, \tag{2.43}$$

where $b \approx 0.72$ is a constant, see Fig. 2.7. Comparing with Eq. (2.39), we find the relative error in the Leegwater approximation:

$$\langle \tau \rangle_W \,/\, \langle \tau_{\rm L} \rangle_W = 1 - O(\Omega^2/W\gamma) \,, \tag{2.44}$$

independent of chain length for $N \gg 1$. This agrees with our previous observations: the Leegwater approach provides an excellent approximation to the quantum transfer time in the regime where quantum enhancement is possible, and the leading correction favors even slightly faster transport than that predicted by the Leegwater formula.

2.4.3 Heuristic derivation of transfer times for the linear chain

Here we give an heuristic derivation of the average transfer time obtained in the previous section. In particular we will analyze the parameter regime where quantum transport outperforms incoherent transport.

Consider a linear chain of N sites. We start at one end of the chain and evaluate the probability to reach the other end where the excitation can escape with a rate $\Gamma_{\rm trap}$.

Let us first compute the average transfer time in the Förster model. To go from site 1 to site 2 takes an average time $1/T_{\rm F}$. The total time required to perform the random walk from site 1 to site N scales as N^2, or more precisely, $N(N-1)/T_{\rm F}$. Moreover, if the probability to be at the N-th site is $1/N$ and the escape rate is $\Gamma_{\rm trap}$

we can estimate the exit time as $N/\Gamma_{\rm trap}$. Adding up the diffusion time and the exit time we have,

$$\tau_{\rm F} = \frac{N(N-1)}{2T_{\rm F}} + \frac{N}{\Gamma_{\rm trap}} = \frac{N}{\Gamma_{\rm trap}} + N(N-1)\left(\frac{6\gamma^2 + W^2}{24\Omega^2\gamma}\right), \tag{2.45}$$

which is exactly the result found by direct calculation, see Eq. (2.38). On the other hand, in the presence of an opening, the Leegwater formulas are modified by the substitution $\gamma \to \gamma + \Gamma_{\rm trap}/2$ for the transfer rate between the last two sites (since in a linear chain only site $N-1$ is connected to the N-th site where the excitation can escape). Needless to say, while for $\Gamma_{\rm trap} \ll \gamma$ the transfer rate in presence of the opening reduces to the incoherent one, for $\Gamma_{\rm trap} \approx \gamma$ the two rates are very different. In particular the rate is maximal for $\gamma + \Gamma_{\rm trap}/2 = W/\sqrt{6}$.

Thus, the (coherent) effects induced by the opening can be included in an (incoherent) model of diffusion using the Leegwater expression. We can estimate the transfer time for the quantum case in a similar way as was done above, namely:

$$\tau_{\rm L} = \frac{N}{\Gamma_{\rm trap}} + \frac{(N-1)(N-2)}{2T_{\rm F}} + \frac{N-1}{T_{\rm L}}. \tag{2.46}$$

This expression, rearranged, is the same as Eq. (2.39). From the above expression we get,

$$\tau_{\rm F} - \tau_{\rm L} = (N-1)\left(\frac{1}{T_{\rm F}} - \frac{1}{T_{\rm L}}\right). \tag{2.47}$$

This last expression is simpler to analyze: quantum transport is better than incoherent transport when $T_{\rm L} > T_{\rm F}$, from which we have:

$$\Gamma_{\rm trap} < \frac{W^2 - 6\gamma^2}{3\gamma}, \tag{2.48}$$

which can be achieved only if $W > \sqrt{6}\gamma$. Moreover for $W \gg \Omega$ and $\Gamma_{\rm trap} > \gamma$,

the optimal quantum transport is obtained for $\Gamma_{\rm trap} = \Gamma_{\rm trap}^{\rm opt} \equiv \sqrt{2/3}W - 2\gamma$ (the same value that maximizes the rate $T_{\rm L}$). We can now compare the optimal quantum transport with the optimal Förster transport obtained for $\Gamma_{\rm trap} \to \infty$. So we have:

$$\tau_{\rm F}^{\rm opt} = \frac{N(N-1)}{2T_{\rm F}}, \tag{2.49}$$

$$\tau_{\rm L}^{\rm opt} = \frac{(N-1)(N-2)}{T_{\rm F}} + \frac{N-1}{T_{\rm L}^{\rm opt}} + \frac{N}{\Gamma_{\rm trap}^{\rm opt}}, \tag{2.50}$$

and for $W \gg \gamma$, $N \gg 1$,

$$\tau_{\rm F}^{\rm opt} - \tau_{\rm L}^{\rm opt} \approx \frac{NW^2}{12\Omega^2\gamma}\,. \tag{2.51}$$

Note that that quantum enhancement due to the opening is proportional to the variance of the static disorder.

2.5 Fully connected networks

In Sec. 2.4 we saw that coherent effects can aid transport through an open linear chain of arbitrary length, as long as the static disorder is sufficiently strong relative to the dephasing rate. To demonstrate the generality of this effect, we now consider a quantum network which, in its degree of connectivity, may be considered to be at the opposite extreme from a linear chain, namely a fully connected network with equal couplings between all pairs of sites, as illustrated in Fig. 2.1 b). Specifically, the Hamiltonian $\rm H_{lin}$ (Eq. (2.1)) for the linear chain is replaced by

$$\rm H_{fc} = \sum_{i=1}^{N} \omega_i \left|i\right\rangle \left\langle i\right| + \Omega \sum_{1\le i<j\le N} \left(\left|i\right\rangle \left\langle j\right| + \left|j\right\rangle \left\langle i\right|\right)\,, \tag{2.52}$$

and the site energies ω_i are again distributed uniformly in $[-W/2, W/2]$. As before, site N is coupled to the continuum with decay rate $\Gamma_{\rm trap}$ (Eq. (2.2)). In the Förster model, then, every site is connected to every other with the incoherent rate

$T_{\rm F}$ (Eq. (2.19), where Δ is the difference between the site energies), whereas in the Leegwater approximation the transfer rates $T_{j\to N}$ and $T_{N\to j}$ are given by the modified rate $T_{\rm L}$ (Eq. (2.24)), which includes the effect of the opening. To simplify the analysis, we focus only on the regime where quantum transport enhancement is most pronounced: This occurs when the opening is comparable to the disorder strength, and the mean level spacing W/N is large compared to the dephasing rate, $\Gamma_{\rm trap}/N \sim W/N \gg \gamma \gg \Omega$. In that case we have $T_{\rm F} \sim \Omega^2\gamma/W^2$ and $T_{\rm L} \sim \Omega^2/W$, so $T_{\rm L} \gg T_{\rm F}$ and to leading order all sites are effectively coupled to site N only. In this regime, the average time to reach the sink starting from site 1 attains the N-independent value

$$\langle\tau_{\rm L}\rangle_W = \frac{3\Gamma_{\rm trap}^2 + 2W^2}{12\Omega^2\Gamma_{\rm trap}}\,. \tag{2.53}$$

We note that this expression agrees, as it must, with the linear chain result (2.39) for the case $N = 2$ in the limit $\Gamma_{\rm trap} \sim W \gg \gamma \gg \Omega$. The transfer time is minimized,

$$\langle\tau_{\rm L}\rangle_W^{\rm min} = W/\sqrt{6}\Omega^2\,, \tag{2.54}$$

when the opening strength is set to the optimal value

$$\Gamma_{\rm trap}^{\rm opt} = \sqrt{2/3}W\,. \tag{2.55}$$

The above discussion addresses the transfer time in the context of the Leegwater approximation. As in the case of the linear chain, an exact numerical evaluation of the average quantum transfer time confirms that the Leegwater approximation provides the leading contribution to the quantum transfer time in the regime of interest. The leading correction for the error takes the form

$$\langle\tau\rangle_W - \langle\tau_{\rm L}\rangle_W \approx (b'N)^2/\sqrt{\gamma W}\,, \tag{2.56}$$

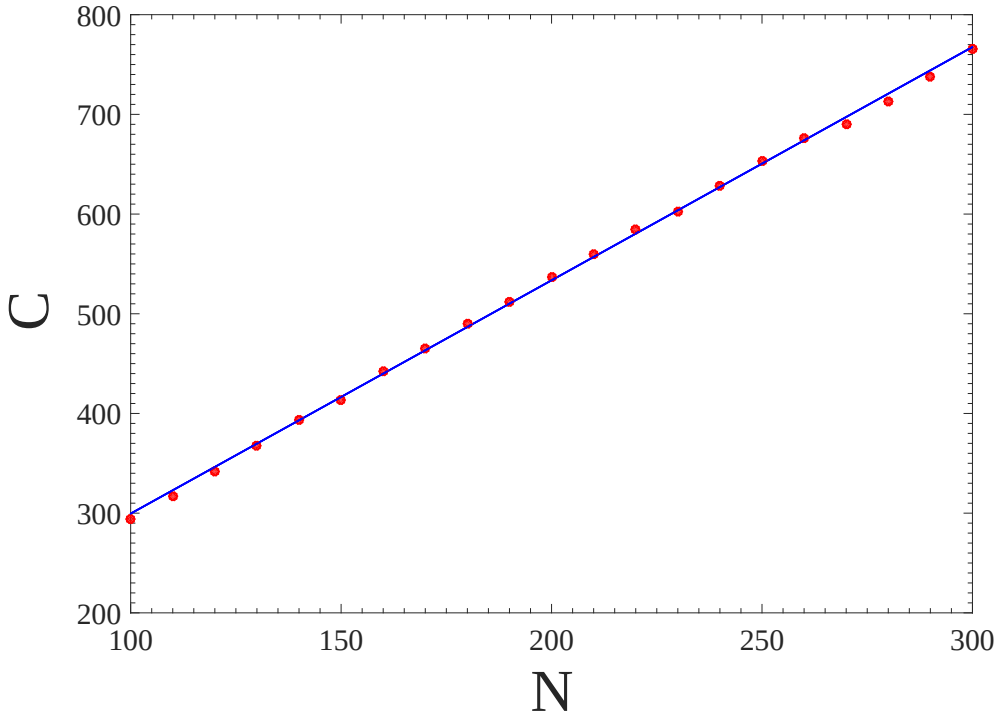

Figure 2.8: The function $C(N)$ in Eq. (2.60), which describes the N-dependence of the incoherent transfer time in the fully connected model, with a fit to $C(N) = 2.34N + 64.55$. Here $W = 5000$, $\Gamma_{\rm trap} = 6000$, and $\gamma = \Omega = 1$.

with $b' \approx 0.37$, as illustrated in Fig. 2.7, so

$$\langle \tau \rangle_W \,/\, \langle \tau_{\rm L} \rangle_W = 1 + O(N^2\Omega^2/W^{3/2}\gamma^{1/2})\,. \tag{2.57}$$

To obtain the corresponding Förster behavior, it is convenient to work in the large-N limit. The probability to jump from site i to site j is given by the Förster transition rate (2.19),

$$(T_{\rm F})_{i\to j} = \frac{2\Omega^2\gamma}{\gamma^2 + (\omega_i - \omega_j)^2}\,. \tag{2.58}$$

Now if we label the sites in order of site energy, $\omega_1 < \omega_2 < \ldots < \omega_N$, for large N we have $(\omega_i - \omega_j)^2 \approx W^2(i-j)^2/N^2$. Since we are working in the regime of very strong disorder, $W \gg N\gamma$, the transition rates simplify to $(T_{\rm F})_{i\to j} \approx 2N^2\gamma\Omega^2/W^2(i-j)^2$.

This corresponds to an $\alpha = 1$ Lévy flight (or Cauchy flight) with typical time scale $\Delta t \sim W^2/N^2\gamma\Omega^2$ for each jump; for an $\alpha = 1$ Lévy flight the average time to travel a distance n scales as n, in contrast with the n^2 scaling of the travel time for ordinary diffusion [56]. Although the initial site is not necessarily site 1 due to the site relabeling, and the site coupled to the sink is not necessarily site N, the initial and final sites are nevertheless separated by a distance of order N. Thus, total time required to travel through the system scales as $\tau \sim N\Delta t$, and we have

$$\langle \tau_{\mathrm{F}} \rangle_W \sim \frac{W^2}{N\gamma\Omega^2} \,. \tag{2.59}$$

The behavior given in Eq. (2.59) is confirmed by exact numerical calculations. Numerically we obtain an excellent fit to

$$\langle \tau_{\mathrm{F}} \rangle_W \approx \frac{W^2}{C(N)\gamma\Omega^2} \,, \tag{2.60}$$

where $C(N) \approx 2.34N + 64.55$. We note that from Eq. (2.59) or Eq. (2.60) the incoherent transfer time may appear to approach 0 in the large-N limit; however one must keep in mind that the above discussion assumes $W/N \gg \gamma$. If we increase N while holding all other system parameters fixed, we find instead that for $N > W/\gamma$, the Förster transfer time saturates at an N-independent value $\langle \tau_{\mathrm{F}} \rangle_W \sim W/\Omega^2$, comparable to the Leegwater prediction. In this limit there is no significant quantum enhancement of transport.

Returning to the regime of primary interest, $W/N \gg \gamma \gg \Omega$ and comparing Eqs. (2.54) and (2.59) we find a very strong coherent enhancement of transport in the fully connected network. Specifically, when the opening strength Γ_{trap} is of order $\Gamma_{\mathrm{trap}}^{\mathrm{opt}}$, the ratio of the Leegwater (or, equivalently, quantum) transfer time to the

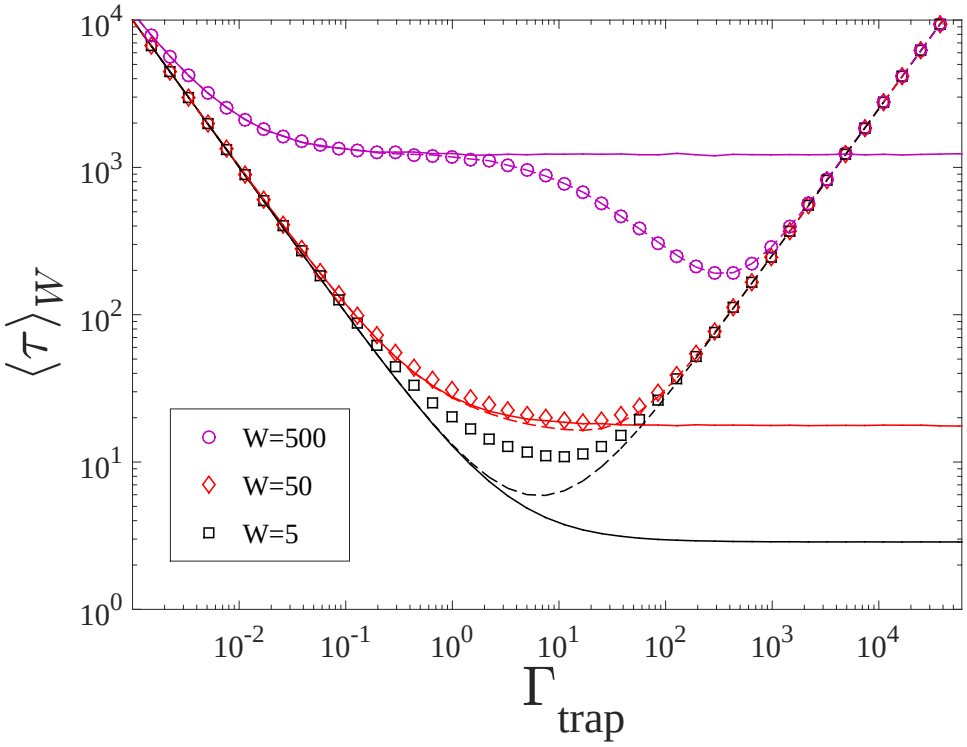

Figure 2.9: Comparison among Förster (solid curves), Leegwater (dashed curves), and quantum (symbols) average transfer times for a fully connected network with $N = 10$ sites and several values of the disorder strength W. Here we fix $\Omega = 1$ and $\gamma = 5$.

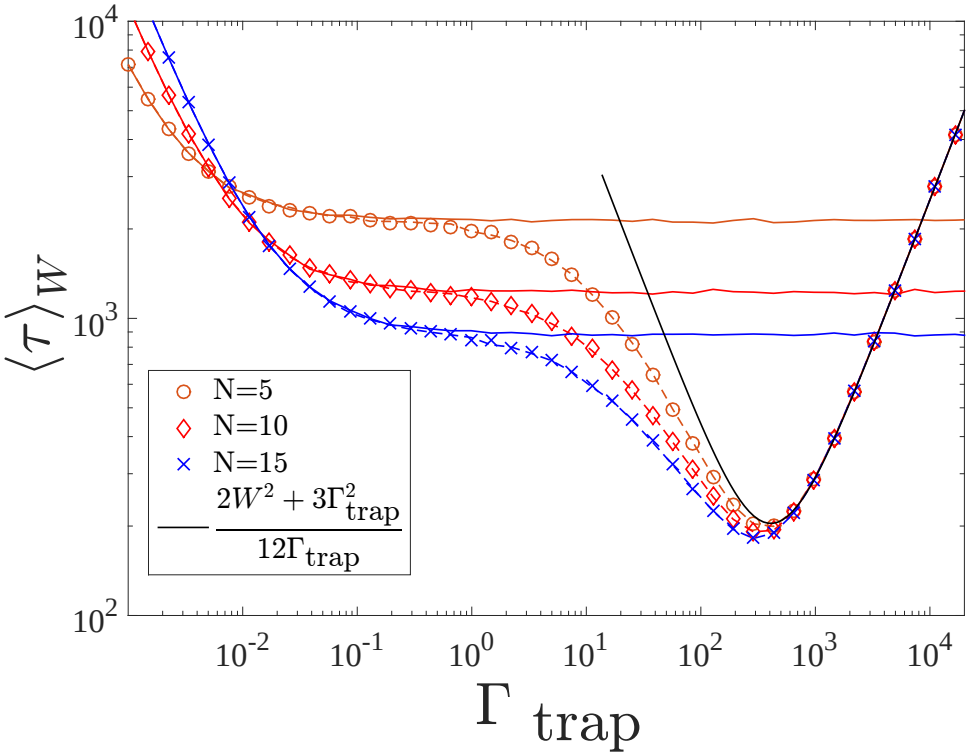

Figure 2.10: Comparison among Förster (solid curves), Leegwater (dashed curves), and quantum (symbols) average transfer times for fully connected networks of several sizes N. Here we fix $W = 500$, $\gamma = 5$, and $\Omega = 1$. The analytic result (2.53) describes the behavior of the Leegwater and quantum ensemble-averaged transfer time in the region of strongest quantum transport enhancement.

incoherent time scales as

$$\frac{\langle \tau_{\rm L} \rangle_W}{\langle \tau_{\rm F} \rangle_W} \sim \frac{\gamma}{W/N} \ll 1\,. \tag{2.61}$$

We note that the condition $W/N \gg \gamma$ which allows quantum mechanics to significantly aid transport in the fully connected network corresponds precisely to the starting assumption underlying the calculations in this Section.

The results in Fig. 2.9 confirm that a very strong quantum enhancement of transport occurs in a fully connected network of $N = 10$ sites for $W \gg N\gamma$ (see the data for $W = 500$ in the figure). Optimal quantum transport appears at the value of the opening given by $\Gamma_{\rm trap}^{\rm opt}$. We also observe excellent agreement between

the exact quantum calculation and the Leegwater approximation in this regime. The Leegwater approximation breaks down for larger relative values of the dephasing rate γ (e.g. $W = \gamma = 5$), but in this range of parameters quantum effects hinder rather than aid transport. Fig. 2.10 illustrates that in the region of strongest quantum transport enhancement ($\Gamma_{\rm trap} \sim \Gamma_{\rm trap}^{\rm opt}$), the quantum behavior is indeed approximately N-independent and is well described by the analytic expression given in Eq. (2.53).

2.6 The FMO complex

The FMO photosynthetic complex has received a lot of attention in recent years as an example of a biological system that exhibits quantum coherence effects even at room temperature [5, 10, 11]. In particular, the interplay of opening and noise in the FMO complex has been already analyzed in Ref. [31], where it was shown that even at room temperature, the superradiance transition is able to enhance transport. Here we examine opening-assisted quantum transport enhancement in the FMO complex and observe that the same behavior obtains here as in the linear chain and fully connected model systems considered in the previous sections.

Each subunit of the FMO complex contains seven chromophores, and may be modeled by the tight-binding Hamiltonian

$$\mathrm{H_{FMO}} = \begin{pmatrix} 200 & -87.7 & 5.5 & -5.9 & 6.7 & -13.7 & -9.9 \\ -87.7 & 320 & 30.8 & 8.2 & 0.7 & 11.8 & 4.3 \\ 5.5 & 30.8 & 0 & -53.5 & -2.2 & -9.6 & 6 \\ -5.9 & 8.2 & -53.5 & 110 & -70.7 & -17 & -63.3 \\ 6.7 & 0.7 & -2.2 & -70.7 & 270 & 81.1 & -1.3 \\ -13.7 & 11.8 & -9.6 & -17 & 81.1 & 420 & 39.7 \\ -9.9 & 4.3 & 6 & -63.3 & -1.3 & 39.7 & 230 \end{pmatrix} \mathrm{cm}^{-1}, \quad (2.62)$$

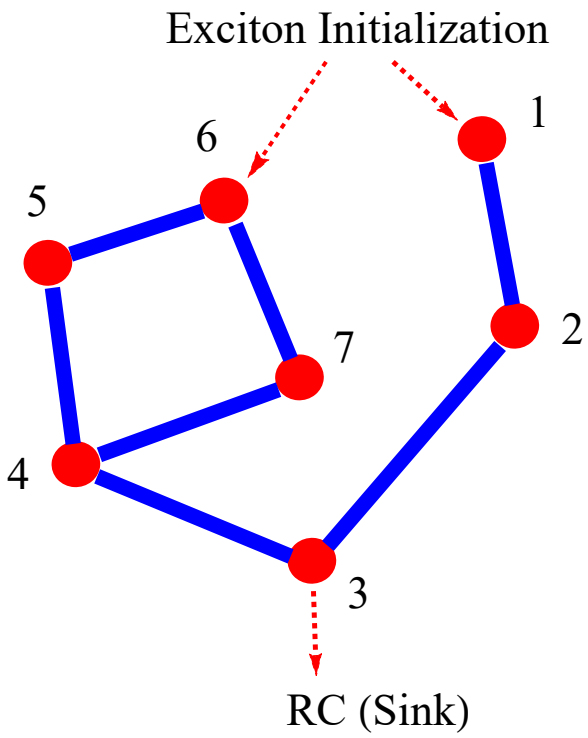

Figure 2.11: A schematic illustration of the FMO Hamiltonian (2.62), with each bond indicating a coupling matrix element of magnitude at least 20 cm^{-1}.

in units where $hc = 1$. We notice that the connectivity between the sites is greater than that in a linear chain, but the inter-site couplings are very non-uniform. Thus, this realistic system may be considered to be intermediate between a chain and a fully connected network. A schematic illustration of the Hamiltonian $\mathrm{H_{FMO}}$, where only off-diagonal elements of magnitude greater than 20 cm^{-1} are indicated by bonds, appears in Fig. 2.11 (but in all calculations below we employ the full Hamiltonian given in Eq. (2.62)).

Since incident photons are believed to create excitations on sites 1 and 6 of the FMO complex [27], we take the initial state of the system to be

$$\rho(0) = \frac{1}{2}\left(|1\rangle\langle 1| + |6\rangle\langle 6|\right) . \tag{2.63}$$

Site 3 is coupled to the reaction center, which serves as the sink for the FMO complex, with decay rate Γ_{trap}. Additionally, an excitation on any site may decay through exciton recombination with rate $\Gamma_{\mathrm{fl}} = (1\ \mathrm{ns})^{-1} = 0.033\ \mathrm{cm}^{-1}$ [27, 29], but this slow decay has a negligible effect on the transfer time τ, as discussed in Sec. 2.2.

The transfer time calculation as a function of reaction center coupling Γ_{trap} is shown in Fig. 2.12 (see also Ref. [31]). For the FMO system, the dephasing rate γ is related to the temperature by the relation $\gamma = 0.52c(T/\mathrm{K})\ \mathrm{cm}^{-1}$, where T/K is the temperature in Kelvin units [10], and results for three values of the temperature (or equivalently, dephasing rate) are shown in the figure. Notably, strong opening-assisted quantum enhancement of transport is seen not only at liquid nitrogen temperature (77 K) but also at room temperature (300 K) where the quantum transfer is up to a factor of 2 faster than that obtained by an incoherent calculation. We also see good agreement between the exact quantum calculation and the Leegwater approximation at room temperature. For comparison, we show an example at very high temperature (1500 K), where the quantum transport enhancement is almost absent.

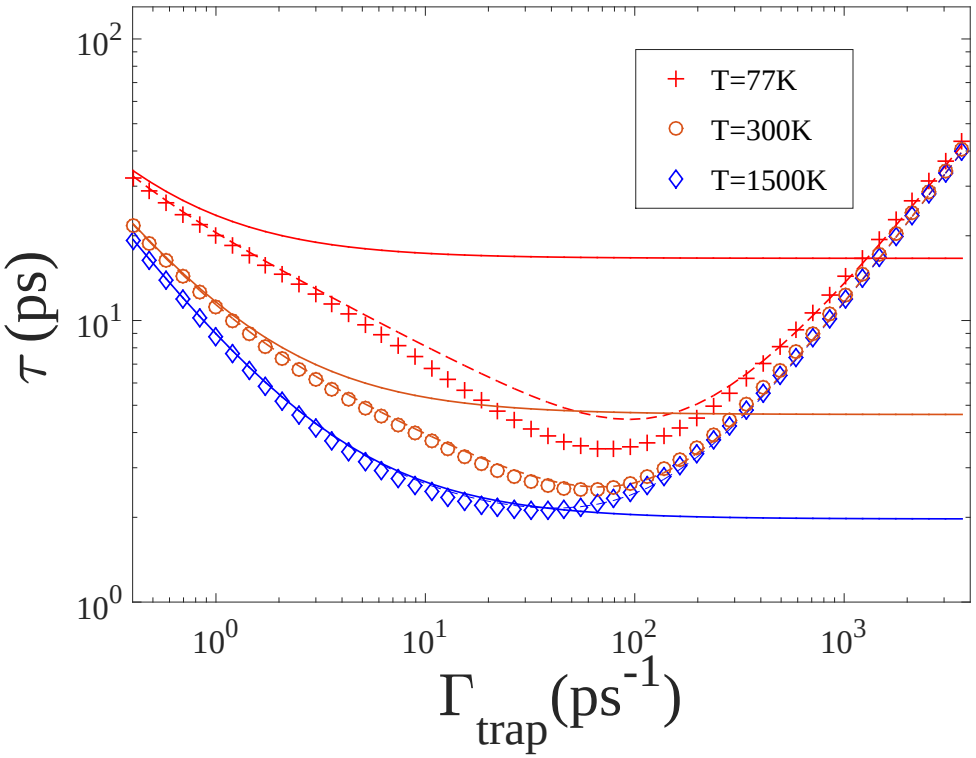

Figure 2.12: The average transfer time for the FMO system is shown as a function of coupling Γ_{trap} between site 3 and the reaction center, at three different temperatures. The Förster, Leegwater, and quantum transfer times are represented by solid curves, dashed curves, and symbols, respectively.

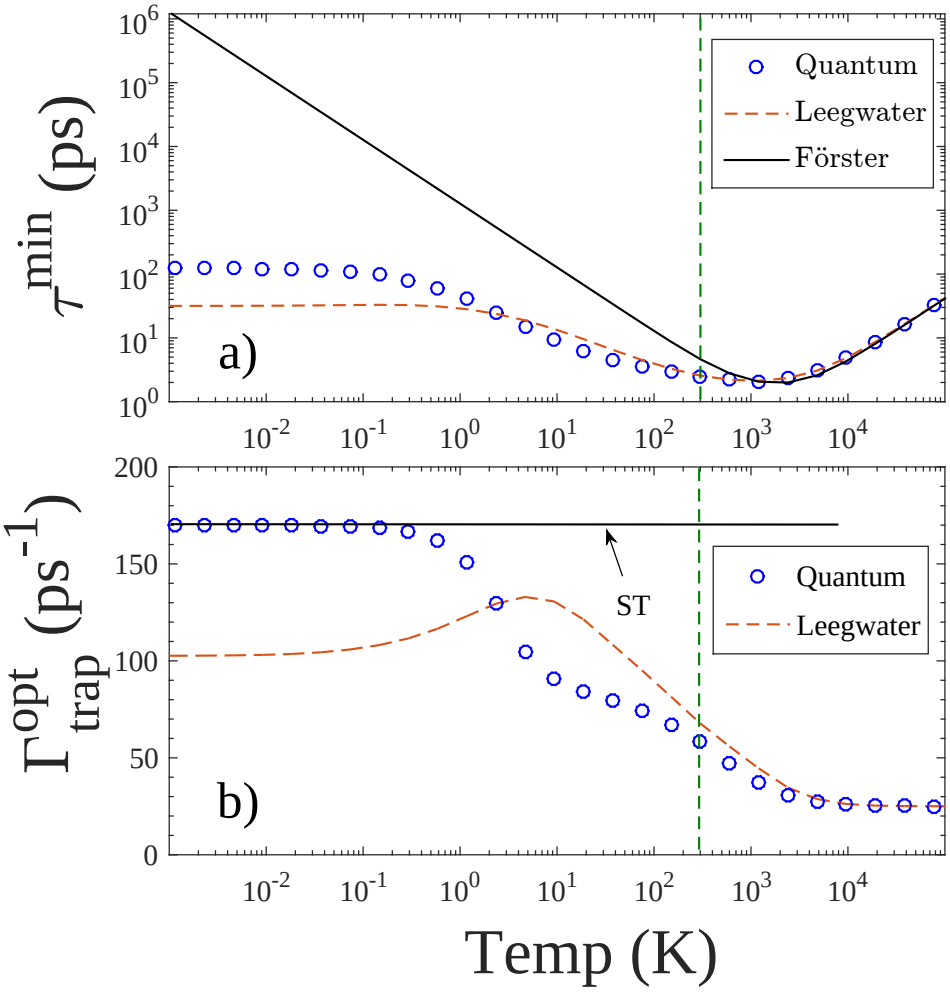

Figure 2.13: a) The minimal transfer time through the FMO complex (optimizing over the coupling Γ_{trap} to the reaction center) is shown as a function of temperature, for the quantum, Leegwater, and incoherent (Förster) calculations. b) The optimal coupling $\Gamma_{\text{trap}}^{\text{opt}}$ is shown as a function of temperature, in the full quantum calculation and in the Leegwater approximation. In the incoherent model, the optimal coupling is always $\Gamma_{\text{trap}}^{\text{opt}} = \infty$. The horizontal solid line indicates the location of the superradiance transition at zero temperature. In both panels, the dashed vertical line indicates room temperature, $T = 300$ K.

Although the "disorder" in the FMO Hamiltonian is fixed, for the purpose of estimating the relevant energy, time, and temperature scales we may analogize this Hamiltonian to one drawn from a disordered ensemble. The variance of the site energies $(H_{\mathrm{FMO}})_{ii}$ is $\sigma^2 = (128\ \mathrm{cm}^{-1})^2$, which corresponds to $W = 443\ \mathrm{cm}^{-1}$. Then we see that room temperature, $T = 300$ K or $\gamma = 156\ \mathrm{cm}^{-1}$, actually corresponds to a marginal case where "static disorder" W and dephasing rate γ are comparable. At even higher (biologically unrealistic) temperatures, e.g. $T = 1500$ K, we have $\gamma = 780\ \mathrm{cm}^{-1} \gg W$, and quantum enhancement of transport is absent, as expected. At lower (also unrealistic) temperatures, e.g. $T = 77$ K, we have $\gamma = 40\ \mathrm{cm}^{-1} \ll W$, corresponding to a regime where opening-assisted quantum transport enhancement is most pronounced. The crossover between the low-temperature regime where coherent effects strongly aid transport and the high-temperature regime where coherent effects provide no advantage is studied quantitatively in Fig. 2.13 a), where the minimal quantum, Leegwater, and Förster transfer times are shown at each temperature (optimizing in each case over the opening strength Γ_{trap}).

Similarly we may estimate the optimal strength of the opening at low temperature using the formula $\Gamma_{\mathrm{trap}}^{\mathrm{opt}} = \sqrt{2/3}W$ obtained for the linear chain and fully connected network at small dephasing and $\Omega \to 0$ (see Eqs. (2.42) and (2.55)). This gives $\Gamma_{\mathrm{trap}}^{\mathrm{opt}} = \sqrt{2/3}(2\pi c)(443\ \mathrm{cm}^{-1}) = 68\ \mathrm{ps}^{-1}$, which is in reasonable qualitative agreement with the location of the Leegwater and quantum minima at liquid nitrogen temperature in Fig. 2.12. (The above formula is valid for inter-site couping $\Omega \to 0$, and therefore is expected to underestimate the true value of $\Gamma_{\mathrm{trap}}^{\mathrm{opt}}$). As expected from our study of the two-site model and linear chain (see Eqs. (2.29) and (2.42)), the location of the minimum shifts to smaller coupling Γ_{trap} as the temperature (dephasing) increases. The full dependence of the optimal opening strength on temperature in the exact quantum calculation as well as in the Leegwater approximation are shown

in detail in Fig. 2.13 b).

2.7 Conclusions

We have analyzed the role of the opening in enhancing coherent transport in the presence of both disorder and dephasing. The effect is investigated in several paradigmatic models, including a two-site system, a linear chain of arbitrary length, and a fully connected network of arbitrary size. For the two-site model, fully analytical expressions exist for both the incoherent and quantum average transfer times, and therefore the regime in which coherent effects aid transport as well as the optimal opening strength at which the effect is maximized may also be obtained analytically. For the linear chain and fully connected network, we are able to find analytical expressions in the semiclassical regime, where dephasing is much stronger than the hopping coupling between the sites. In this case quantum transport can be described with an incoherent master equation where the rates incorporate the effect of the opening, as suggested by Leegwater. Again, the different efficiencies of quantum and incoherent transport can be compared to identify the regime in which coherent effects aid transport. In this regime we find the optimal opening able to maximize transport efficiency. We see very generally that quantum transport can outperform incoherent transport even at high rates of dephasing (or dynamic disorder), as long as the static disorder strength is sufficiently large. The optimal strength of the opening grows linearly with the disorder strength. An analysis of the FMO natural photosynthetic complex confirms the role of the opening in enhancing coherent transport in realistic models, even at room temperature.

Chapter 3

Optimal Dephasing Rate for Exciton Energy Transfer in Disordered Linear Chains

3.1 Introduction

The optimization of excitonic and charge transport is a central problem for building quantum devices with different functions, including sensing, computing, and light-harvesting. Theoretically, the problem is challenging due to the interplay of different environments. Under low light intensity, in many natural photosynthetic systems or in ultra-precise photon sensors, the single-excitation approximation is usually valid. In this case the system is equivalent to a quantum network where one excitation can hop from site to site [7, 16, 17, 20, 21]. For a realistic description of the quantum transport problem, however, one has to consider not only the quantum coherent evolution, but also the coupling to multiple environments. These include an external acceptor system, where the excitation can be donated and trapped, and the coupling with a phonon bath, which can induce different types of disorder: Static disorder (position dependent but time independent) and noise (time-dependent dis-

order).

From the study of natural photosynthetic complexes [5, 10, 11, 12, 13] has emerged the idea that in the optimal transport regime the energy scale of the coherent internal coupling is the same as the scale of the coupling to the external environment. This leaves little room for perturbative simplifications, and the analysis of the interplay of internal and external coupling must be carried out with care. Another important issue is related to finite-size effects. Indeed, many relevant natural and artificial quantum network are made of a few two-level systems. For instance, the FMO complex in green sulphur bacteria, which is thought to have the role of a quantum wire, is made of eight bacterioclorophyll a molecules [5]. The LHI and LHII [4, 18] complexes in purple bacteria are made of 32 and 16-18 molecules, respectively. So the infinite system size limit also cannot be used to simplify the problem of exciton transport.

In Chapter 2 [57], exciton transport in different quantum networks was considered in the semiclassical limit, focusing on the role of the coupling to the external acceptor system, which can induce coherent effects such as supertransfer of the excitation. Here we focus our attention on the case of a linear chain of sites with nearest-neighbor coherent hopping of the excitation. Without invoking the semiclassical limit (where dephasing is large with respect to the coherent nearest-neighbor coupling), we analyze here the problem of optimal transport. We focus on the role of dephasing noise (time-dependent perturbations) in enhancing transport. It is well known that noise is not always detrimental to transport and in some situations may enhance efficiency [27, 28, 29].

Several works in the literature aim to understand the parameter regime in which transport efficiency is maximized. Some general principles that might be used as a guide to understand how optimal transport can be achieved have been proposed:

Enhanced noise assisted transport [27, 29], the Goldilocks principle [30], and superradiance in transport [31].

Specifically, transport in one-dimensional chains has been studied in depth recently in the context of closed systems [7, 30, 47]. The results obtained for a one-dimensional chain of length N can be summarized as follows: While for zero static disorder, dephasing never helps transport, in the presence of static disorder there may be a nonzero optimal dephasing $\gamma^{\rm opt}$ for transport. If we call W the strength of static disorder and Ω the coherent nearest-neighbor hopping, two main regimes have been identified previously. *i*) For $W \gg \Omega$, where the localization length $\xi \leq 1$, we have $\gamma^{\rm opt} \propto W$, independent of Ω. *ii*) For $\Omega/\sqrt{N} \ll W \ll \Omega$, where $1 \ll \xi \ll N$, we have nonlinear dependence on the disorder strength, $\gamma^{\rm opt} \propto W^2/\Omega$. Note that in both regimes the optimal dephasing is independent of N. On the other hand, the role of the coupling to the acceptor systems and the value of the critical disorder needed for dephasing to help transport has not been investigated fully.

Here we estimate semi-analytically the value of the critical minimal disorder $W^{\rm cr}$ above which dephasing noise aids transport in a one-dimensional chain with nearest-neighbor hopping. Contrary to what one might expect, dephasing helps transport not only in the localized regime, when $\xi < N$, but also in the deep ballistic regime, when $\xi \gg N$, due to a competition between the effects of static and dynamic disorder on transport. Another important point is that the critical disorder $W^{\rm cr}$ depends on the coupling to the acceptor system. We also find that in the deep ballistic regime the optimal dephasing $\gamma^{\rm opt}$ is not size-independent but decreases with the chain length N, up to a length determined by $N \approx \xi$, where the optimal dephasing becomes independent of N.

The chapter is organized as follows: In Sec. 3.2 we define the transport model, including the effects of dephasing, disorder, and coupling to the acceptor system. In

Sec. 3.3 we obtain analytic and numerical results for the simplest finite-length chains: $N = 2$ and $N = 3$. Then in Sec. 3.4 we examine the behavior for general N and obtain two separate delocalized regimes where the optimal dephasing displays N-dependent behavior. We summarize our results in Sec. 3.5.

3.2 Model description

We study the optimal dephasing for exciton energy transfer (EET) in linear chains in the presence of disorder. The time evolution of the closed system can be expressed as

$$i\hbar\dot{\rho}(t) = [H_{\text{sys}}, \rho(t)] \ . \tag{3.1}$$

The system Hamiltonian is usually expressed in the site basis as

$$H_{\text{sys}} = \sum_{i=1}^{N} \hbar\omega_i \left|i\right\rangle \left\langle i\right| + \sum_{l,m}^{N} J_{lm} \left|l\right\rangle \left\langle m\right| , \tag{3.2}$$

where we work in the single-exciton regime, with state $|i\rangle$ representing an excitation on site i only, $\hbar\omega_i$ are the site energies, and J_{lm} are the inter-site couplings. EET systems are open and connect to acceptor systems, which serve as sinks. Here, we take site N to be connected to the sink. The effects of the opening are conventionally addressed by augmenting the system Hamiltonian with a non-Hermitian term:

$$-i\mathcal{W} = -i\frac{\Gamma_{\text{trap}}}{2} \left|N\right\rangle \left\langle N\right| . \tag{3.3}$$

Consequently the time evolution of the reduced density matrix ρ of the system will be described as

$$i\hbar\dot{\rho} = [H_{\text{sys}}, \rho] - i\left\{\mathcal{W}, \rho\right\} . \tag{3.4}$$

EET systems are subject to background noise, which results in dephasing. We

use the Haken-Strobl-Reineker (HSR) model [53] to describe the dephasing behavior of the system as

$$\dot{\rho}_{ij} = -\gamma(1 - \delta_{ij})\rho_{ij}. \tag{3.5}$$

Finally, the full system dynamics can be expressed as

$$\dot{\rho}_{ij} = -\frac{i}{\hbar}(H_{\text{eff}}\,\rho - \rho\,H_{\text{eff}}^{\dagger})_{ij} - \gamma(1 - \delta_{ij})\rho_{ij}, \tag{3.6}$$

where $H_{\text{eff}} = H_{\text{sys}} - i\mathcal{W}$ is the effective non-Hermitian Hamiltonian of the system.

The efficiency of EET can be measured by the total population trapped by the sink [29, 48]

$$\eta = \Gamma_{\text{trap}} \int_0^\infty \rho_{NN}(t)\,dt\,, \tag{3.7}$$

and the average transfer time to the sink [27]

$$\tau = \Gamma_{\text{trap}} \int_0^\infty t\,\rho_{NN}(t)\,dt/\eta\,. \tag{3.8}$$

In this work, we neglect the fluorescence effect of excitons so that $\eta = 1$, and the average transfer time τ reduces to

$$\tau = \Gamma_{\text{trap}} \int_0^\infty t\rho_{NN}(t)\,dt\,. \tag{3.9}$$

We note that if decay via fluorescence is explicitly included, we have $\eta = 1/\left(1 + \Gamma_{\text{fl}}\tau\right)$ for small fluorescence rate Γ_{fl} [54], and thus minimizing the transfer time τ is equivalent to maximizing the efficiency η.

Finally, if the master equation (3.6) is expressed in terms of the Liouville superoperator $\mathcal{L}$

$$\dot{\rho}(t) = -\mathcal{L}\rho(t)\,, \tag{3.10}$$

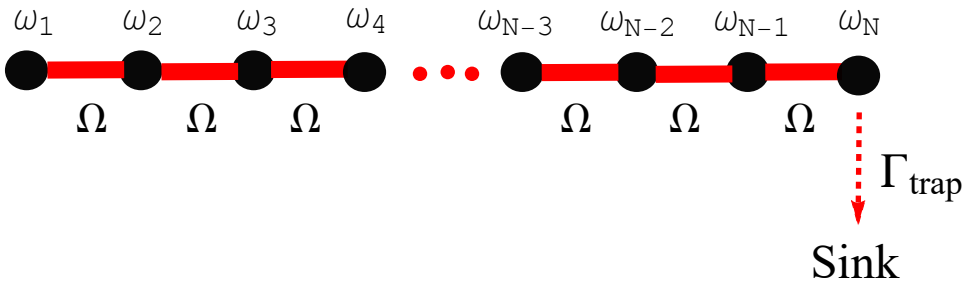

Figure 3.1: A schematic of a disordered linear chain that is coupled to a sink.

we have

$$\tau = \frac{\Gamma_{\text{trap}}}{\eta}(\mathcal{L}^{-2}\rho(0))_{\text{NN}}\,. \tag{3.11}$$

In reality EET systems are often disordered. Here we consider Anderson-type disorder, with the site energies ω_i uniformly and independently distributed in the interval $[-W/2, W/2]$, where W denotes the disorder strength. The disorder-averaged transfer time is then calculated as

$$\langle\tau\rangle_W = \frac{1}{W^n}\int_{-W/2}^{W/2}\dots\int_{-W/2}^{W/2}\tau(\omega_1,\omega_2,\dots,\omega_n)\,d\omega_1\,d\omega_2\dots d\omega_n. \tag{3.12}$$

For linear chains with uniform couplings, J_{lm} takes the form $\text{J}_{\text{lm}} = \delta_{|l-m|,1}\Omega$, where Ω is the coupling constant. Furthermore, in the following we choose the initial state to be $\rho(0) = |1\rangle\langle 1|$ and set $\hbar = 1$ for simplicity.

3.3 Optimal dephasing for 2- and 3-site chains

3.3.1 Explicit solution and optimal dephasing for the 2-site model

For a two-site chain ($N = 2$), we have obtained in Ref. [57] a simple analytic form for τ by solving Eq. (3.11) exactly with $\rho(0) = |1\rangle\langle 1|$:

$$\tau_2 = \frac{1}{2\Omega^2}\left(\frac{4\Omega^2}{\Gamma_{\rm trap}} + \gamma + \frac{\Gamma_{\rm trap}}{2} + \frac{(\omega_1 - \omega_2)^2}{\gamma + \frac{\Gamma_{\rm trap}}{2}}\right), \tag{3.13}$$

where the subscript 2 here and in the following denotes the chain length. After integration over disorder using Eq. (3.12), Eq. (3.13) becomes

$$\langle\tau_2\rangle_W = \frac{1}{2\Omega^2}\left(\frac{4\Omega^2}{\Gamma_{\rm trap}} + \gamma + \frac{\Gamma_{\rm trap}}{2} + \frac{W^2}{6(\gamma + \frac{\Gamma_{\rm trap}}{2})}\right). \tag{3.14}$$

We see from Eq. (3.14) that the average transfer time behaves monotonically with static disorder strength W, i.e., increasing disorder always slows down transport. On the other hand, there is a complex interplay between static disorder W and dephasing γ, and this interplay depends in turn on the strength of the opening $\Gamma_{\rm trap}$. In particular, $\langle\tau_2\rangle_W$ has a minimum in γ when $W > W_2^{\rm cr}$, where

$$W_2^{\rm cr} = \sqrt{6}\Gamma_{\rm trap}/2 \tag{3.15}$$

is the critical strength of disorder for a given degree of openness. Thus, dephasing can aid transport when disorder is sufficiently strong, $W > W_2^{\rm cr}$, and dephasing will always retard transport when $W < W_2^{\rm cr}$. In the regime $W > W_2^{\rm cr}$, the optimal rate

of dephasing is given exactly by

$$\gamma_2^{\rm opt} = \frac{W}{\sqrt{6}} - \frac{\Gamma_{\rm trap}}{2} = \frac{W - W_2^{\rm cr}}{\sqrt{6}}\,. \tag{3.16}$$

3.3.2 The 3-site chain – symmetry between large and small opening

For a chain of length $N = 3$, the exact transfer time τ_3 may be written down explicitly for a given realization of the disorder, for any dephasing rate and any coupling strength to the sink. The result, shown in Eq. (A.1) in Appendix A, is unwieldy to work with analytically except in limiting cases; however it is easy to perform numerically the disorder integration given by Eq. (3.12). At first glance, the behavior is qualitatively similar to that of the $N = 2$ chain, as illustrated in Fig. 3.2. At fixed $\Omega = 1$ and weak disorder (small W), the transfer time τ_3 increases monotonically with dephasing rate γ, but as disorder increases, a minimum in γ appears and grows. The critical disorder in this case is seen numerically to be $W_3^{\rm cr} \approx 1$ for both $\Gamma_{\rm trap} = 1$ and $\Gamma_{\rm trap} = 10$.

In Fig. 3.3, for each value of the opening $\Gamma_{\rm trap}$ we calculate the ensemble-averaged transfer time $\langle\tau_3\rangle_W$ as a function of dephasing γ and disorder W, and obtain the disorder value $W_3^{\rm cr}$ at which τ_3 develops a minimum as a function of γ. Looking more closely at Fig. 3.3, we find an important qualitative difference in the system's behavior as compared with the 2-site case. For the 2-site chain, the critical disorder is always proportional to the opening strength, $W_2^{\rm cr} = \sqrt{6}\Gamma_{\rm trap}/2$, regardless of the value of Ω. Now for the 3-site chain, the critical disorder is again proportional to $\Gamma_{\rm trap}$ for small opening, but for large opening the critical disorder *decreases* with the opening strength. (More precisely, we have $W_3^{\rm cr} = \Gamma_{\rm trap}$ for $\Gamma_{\rm trap} \ll \Omega$ and $W_3^{\rm cr} = 6\sqrt{2}\Omega^2/\Gamma_{\rm trap}$ for $\Gamma_{\rm trap} \gg \Omega$, as will be obtained analytically below.)

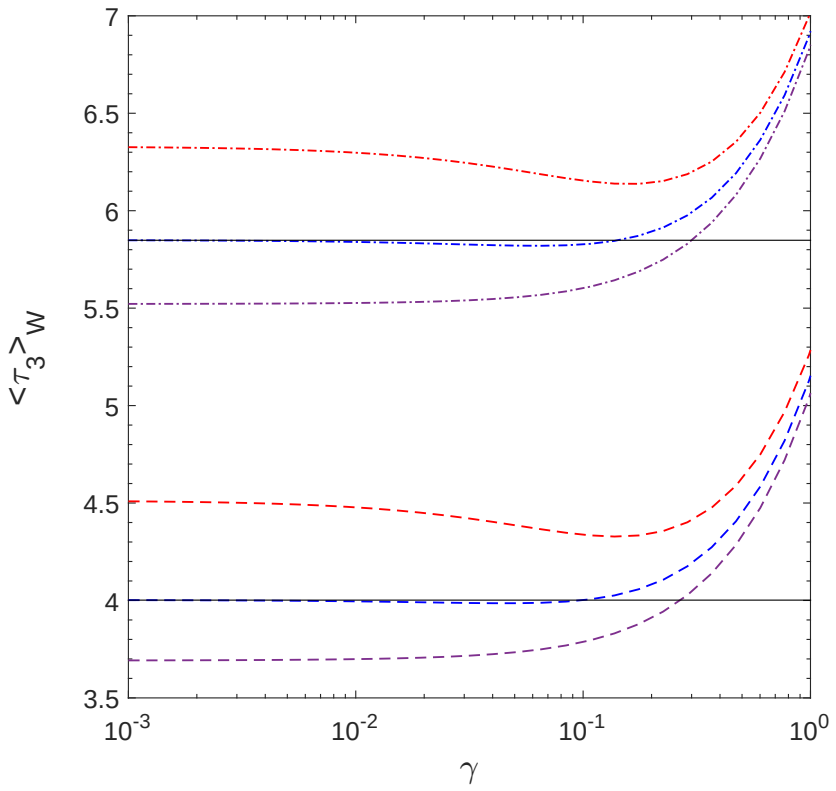

Figure 3.2: Plot of the average transfer time $\langle \tau_3 \rangle_W$ as a function of dephasing rate γ for a 3-site chain. Here we fix inter-site coupling $\Omega = 1$ while varying the opening Γ_{trap} and disorder strength W. The three dashed curves are for opening $\Gamma_{\text{trap}} = 1$, and the three dot-dashed curves are for opening $\Gamma_{\text{trap}} = 10$; within each group from top to bottom we have $W = 1.5$, 1.1, and 0.7. Physically, the presence of a minimum for $W > 1$ indicates that appropriate dephasing can enhance the transport.

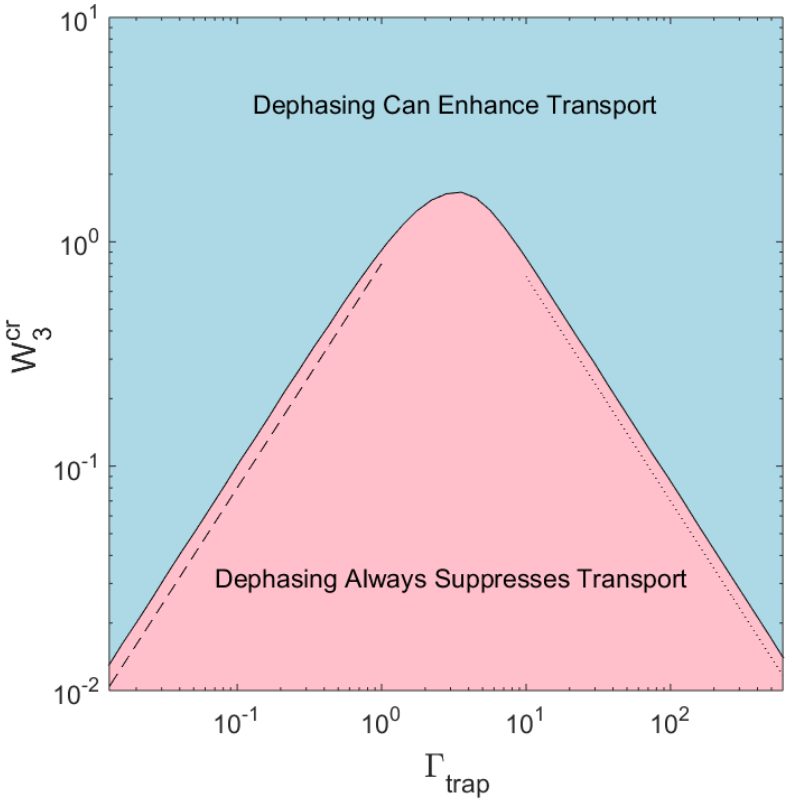

Figure 3.3: Plot of critical disorder strength W_3^{cr} as a function of opening Γ_{trap} in a 3-site chain. The curve separates two transport regimes. In the upper region of the phase diagram (light blue), dephasing can enhance transport while in the lower the lower region (pink), dephasing always suppresses transport. The straight lines of slope +1 and -1 indicate the scaling for small and large opening Γ_{trap}, respectively. Here we fix units where $\Omega = 1$.

The symmetry between large and small opening is related to the superradiance transition in open quantum systems, where for sufficiently large opening a segregation of resonances into superradiant states (strongly coupled to the sink) and subradiant states (trapped away from the sink) occurs, with the result that escape to the sink is suppressed [9, 22, 33, 34, 35, 36]. Transport to the sink in the clean quantum system is maximized at the superradiance transition. In the case of the clean $N-$site chain (with no disorder or dephasing), the transfer time is given by

$$\tau = \frac{N}{\Gamma_{\text{trap}}} + \frac{(N-1)\Gamma_{\text{trap}}}{4\Omega^2}\,, \tag{3.17}$$

see Ref. [57], and thus transport to the sink is optimized at $\Gamma_{\text{trap}} = 2\sqrt{N/(N-1)}\Omega$, or $\Gamma_{\text{trap}} = \sqrt{6}\Omega$ for $N = 3$.

Analytics for small opening

We now obtain analytically the critical disorder for the 3-site chain. We break up the problem into two regimes, starting with the regime of weak opening: $\Gamma_{\text{trap}} \ll \Omega$. After expanding τ_3 from Appendix A in powers of Ω^{-1} assuming Ω is large compared to all other energy scales in the problem, and integrating the expanded expression over disorder using Eq. (3.12), we obtain

$$\langle \tau_3 \rangle_W = \frac{3}{\Gamma_{\text{trap}}} + \Omega^{-2}\left(\frac{3\gamma}{2} + \frac{\Gamma_{\text{trap}}}{2} - \frac{W^2}{12\,(2\gamma+\Gamma_{\text{trap}})} + \frac{5W^2}{12\,(4\gamma+\Gamma_{\text{trap}})}\right) + O\left(\Omega^{-4}\right). \tag{3.18}$$

Differentiating $\langle \tau_3 \rangle_W$ with respect to γ, and neglecting $O(\Omega^{-4})$ terms, we find

$$\frac{\partial \langle \tau_3 \rangle_W}{\partial \gamma} \approx \frac{1}{12\Omega^2}\left[18 + W^2\left(\frac{2}{(2\gamma+\Gamma_{\text{trap}})^{\,2}} - \frac{20}{(4\gamma+\Gamma_{\text{trap}})^2}\right)\right]. \tag{3.19}$$

Now $\frac{2}{(2\gamma+\Gamma_{\text{trap}})^2} - \frac{20}{(4\gamma+\Gamma_{\text{trap}})^2}$ is always negative for non-negative γ and Γ_{trap}. Furthermore, the quantity in square brackets in Eq. (3.19) increases monotonically from

$18(1 - W^2/\Gamma_{\rm trap}^2)$ to 18 as γ increases from 0 to ∞. Thus for $W < \Gamma_{\rm trap}$, Eq. (3.19) is always positive, and dephasing always retards transport. For $W > \Gamma_{\rm trap}$, on the other hand, Eq. (3.19) increases monotonically in γ from below 0 to above 0, i.e., the mean transfer time $\langle \tau_3 \rangle_W$ exhibits a minimum as a function of γ. Thus, the critical disorder strength for weak opening is given by

$$W_3^{\rm cr} = \Gamma_{\rm trap}\,. \tag{3.20}$$

What about the optimal dephasing $\gamma_3^{\rm opt}$? As a function of disorder strength W when $W > W_3^{\rm cr}$, this is given in general by the solution of a quartic equation. Nevertheless, three relatively simple regimes may be distinguished.

(i) For weak disorder only slightly above the critical value, $0 < W - W^{\rm cr} \ll W^{\rm cr}$, we may expand Eq. (3.19) and obtain $\gamma_3^{\rm opt} \approx \frac{9}{38}(W - W_3^{\rm cr})$.

(ii) For moderate disorder, $W^{\rm cr} \ll W \ll \Omega$, $\gamma^{\rm opt}$ will be large compared to $W_3^{\rm cr} = \Gamma_{\rm trap}$, and thus we may take $\gamma \gg \Gamma_{\rm trap}$ in Eq. (3.19). We then have $\gamma_3^{\rm opt} \approx W/2\sqrt{6}$.

(iii) Finally, one may consider the behavior for strong disorder, $W_3^{\rm cr} \ll \Omega \ll W$. This is outside the range of validity of the above derivation, since Ω is no longer the largest energy scale. In this parameter regime, to be discussed further in Sec. 3.4.2, the optimal dephasing rate converges to the N-independent form $\gamma^{\rm opt} \approx W/\sqrt{6}$.

Interestingly, in each of the three ranges of the disorder strength W, the optimal dephasing rate $\gamma_3^{\rm opt}$ grows linearly with W, but the coefficient is different in each case. In Sec. 3.4.2, we will see that each of the three regimes identified here for $N = 3$ has a counterpart at large N, but each is associated with a different scaling with system size N.

Analytics for large opening

Now we consider the strong opening scenario, $\Gamma_{\rm trap} \gg \Omega$. As far as the scaling analysis is concerned, a large opening can be thought as a small opening with the effective small opening strength $\Gamma'_{\rm trap} = \Omega^2/\Gamma_{\rm trap}$. So starting from the exact expression for τ_3 in Appendix A, we may change variables from $\Gamma_{\rm trap}$ to $\Gamma'_{\rm trap}$, and expand τ_3 assuming Ω is very large (compared to all ω_i, γ, and $\Gamma'_{\rm trap}$). Integrating over disorder, we obtain

$$\langle \tau_3 \rangle'_W = \frac{1}{2\Gamma'_{\rm trap}} + \frac{18\left(\gamma + 2\Gamma'_{\rm trap}\right) + \frac{W^2}{\gamma + 2\Gamma'_{\rm trap}}}{\Omega^2} + O\left(\frac{1}{\Omega^4}\right). \tag{3.21}$$

Straightforward algebra now shows that for strong opening the critical disorder is given by

$$W_3^{\rm cr} = 6\sqrt{2}\Gamma'_{\rm trap} = 6\sqrt{2}\Omega^2/\Gamma_{\rm trap}\,, \tag{3.22}$$

and the optimal dephasing rate above critical disorder is seen to be

$$\gamma_3^{\rm opt} = (W - W_3^{\rm cr})/3\sqrt{2}\,. \tag{3.23}$$

3.4 Optimal dephasing for long chains

3.4.1 Critical disorder strength for long chains

We now consider how the results obtained above for 2- and 3-site chains may extend to chains of general length N. To begin with, we generalize the results of Fig. 3.3 to N sites. Once again, without loss of generality we choose units where hopping $\Omega = 1$ and evaluate numerically, as a function of opening $\Gamma_{\rm trap}$, the critical disorder $W^{\rm cr}$ at which the ensemble-averaged transfer time $\langle \tau(\gamma) \rangle_W$ develops a minimum as a function of dephasing rate γ. For general N, Monte Carlo integration is used to evaluate the disorder average. The results, for selected values of N, are

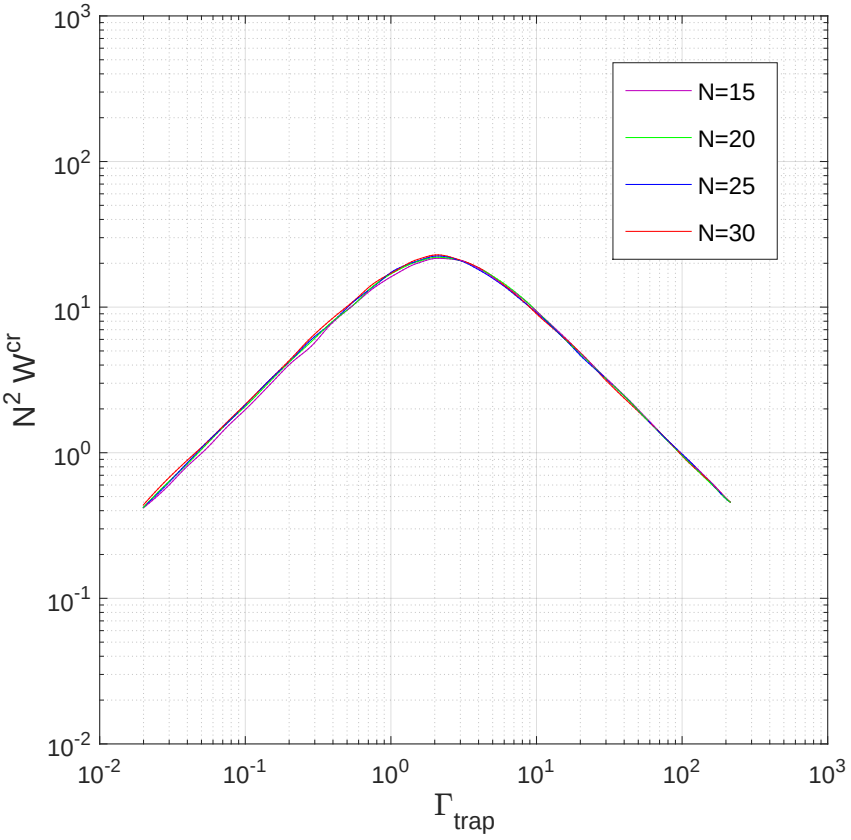

Figure 3.4: Plot of the rescaled critical disorder N^2W^{cr} as a function of opening Γ_{trap} for various chain lengths N. Here we fix $\Omega = 1$.

shown in Fig. 3.4. We notice in Fig. 3.4 the same qualitative behavior observed earlier in Fig. 3.3 for the 3-site chain. Furthermore, we see empirically that the behavior becomes N-independent for large N when the rescaled disorder strength $N^2 W^{\mathrm{cr}}$ is plotted as a function of opening Γ_{trap}, indicating that the critical disorder scales as

$$W^{\mathrm{cr}} \sim \frac{1}{N^2} \tag{3.24}$$

for all values of Γ_{trap}. In particular, comparing with the results for $N = 3$, we have

$$W^{\mathrm{cr}} \sim \frac{\Gamma_{\mathrm{trap}}}{N^2} \tag{3.25}$$

for small opening, $\Gamma_{\mathrm{trap}} \ll \Omega$, and

$$W^{\mathrm{cr}} \sim \frac{\Omega^2}{N^2 \Gamma_{\mathrm{trap}}} \tag{3.26}$$

for large opening, $\Gamma_{\mathrm{trap}} \gg \Omega$.

We notice that W^{cr} approaches zero as the chain length N goes to infinity. This is consistent with the fact that for an infinitely long chain, the system is localized at arbitrarily weak disorder, and any amount of dephasing can break the localization, thus aiding transport.

Unfortunately, an analytic understanding of the empirical scaling behavior (3.24) is not presently available; the analysis would require a non-perturbative treatment of the effect of the opening Γ_{trap}, since near critical disorder Γ_{trap} will be large compared to both disorder W and dephasing strength γ.

3.4.2 Optimal dephasing as a function of disorder

We now consider the optimal dephasing for long chains when $W > W^{\mathrm{cr}}$. Numerical results for two values of Γ_{trap} (one corresponding to a small opening and the

other to a large opening), are shown in Fig. 3.5. We see that the optimal dephasing increases monotonically with the disorder strength. However, several distinct parameter regimes can be identified, which are in direct correspondence with the three regimes obtained for $N = 3$ in Sec. 3.3.2. Notably, each regime shows its own scaling behavior with the chain length N.

Weak disorder: $W - W^{\rm cr} \sim W^{\rm cr}$

We first consider W just slightly above the critical disorder, $0 < W - W^{\rm cr} \sim W^{\rm cr}$. As seen in Fig. 3.5, here the optimal disorder $\gamma^{\rm opt}$ grows linearly with $W - W^{\rm cr}$, just as it does for $N = 2$ and $N = 3$. To ascertain the N-dependence for long chains, in Fig. 3.6 we study $\gamma^{\rm opt}$ as a function of N for $W = 2W^{\rm cr}$ and several (large and small) values of the opening strength $\Gamma_{\rm trap}$. We observe the scaling $\gamma^{\rm opt} \sim 1/N^3$ when other parameters are held fixed, which combined with Eq. (3.24) implies

$$\gamma^{\rm opt} \sim \frac{W - W^{\rm cr}}{N} \,. \tag{3.27}$$

Moderate disorder: $\Gamma_{\rm trap}/\sqrt{N} \ll W \ll \Omega/\sqrt{N}$

Here we consider the behavior where disorder (and dephasing) are strong compared to the opening size but still weak compared to the hopping amplitude. Thus, we are interested in the regime $\Gamma_{\rm trap} \ll W \sim \gamma \ll \Omega$ where any required N dependence is temporarily omitted from the inequalities.

It is convenient to begin with a clean open chain in the presence of dephasing. Here the transfer time may be obtained exactly as

$$\tau = \frac{N}{\Gamma_{\rm trap}} + \frac{N(N-1)\gamma + (N-1)\Gamma_{\rm trap}}{4\Omega^2} \,, \tag{3.28}$$

to be compared with Eq. (3.17) for the special case $\gamma = 0$. Now we consider expanding

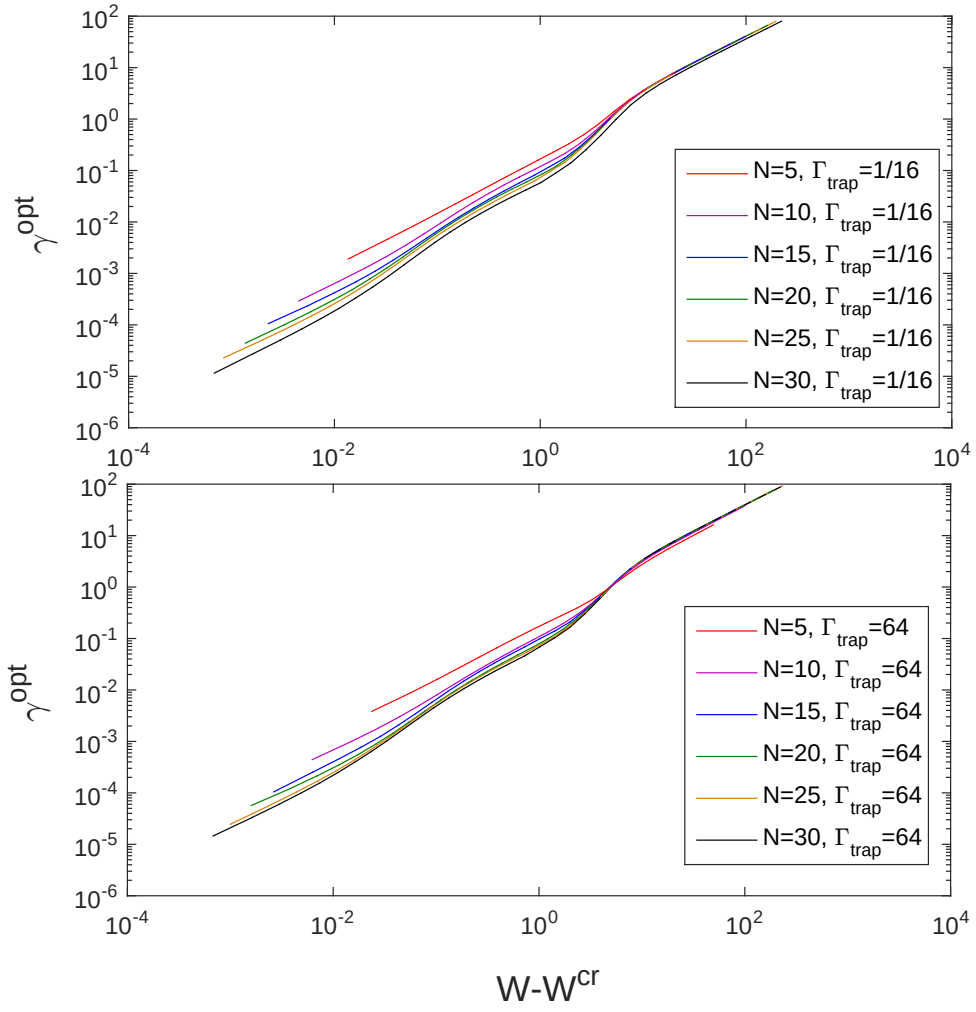

Figure 3.5: Optimal dephasing rate $\gamma^{\rm opt}$ is plotted as a function of $W - W^{\rm cr}$ for chains of different length N, where in each curve the minimum value of W is $1.4W^{\rm cr}$ and the critical disorder $W^{\rm cr}$ is itself a function of N. Here we again fix $\Omega = 1$. The top and bottom panels show results for $\Gamma_{\rm trap} = 1/16$ and 64, providing examples respectively of the small-opening and large-opening wings in Fig. 3.4. In each panel, three distinct regimes may be observed: For weak disorder we have $\gamma^{\rm opt} \sim (W - W^{\rm cr})/N$ (Eq. (3.27)), for moderate disorder we find $\gamma^{\rm opt} \sim W/\sqrt{N}$ (Eq. (3.30)), and for the strongest disorder, $\gamma^{\rm opt} \sim W/\sqrt{6}$ (Eq. (3.32)).

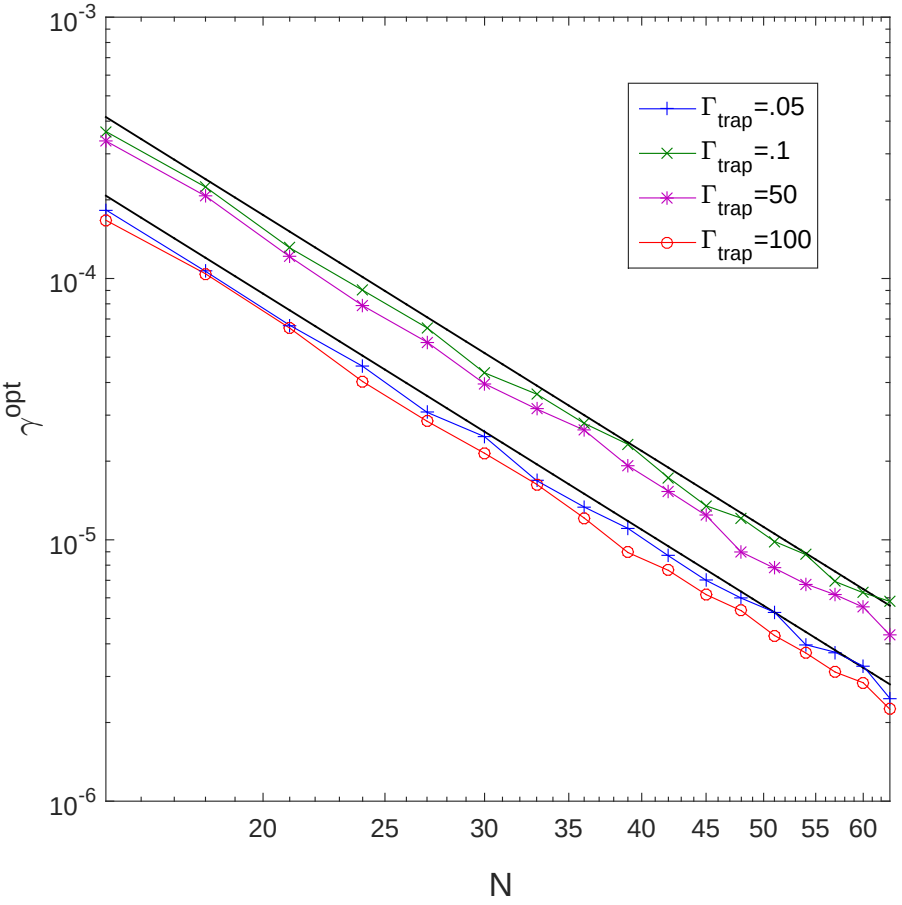

Figure 3.6: Optimal dephasing rate $\gamma^{\rm opt}$ is shown as a function of N with $W = 2W^{\rm cr}$ for several values of the opening strength $\Gamma_{\rm trap}$. Here $\Omega = 1$. The two black solid lines illustrate scaling proportional to $1/N^3$, implying $\gamma^{\rm opt} \sim (W - W^{\rm cr})/N$ for W close to $W^{\rm cr}$.

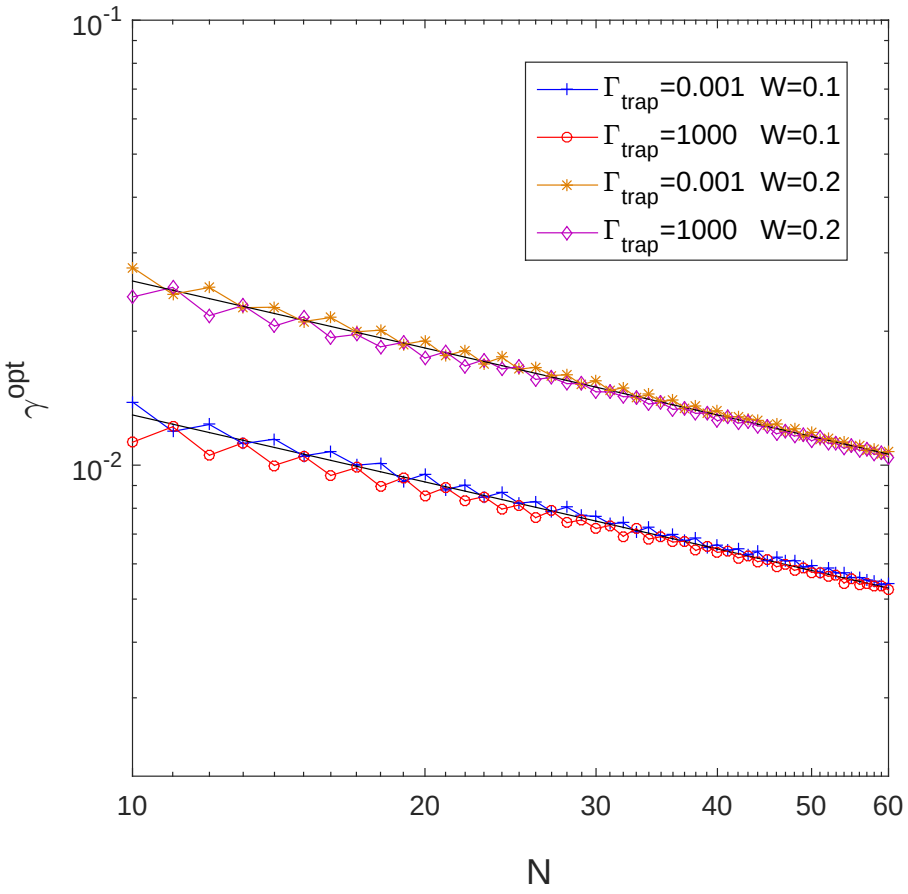

Figure 3.7: Optimal dephasing $\gamma^{\rm opt}$ is shown as a function of chain length N in the moderate-disorder regime, for several values of opening $\Gamma_{\rm trap}$ and disorder strength W. Here $\Omega = 1$. We observe good agreement with Eq. (3.30), as shown by the solid lines.

in both disorder strength W and opening $\Gamma_{\rm trap}$ assuming that the opening is small compared to Ω (i.e., we work in a regime analogous to that considered in Sec. 3.3.2 for $N = 3$; an analogous treatment for $\Gamma_{\rm trap} \gg \Omega$ may be considered as in Sec. 3.3.2). Beginning with Eq. (3.28) for $W = 0$ and comparing with the results (3.14) and (3.18) for $N = 2$ and 3 respectively, we conjecture that for large N the expansion takes the form

$$\begin{aligned}\langle\tau\rangle_W &= \frac{N}{\Gamma_{\rm trap}} + \frac{1}{\Omega^2}\left[\left(\frac{N(N-1)}{4}\gamma + a(N)\frac{W^2}{\gamma}\right) + \Gamma_{\rm trap}\left(\frac{N-1}{4} - b(N)\frac{W^2}{\gamma^2}\right)\right. \\ &+ \left. O\left(\Gamma_{\rm trap}^2\right)\right] + \frac{1}{\Omega^4}\left[c(N)W^2\gamma + d(N)\frac{W^4}{\gamma} + O(\Gamma_{\rm trap})\right] + O\left(\frac{1}{\Omega^6}\right) . \quad (3.29)\end{aligned}$$

Numerically, we find $a(N) = a_0 N$, $b(N) = b_0$, $c(N) = c_0 N^3$, and $d(N) = d_0 N^2$ for large N. In particular, $a_0 \approx 0.042$.

For sufficiently large Ω and small $\Gamma_{\rm trap}$ we may restrict our attention to the term $\left(\frac{N(N-1)}{4}\gamma + a_0 N\frac{W^2}{\gamma}\right)/\Omega^2$ only, which implies that the optimal dephasing in this regime should behave as

$$\gamma^{\rm opt} \approx \frac{2\sqrt{a_0}\,W}{\sqrt{N}} \approx 0.41\frac{W}{\sqrt{N}} . \quad (3.30)$$

This predicted behavior with system size N for moderate disorder strength is confirmed in Fig. 3.7. We observe in Fig. 3.7 that while Eq. (3.30) was obtained in the context of $\Gamma_{\rm trap} \ll \Omega$, the same scaling behavior, $\gamma^{\rm opt} \sim 1/\sqrt{N}$, holds for $\Gamma_{\rm trap} \gg \Omega$ where the effective opening $\Omega^2/\Gamma_{\rm trap}$ is small.

Now to understand the range of validity of Eq. (3.30), we need to take a closer look at the two expansions in Eq. (3.29). On the one hand, our approximation breaks down for small disorder and dephasing when the terms proportional to $\Gamma_{\rm trap}$ become comparable to the $\Gamma_{\rm trap}$-independent terms we have been considering. This occurs when $\gamma^{\rm opt} \sim \Gamma_{\rm trap}/N$, or equivalently $W \sim \Gamma_{\rm trap}/\sqrt{N}$. On the other

hand, the approximation also breaks down for larger disorder (and dephasing), when the $1/\Omega^4$ contribution becomes comparable to that of the $1/\Omega^2$ terms in the expansion. This occurs when $W \sim \Omega/\sqrt{N}$, which not coincidentally corresponds to the localization border where the localization length near the middle of the energy band, $\xi \approx 100\,\Omega^2/W^2$ [58], becomes comparable to the chain length N.

Thus the moderate-disorder regime in which the scaling of the optimal dephasing rate is given by Eq. (3.30) extends over the range $\Gamma_{\rm trap}/\sqrt{N} \ll W \ll \Omega/\sqrt{N}$. We note that in the moderate-disorder regime as well as in the weak-disorder regime, the eigenstates are delocalized and wave packet motion is ballistic. Nevertheless, in both regimes we have shown that dephasing will aid transport.

Strong disorder: $W \gg \Omega/\sqrt{N}$

Finally, in the strong disorder regime, defined by $W \gg \Omega/\sqrt{N}$, the quantum eigenstates are localized, and the dynamics is diffusive. This regime has previously been studied in Refs. [7, 30, 47]. More precisely, this regime comprises two subregimes: For $\Omega/\sqrt{N} \ll W \ll \Omega$, one has $1 \ll \xi \ll N$, and the optimal dephasing rate is given by $\gamma^{\rm opt} \sim \Omega/\xi \sim W^2/\Omega$. Upon further increase of the disorder, we reach $W \gg \Omega$, implying a localization length $\xi \sim 1$, and the optimal dephasing is then simply proportional to the disorder: $\gamma^{\rm opt} \sim W$. Throughout the strong-disorder regime, the optimal dephasing is controlled by motion on the scale of a localization length, and as a consequence $\gamma^{\rm opt}$ is N-independent.

Specifically, for $W \gg \Omega$, the Leegwater classical-like approximation applies [55], and the transfer time is given by [57]

$$\langle \tau_{\rm L} \rangle_W = \frac{N}{\Gamma_{\rm trap}} + \frac{N\,(N-1)}{4\Omega^2}\left[\gamma + \frac{\Gamma_{\rm trap}}{N} + \frac{W^2}{6\gamma}\left(1 - \frac{2\Gamma_{\rm trap}}{N(2\gamma+\Gamma_{\rm trap})}\right)\right]. \qquad (3.31)$$

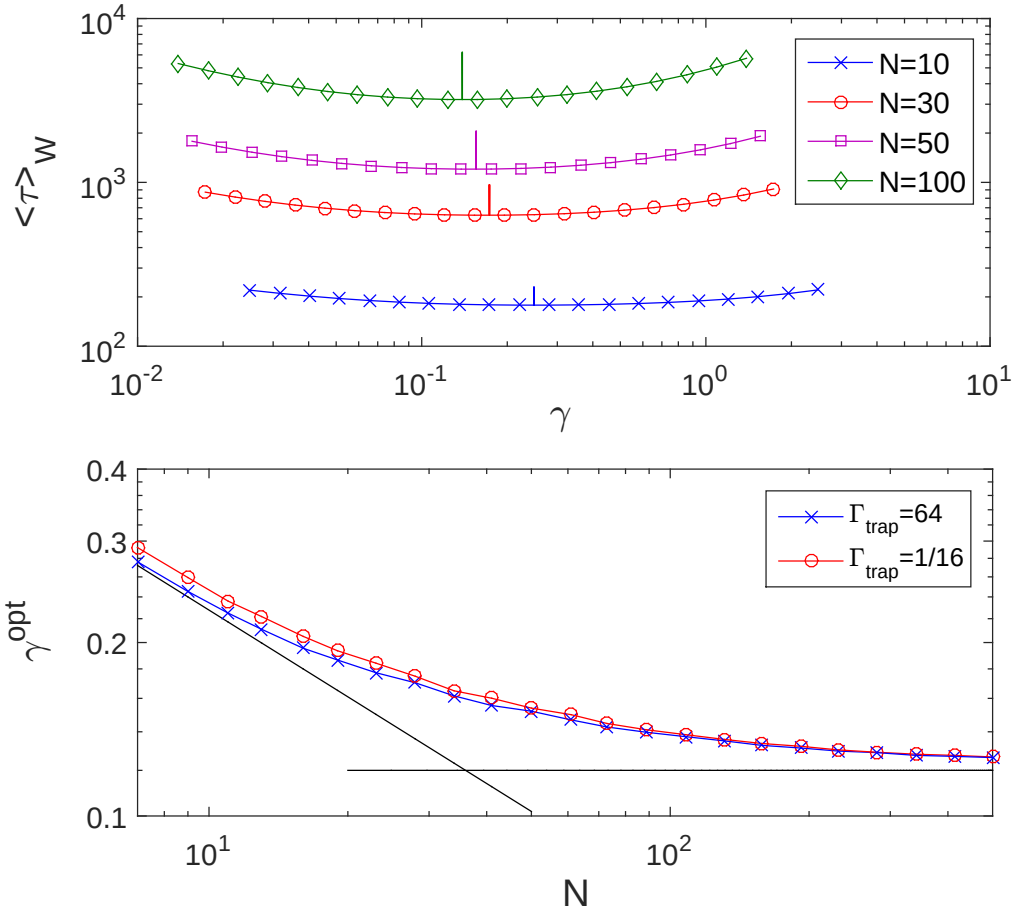

Figure 3.8: Upper panel: The disorder-averaged transfer time $\langle\tau\rangle_W$ is shown as a function of dephasing rate γ for chains of several lengths N. Here $\Omega = 1$, $W = 2$, and $\Gamma_{\rm trap} = 1/16$. In each case, the vertical line indicates the optimal dephasing rate $\gamma^{\rm opt}$. Lower panel: The optimal dephasing $\gamma^{\rm opt}$ is shown as a function of chain length N in the crossover between the moderate-disorder and strong disorder regimes. Here $\Omega = 1$, $W = 2$, and two values of the opening $\Gamma_{\rm trap}$ are presented, corresponding to the weak-opening and strong-opening scenarios. The solid lines represent the $N^{-1/2}$ scaling of Eq. (3.30) in the moderate-disorder regime and the N-independent behavior observed for strong disorder.

The optimal dephasing in this regime is

$$\gamma^{\rm opt} \approx \frac{W}{\sqrt{6}}\,. \tag{3.32}$$

In Fig. 3.8 we examine explicitly the crossover between the moderate-disorder regime, where motion is ballistic and $\gamma^{\rm opt}$ scales with N in accordance with Eq. (3.30), and the strong-disorder regime where localization obtains and $\gamma^{\rm opt}$ becomes N- independent.

3.5 Conclusions

We have systematically studied the effect of dephasing on transport in open disordered chains of arbitrary length. For disorder above a critical value $W^{\rm cr}$, dephasing has been shown to aid transport. We have obtained the scaling of the critical disorder strength $W^{\rm cr}$ with the chain length N; furthermore we have seen that $W^{\rm cr}$ varies linearly or inversely with the opening strength $\Gamma_{\rm trap}$ when $\Gamma_{\rm trap}$ is small or large, respectively, as may be seen analytically in a 3-site model. Thus, $W^{\rm cr} \sim \Gamma_{\rm trap}/N^2$ for $\Gamma_{\rm trap} \ll \Omega$ and $W^{\rm cr} \sim \Omega^2/N^2\Gamma_{\rm trap}$ for $\Gamma_{\rm trap} \gg \Omega$, where the hopping amplitude Ω sets the overall energy scale. Consequently, $W^{\rm cr}$ vanishes and the optimal dephasing rate is always nonzero in the limit of very small or very large opening (as well as in the limit of a long chain).

For $W > W^{\rm cr}$, three distinct regimes have been obtained for the behavior of the optimal dephasing rate $\gamma^{\rm opt}$. For W close to $W^{\rm cr}$, we have $\gamma^{\rm opt} \sim (W - W^{\rm cr})/N$, whereas for $\Gamma_{\rm trap}/\sqrt{N} \ll W \ll \Omega/\sqrt{N}$, the optimal dephasing becomes opening-independent and scales as $\gamma^{\rm opt} \sim W/\sqrt{N}$. In both the weak- and moderate-disorder regimes, dephasing aids transport even though eigenstates are delocalized and motion is ballistic. Finally, for sufficiently strong disorder, $W \gg \Omega/\sqrt{N}$, the quantum states becomes localized and the optimal dephasing rate becomes N-independent, as has

been seen in previous works.

Chapter 4

Optimization of Lossy Mach-Zehnder Interferometer with Varying Prior Phase Uncertainties Using Photon-Counting Detection

4.1 Introduction

The goal of quantum metrology is to explore methods of obtaining high precision measurements in a quantum framework that are not possible classically. Of major interest in this field is the use of quantum optical states (e.g. entangled states or squeezed states), and various measurement schemes have been explored to measure relative phase precisely in a Mach-Zehnder-like interferometer (MZI). Historically, interferometers have been widely used for measuring small displacements. In 1887, the Michelson-Morley experiment showed strong proof against the existence of the aether, while today Michelson-Morley interferometers (MMI), which are mathematically equivalent to MZI, are used for example to detect gravitational waves, in projects such as the Laser Interferometer Gravitational-Wave Observatory (LIGO).

The precision of a classical interferometer (with one of the two arms fed with vacuum) is limited by the shot noise limit $\delta\phi_{\mathrm{SNL}} \geq 1/\sqrt{N}$, where $\delta\phi$ is the minimal detectable relative phase and N is the total or average number of particles (photons in our case) entering into the interferometer. In 1981, Caves showed that by using coherent light together with squeezed vacuum one could achieve sub-shot-noise sensitivities [59]. Since then, a lot of work has been done in order to reach the smallest possible phase uncertainty, given by the Heisenberg limit $\delta\phi_{\mathrm{H}} \sim 1/N$ [60, 61, 62, 63, 64, 65, 66, 67].

Several different measurement schemes are used in the literature, including parity measurement [68], "optimal measurement" [61], and photon-counting measurement [60, 69]. For photon-counting measurement, the standard error propagation formula $\Delta\phi = \Delta\hat{J}_z/|d\hat{J}_z/d\phi|$ is used in several works [60, 62], which is valid only when the probability distributions are Gaussian [70]. Another approach to extract the phase uncertainty from a photon-counting measurement is to calculate the classical Fisher Information F and apply the Cramer-Rao inequality $(\delta\phi)^2 \geq 1/(MF)$ which saturates when the number of measurements M approaches infinity [70, 71]. The classical Fisher Information can be maximized over all possible measurements, which generally are not photon-counting measurements [72, 73, 74]. Additionally, Berry and Wiseman proposed the almost optimal adaptive measurement, which can be achieved by photon counting [69]. Adaptive measurement has been further studied by Wiseman and Killip [75, 76].

In many works in the literature, the limit of both a large number of measurements and a large number of photons is assumed, and thus the prior uncertainty in the phase shift before each successive measurement may be assumed to be already small. But it is also interesting to ask how well can we do in a situation where the resources for each measurement and the number of measurements are both limited, and when

we try to obtain the best estimate for the phase shift with poor prior knowledge (for instance, if we only know a priori that the phase is somewhere between 0 and π). The problem is also very relevant to adaptive measurement schemes, where the choice of probe state for the next step is highly related to previous measurement results. This kind of problem has been studied for covariant measurements [77, 78].

In practice, we need to consider photon loss for quantum states of light and how they will degrade the sensitivity of the interferometer. Lossy interferometric systems have been widely studied [79, 80, 81, 82, 83, 84].

It has been shown in [85] that N00N states can achieve the Heisenberg limit given a large enough number of identical measurements. The assumption of a large number of measurements in [85] simplifies the expressions for phase uncertainties but makes the results inapplicable for a small number of measurements. What we will present below does not make any assumptions on the number of measurements, and the expressions for the phase uncertainties are exact. So we will see how optimal input states evolve when the number of measurements increases. However, our results suggest along with those in [85] that N00N states are the ultimate optimal states, which give the best measurement sensitivity locally for the relative phase in MZI.

The present chapter is organized as follows. In Section 4.2, the problem is described and the exact expressions that enter into the optimization are presented. In Section 4.3, we characterize optimal states in detail in the case of a flat prior phase probability distribution and no photon loss. We also discuss limiting behaviors of the optimal states, and the scaling relations associated with transitions between different regimes in parameter space. In section 4.4, photon loss is included in the calculation, which modifies the shape of the optimal states and increases the post-measurement variance. Results are presented as a function of the loss rate, for losses in either one or both arms of the interferometer. In Section 4.5, we test the stability of the optimal

states with respect to a change in the prior phase probability distribution. The results show that optimal states are changed only slightly, provided the distribution is symmetric. Finally, in Section 4.6, we present the conclusions.

4.2 Phase measurement formalism for a lossy interferometer

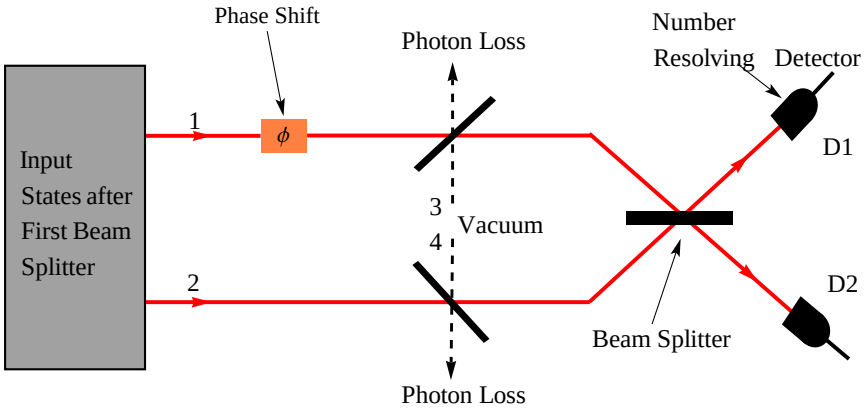

Figure 4.1: Schematic of a Mach-Zehnder-like interferometer. We are considering input states after the first beam splitter in the standard Mach-Zehnder interferometer. Photon loss is modeled by two beam splitters after the phase shift, and perfect detection is assumed at the two number-resolving detectors.

We wish to find the optimal input quantum states for a lossy Mach-Zehnder interferometer assuming the output state is measured using photon counting detection techniques. We model photon loss by two passive beam splitters and two imaginary arms labeled 3 and 4 in Fig. 4.1 [71, 81]. An arbitrary pure-state input with definite photon number N can be written as

$$|\psi\rangle_{\text{in}} = \sum_{k=0}^{N} c_k \, |N-k, k, 0, 0\rangle = \sum_{k=0}^{N} c_k \frac{(\hat{a}_1^\dagger)^{N-k} (\hat{a}_2^\dagger)^k}{\sqrt{(N-k)!k!}} \, |0\rangle \ , \tag{4.1}$$

where $|N-k, k, 0, 0\rangle$ represents a basis state with $N-k$ photons in arm 1, k photons

in arm 2, and 0 photons in imaginary arms 3, 4, and $\hat{a}_i^\dagger$ is the photon creation operator in arm i.

The phase shift acts as $e^{i\phi\hat{n}_1}$, where $\hat{n}_1$ is the number operator on arm 1. So the state after the phase shifter is

$$|\psi'\rangle = \sum_{k=0}^{N} c_k \frac{e^{i(N-k)\phi}(\hat{a}_1^\dagger)^{N-k}(\hat{a}_2^\dagger)^k}{\sqrt{(N-k)!k!}} |0\rangle . \tag{4.2}$$

Next, the state passes through two fictitious beam splitters that represent photon loss in each arm. One beam splitter acts as a unitary transformation on creation operators for real arm 1 and imaginary arm 3, and can be represented by

$$\begin{pmatrix} \hat{a}_{1,\text{out}}^\dagger \\ \hat{a}_{3,\text{out}}^\dagger \end{pmatrix} = U_1 \begin{pmatrix} \hat{a}_{1,\text{in}}^\dagger \\ \hat{a}_{3,\text{in}}^\dagger \end{pmatrix} , \tag{4.3}$$

where the "in" and "out" subscripts label creation operators before and after the beam splitter, respectively. U_1 is a 2×2 unitary matrix that can be represented as

$$U_1 = \begin{pmatrix} \cos\alpha & \sin\alpha \\ -\sin\alpha & \cos\alpha \end{pmatrix} . \tag{4.4}$$

Physically, $\sin^2\alpha$ is the photon loss fraction in arm 1. The fictitious beam splitter acting on physical arm 2 and imaginary arm 4 is represented in the same way, with 2×2 matrix U_2 and fractional loss $\sin^2\beta$. The multi-photon state becomes

$$|\psi''\rangle = \sum_{k=0}^{N} \frac{c_k e^{i(N-k)\phi}}{\sqrt{(N-k)!k!}} (\cos\alpha\,\hat{a}_1^\dagger + \sin\alpha\,\hat{a}_3^\dagger)^{N-k} (\cos\beta\,\hat{a}_2^\dagger + \sin\beta\,\hat{a}_4^\dagger)^k |0\rangle . \tag{4.5}$$

Finally, after the last beam splitter, with angle parameter γ, we have

$$\begin{aligned} |\psi'''\rangle = \sum_{k=0}^{N} \frac{c_k e^{i(N-k)\phi}}{\sqrt{(N-k)!k!}} [\cos\alpha(\cos\gamma\,\hat{a}_1^\dagger + \sin\gamma\,\hat{a}_2^\dagger) + \sin\alpha\,\hat{a}_3^\dagger]^{N-k} \\ \times [\cos\beta(-\sin\gamma\,\hat{a}_1^\dagger + \cos\gamma\,\hat{a}_2^\dagger) + \sin\beta\,\hat{a}_4^\dagger]^k\,|0\rangle\ . \end{aligned} \tag{4.6}$$

Expanding Eq. (4.6), we will obtain a polynomial of the form

$$|\psi'''\rangle = \sum_{l=0}^{N} \sum_{\mu=0}^{N-l} \sum_{\nu=0}^{l} g_{l\mu\nu} (\hat{a}_1^\dagger)^\mu (\hat{a}_2^\dagger)^{N-l-\mu} (\hat{a}_3^\dagger)^\nu (\hat{a}_4^\dagger)^{l-\nu}\,, \tag{4.7}$$

where l is the number of photons lost. The coefficients $g_{l\mu\nu}$ are polynomials of degree N in $\cos\alpha$, $\sin\alpha$, $\cos\beta$, $\sin\beta$, $\cos\gamma$, and $\sin\gamma$; they may be obtained explicitly for given N using for example symbolic computational software such as Wolfram Mathematica.

The probability of detecting μ photons in detector 1 and $N-l-\mu$ in detector 2 is given by

$$P_m(\phi) = \sum_{\nu=0}^{l} \left| \sqrt{\nu!(l-\nu)!\mu!(N-l-\mu)!}\, g_{l\mu\nu} \right|^2, \tag{4.8}$$

where we will use $m = (\mu, N-l-\mu)$ to label the $(N+1)(N+2)/2$ possible outcomes of the measurement. $P_m(\phi)$ is the probability distribution of observing outcome m given the phase shift ϕ, in other words $P_m(\phi) = P(m|\phi)$, satisfying $\sum_m P(m|\phi) = \sum_m P_m(\phi) = 1$.

According to Bayes' theorem, the probability that the true phase is ϕ given measurement outcome m is

$$P(\phi|m) = \frac{P(\phi)P(m|\phi)}{P(m)}, \tag{4.9}$$

where $P(\phi)$ is the prior phase distribution before measurement and $P(m)$ can be obtained by normalization. Since the phase has periodicity of 2π, we work with ϕ in the interval $[-\pi, \pi]$.

In particular, without loss of generality, we will consider arbitrary prior phase interval $[-\Delta/2, \Delta/2]$, where $0 < \Delta \leq \pi$. (The reason for the restriction to uncertainty intervals of size no greater than π is explained in Sec. 4.3.) So $P(\phi)$ now satisfies the normalization condition:

$$\int_{-\Delta/2}^{\Delta/2} P(\phi)\, d\phi = 1. \tag{4.10}$$

Eq. (4.9) can be extended to M measurements:

$$P(\phi|m_1, m_2, ..., m_M) = \frac{1}{\mathcal{N}} P(\phi)P(m_1|\phi)P(m_2|\phi)...P(m_M|\phi), \tag{4.11}$$

where the normalization $\mathcal{N}$ is given by

$$\mathcal{N} = \int_{-\Delta/2}^{\Delta/2} P(\phi')P(m_1|\phi')P(m_2|\phi')...P(m_M|\phi')\, d\phi'\,. \tag{4.12}$$

From the likelihood function $P(\phi|m_1, m_2, ..., m_M)$, we can obtain the unbiased phase estimator defined as the mean of the likelihood function,

$$\begin{aligned} \tilde{\phi}_{m_1 m_2 ... m_M} &= \int_{-\Delta/2}^{\Delta/2} \phi'\, P(\phi'|m_1, m_2, ..., m_M)\, d\phi' \\ &= \frac{\int_{-\Delta/2}^{\Delta/2} \phi'\, P(\phi') \prod_{i=1}^{M} P(m_i|\phi')\, d\phi'}{\int_{-\Delta/2}^{\Delta/2} P(\phi'') \prod_{i=1}^{M} P(m_i|\phi'')\, d\phi''}\,, \end{aligned} \tag{4.13}$$

where $\tilde{\phi}_{m_1 m_2 ... m_M}$ is associated with outcome sequence $m_1, m_2, ..., m_M$, occurring with

probability $\prod_{i=1}^{M} P(m_i|\phi)$. Each measurement outcome sequence $m_1 m_2 ... m_M$ will produce its own phase estimator $\tilde{\phi}$ for the same true phase shift ϕ. Then $(\phi - \tilde{\phi}_{m_1 m_2 ... m_M})^2$ is the squared measurement error for that specific outcome sequence. Summing over all the outcomes, we obtain the variance, or expected mean squared measurement error, for a specific true phase shift ϕ:

$$(\delta\phi)^2_\phi = \sum_{m_1, m_2, ..., m_M} \prod_{i=1}^{M} P(m_i|\phi)(\phi - \tilde{\phi}_{m_1 m_2 ... m_M})^2. \tag{4.14}$$

In reality, however, we don't know the true phase shift. What we do know is the prior distribution of the phase shift, $P(\phi)$. So, integrating over all possible values of ϕ, we obtain the expected mean squared measurement error for a prior distribution $P(\phi)$,

$$(\delta\phi)^2 = \sum_{m_1, m_2, ..., m_M} \int_{-\Delta/2}^{\Delta/2} (\phi - \tilde{\phi}_{m_1 m_2 ... m_M})^2 P(\phi) \prod_{i=1}^{M} P(m_i|\phi)\, d\phi, \tag{4.15}$$

where we have interchanged the order of integration and summation. For the case of a single measurement, which is the primary focus of the present work, this expression reduces to

$$(\delta\phi)^2 = \sum_{m} \int_{-\Delta/2}^{\Delta/2} (\phi - \tilde{\phi}_m)^2 P(\phi) P(m|\phi)\, d\phi\,, \tag{4.16}$$

where

$$\tilde{\phi}_m = \frac{\int_{-\Delta/2}^{\Delta/2} \phi'\, P(\phi') P(m|\phi')\, d\phi'}{\int_{-\Delta/2}^{\Delta/2} P(\phi'') P(m|\phi'')\, d\phi''}\,. \tag{4.17}$$

We recall that $(\delta\phi)^2$ is a function of the prior uncertainty interval Δ (and, more generally, of the prior distribution $P(\phi)$, if the prior distribution is not flat), as well as of photon number N, input state coefficients c_k, and the three beam splitter parameters α, β, γ. The next step is to minimize $(\delta\phi)^2$ given certain constraints to

find what the optimal input states look like in different scenarios. One trick about the optimization that deserves to be mentioned is that the phase estimators $\tilde{\phi}_m$ in Eq. (4.16) can be treated as free optimization variables, instead of functions of the input states coefficients c_k and other variables. Indeed, the phase estimators $\tilde{\phi}_m$ that minimize the variance in Eq. (4.16) will be identical to those given by the mean of the phase distribution $P(\phi|m)$, as in Eq. (4.17). (This is analogous in spirit to the fact that the axis position that minimizes the moment of inertia is precisely the center of mass.) Treating the phase estimators $\tilde{\phi}_m$ as free parameters is computationally advantageous in many cases.

4.3 Optimal states and variance for zero loss and flat prior phase distribution

In this section, we start out with no photon loss ($\alpha, \beta = 0$, corresponding to removal of the two beam splitters intended for modeling photon loss) and flat prior phase distribution, $P(\phi) = 1/\Delta$ for $-\Delta/2 \leq \phi \leq \Delta/2$. Nonzero photon loss and different prior phase distributions will be considered in Secs. 4.4 and 4.5, respectively. Now the variance $(\delta\phi)^2$ is a function of photon number N, input state coefficients c_k, phase interval Δ, and beam splitter parameter γ. We fix N and Δ for each run, seeking the optimal coefficients c_k and splitter angle γ that minimize the output variance $(\delta\phi)^2$. The results of optimization show that the optimal beam splitter parameter γ invariably takes values $\eta\pi/2 + \pi/4$ ($\eta \in \mathbb{Z}$) for all N and Δ, which means the optimal beam splitter right before the detectors is a always a 50:50 beam splitter. The above results continue to apply in situations with photon loss. So without loss of generality, in the following we set $\gamma = \pi/4$.

The optimization results also show that the optimal input state coefficients c_k obey a symmetry with respect to interchange of the mode numbers 1 and 2. Specifi-

cally, if we express the coefficients in polar form as $c_k = r_k e^{i\theta_k}$ (with real r_k, θ_k), then the optimal parameters r_k, θ_k satisfy

$$r_k = r_{N-k} \geq 0, \quad \theta_k = -\theta_{N-k}, \tag{4.18}$$

where $k = 0, 1, \ldots, N$. Eq. (4.18) holds in general for all $\Delta \in (0, 2\pi]$, but it implies $P(m|\phi) = P(m|\phi + \pi)$, which gives rise to ambiguities in the phase estimators $\tilde{\phi}_m$ for $\Delta > \pi$. To eliminate these ambiguities, we will henceforth restrict ourselves to prior phase uncertainty intervals $\Delta \leq \pi$.

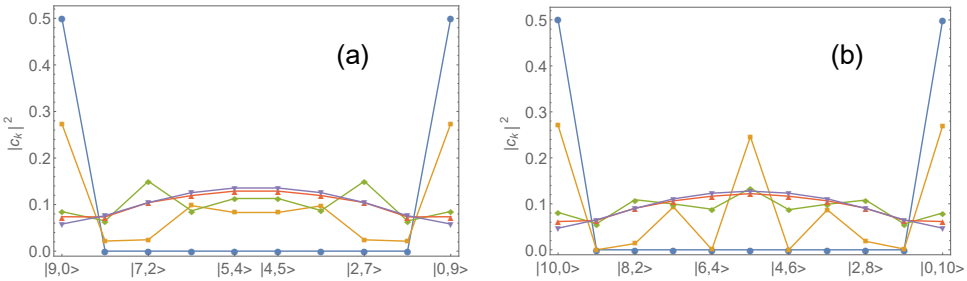

Figure 4.2: The structure of the optimal input state $|\psi\rangle_{\text{in}}$ is shown for $N = 9$ photons in panel (a) and $N = 10$ in panel (b), for different values of the initial phase uncertainty Δ. In each panel, the blue circles, yellow squares, green diamonds, red triangles, and blue upside-down triangles label $\Delta/\pi = 0.1$, 0.2, 0.3, 0.4, and 0.5, respectively.

The specific form of the optimal states is determined by the size of the prior phase uncertainty interval Δ and the photon number N. Several examples of optimal states are depicted in Fig. 4.2, where we see that as Δ increases for a given photon number, the states shift from being concentrated at the edges $|N, 0\rangle$ and $|0, N\rangle$ to being suppressed at the edges.

Specifically, three distinct regimes are identified as shown in Fig. 4.3: a N00N state regime valid for small prior phase uncertainty or small photon number, a quasi-Gaussian regime valid for large prior uncertainty or large photon number, and an in-

termediate regime with more complicated optimal input state structure. The boundaries between these regimes follow a $\Delta \sim 1/N^z$ scaling with $z \approx 1$, as seen in Fig. 4.3, so in particular the quasi-Gaussian regime obtains for $N\Delta \gg 1$ and the N00N regime obtains for $N\Delta \ll 1$. The reasons for this scaling of the two boundary lines are discussed below.

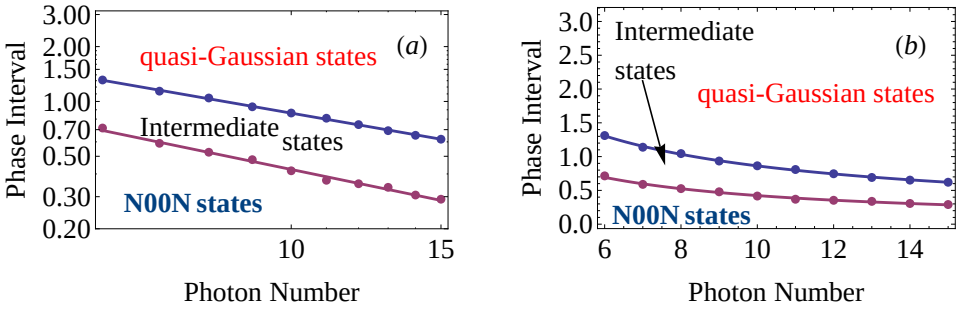

Figure 4.3: The regions in $N - \Delta$ space are identified in which the optimal input states are N00N states, intermediate states, or quasi-Gaussian states. Panel (a) shows the behavior on a log-log scale, whereas in panel (b) the same data are shown on a linear plot. The boundary between the N00N and intermediate regimes has been fit to the form $\Delta = 3.9/N^{0.96}$; the boundary between the intermediate and quasi-Gaussian regimes has the fitted behavior $\Delta = 5.6/N^{0.81}$.

The N00N states,

$$|\psi\rangle_{\text{N00N}} = \frac{|N,0\rangle + e^{\pm i\pi/2}\,|0,N\rangle}{\sqrt{2}} \tag{4.19}$$

are optimal for small prior uncertainty, which is the regime that has been considered in earlier works [78, 86]. An example is the optimal state for $\Delta/\pi = 0.1$ in Fig. 4.2. The intermediate region in Fig. 4.3 may contain multiple classes of states and no simple analytical expressions for the states are available in this region. In Fig. 4.2, $\Delta/\pi = 0.2$ and 0.3 provide examples of optimal states in this intermediate regime.

In the upper-right region identified as "quasi-Gaussian" in Fig. 4.3, we find that the optimal input states have amplitudes that are symmetric under interchange

of modes 1 and 2, and the phases follow a fixed pattern:

$$r_k = r_{N-k}, \quad \theta_k = \theta_0 + sk\pi/2\,, \tag{4.20}$$

where $s = \pm 1$. We notice that Eq. (4.20) is consistent with Eq. (4.18) up to an irrelevant global phase θ_0. Furthermore, the amplitude r_k is peaked at $k \approx N/2$ where the photons are evenly distributed between the two modes, specifically we have

$$r_{k+1} > r_k \tag{4.21}$$

for $0 \leq k \leq N/2 - 1$. $\Delta/\pi = 0.4$ and 0.5 in Fig. 4.2 provide examples of states in this regime. Their behavior is in sharp contrast with the N00N states, where all photons are either in mode 1 or mode 2. Analyzing the optimal input states more closely, we find that they can be fit very well to a quasi-Gaussian form:

$$|\psi\rangle_{\mathrm{qG}} = \frac{\sum_{k=0}^{N} e^{-\rho(k-N/2)^2 - \rho'(k-N/2)^4 + isk\pi/2}}{\sqrt{\sum_{k'=0}^{N} \left(e^{-\rho(k'-N/2)^2 - \rho'(k'-N/2)^4}\right)^2}} |N-k, k\rangle\,, \tag{4.22}$$

where $s = \pm 1$ as before, and ρ, ρ' are functions of N and Δ. Two examples of optimal states are shown in Fig. 4.4, where fits to the quasi-Gaussian form of Eq. (4.22) are compared with fits to a pure Gaussian (Eq. (4.22) with $\rho' = 0$). We see that the quasi-Guassian form with only a quartic correction in the exponent is sufficient to reproduce the exact optimal states almost exactly, even for modest values of the photon number N. Thus, the optimal input states in the quasi-Gaussian regime can be well described using only two parameters ρ and ρ', and it is sufficient to find the optimal values of these two parameters, i.e., the values that minimize the post-measurement variance (4.16), for given values of N and Δ.

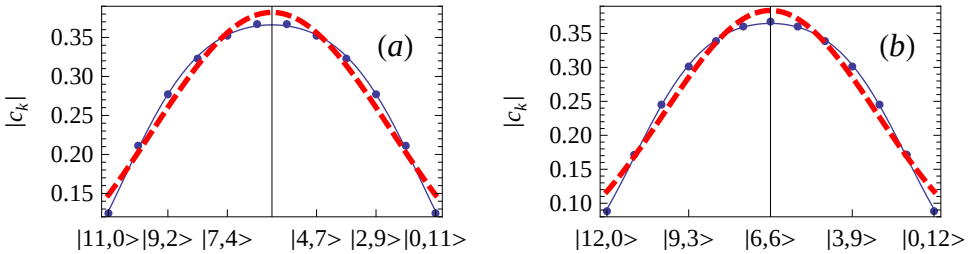

Figure 4.4: Amplitudes $r_k = |c_k|$ of the optimal states for (a) $N = 11, \Delta = 0.8\pi$ and (b) $N = 12, \Delta = 0.9\pi$. The solid and dashed lines represent fits to the quasi-Gaussian form of Eq. (4.22) and to a pure Gaussian (Eq. (4.22) with $\rho' = 0$), respectively.

Further study of ρ and ρ' shows that for large N we have $\rho \propto 1/N$ and $\rho' \propto 1/N^3$. This scaling implies that for sufficiently large N the quartic term in the exponent will be suppressed, reducing Eq. (4.22) to a pure Gaussian form.

When we do constrain the input states to obey the Gaussian form (Eq. (4.22) with $\rho' = 0$), which is valid for sufficiently large photon number N, we find that the optimal ρ scales as $\rho \propto \Delta$ to a good approximation. Thus when N is large, $\rho \approx c_\rho \Delta/N$ where c_ρ is a constant, ρ' may be ignored, and Eq. (4.22) reduces to a Gaussian state,

$$|\psi\rangle_{\mathrm{G}} = \sum_{k=0}^{N} \frac{e^{-c_\rho(\Delta/N)(k-N/2)^2 + isk\pi/2}}{\sqrt{\sum_{k=0}^{N} \left(e^{-c_\rho(\Delta/N)(k-N/2)^2}\right)^2}} |N-k, k\rangle \,. \tag{4.23}$$

In the state given by Eq. (4.23), the variance of the photon number difference between two arms, $\Delta n = n_1 - n_2 = (N-k) - k$, behaves as $(\Delta n)^2 \propto N/\Delta$. The uncertainty relation between phase and photon number, $\Delta\phi\Delta n \sim 1$, implies that input states of the form (4.23) will give uncertainties in the measured phase scaling at best as

$$(\Delta\phi)^2_{\mathrm{qG}} \sim \frac{\Delta}{N} \,. \tag{4.24}$$

Now the uncertainty in the measured phase can be no larger than the prior uncertainty, so we have $\Delta/N \lesssim \Delta^2$ or $\Delta > 1/N$. This suggests that the quasi-Gaussian regime can only hold for $N\Delta \gtrsim 1$. This predicted scaling $\Delta_{\mathrm{qG-I}} \sim 1/N$ for the transition line between quasi-Gaussian states and intermediate states is in reasonable agreement with that obtained numerically for moderate N, as shown in Fig. 4.3.

The transition line between N00N states and the intermediate regime is also straightforward to understand. N00N states have an N-fold ambiguity in phase detection, i.e., when a N00N state is used as the input state, $P(m|\phi)$ is invariant under the shift $\phi \to \phi + 2\pi/N$. Thus N00N states can only be appropriate when $\Delta \lesssim 1/N$, which implies a scaling $\Delta_{\mathrm{N-I}} \sim 1/N$ for the transition line between N00N states and intermediate states, in good agreement with the numerical result in Fig. 4.3.

The scaling of the two transition lines in Fig. 4.3 suggests that for large N the intermediate states are confined to a strip of width ~ 1 in the $\log N - \log \Delta$ space. When N is large, the area of this strip is negligible compared to the area of the whole space, and the intermediate states are therefore unlikely to be optimal. So the details of the intermediate states are less important for optimal phase measurement.

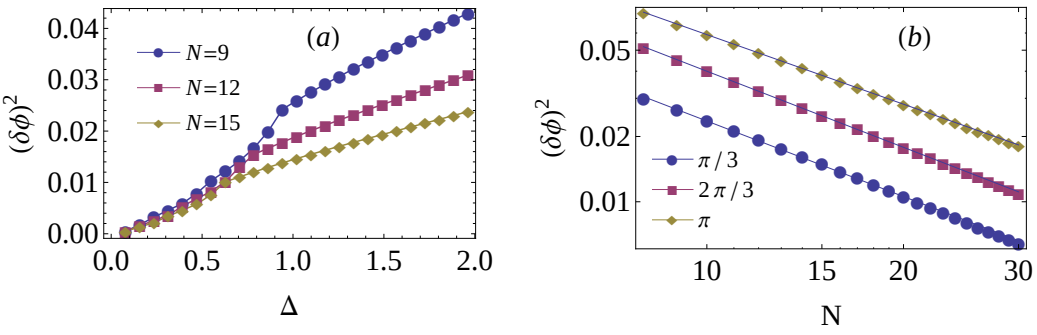

Figure 4.5: The variance $(\delta\phi)^2$ is shown (a) as a function of prior phase uncertainty Δ for several values of photon number N and (b) as a function of N for several values of Δ. The lines in (b) are best fits to a power-law behavior: $(\delta\phi)^2 = 0.338/N^{1.16}$, $0.586/N^{1.17}$, and $0.687/N^{1.07}$ for $\Delta = \pi/3$, $\Delta = 2\pi/3$, and $\Delta = \pi$, respectively.

The transitions between different optimal input state regimes in different regions are also reflected in the output variance $(\delta\phi)^2$ viewed as a function of input uncertainty Δ, as shown in Fig. 4.5(a). For large Δ, we observe $(\delta\phi)^2 \sim \Delta$, consistent with Eq. (4.24), whereas for small Δ we have the $(\delta\phi)^2 \sim \Delta^2$ behavior (independent of N) expected for input N00N states. In Fig. 4.5(b) the output variance is shown to vary inversely with N when N is sufficiently large as to be in the quasi-Gaussian regime, again in agreement with Eq. (4.24) and also with the scaling implied by the shot noise limit. The data in Fig. 4.5(b) for $N > 20$ were obtained restricting the input states to have the form Eq. (4.20). The use of constraint (4.20) reduces the number of optimization parameters by a factor of 4, allowing direct optimization to be viable for much greater values of N.

4.4 Optimal states and variance with photon loss

In the previous section, the limiting scenario of negligible photon loss was assumed. Here, we will discuss how the optimal states and output variance change in presence of nonzero photon loss. Loss is modeled via a fictitious beam splitter in each arm, as discussed in Sec. 4.2. Since the outcome does not depend on the photon loss occurring before or after the phase shift [87], this way of modeling photon loss can account for photon loss anywhere in the paths upstream from the photodetectors.

For now, a flat prior phase distribution is still assumed. Unsurprisingly, the output variance $(\delta\phi)^2$ increases monotonically with the loss rate, i.e., the information gain for the measurement decreases, as depicted in Fig. 4.6. We see in Fig. 4.6 that the variance is a linear function of loss rate to first order, no matter whether the photon loss exists in one arm or both. For the standard interferometric limit (SIL), it has been shown that $(\delta\phi_{\mathrm{SIL}})^2 = 1/N(1-\epsilon)$ [81], where ϵ is the loss rate for both arms. Generalizing to $(\delta\phi)^2 \propto 1/(N(1-\epsilon))^\lambda$ and expanding to first order in ϵ,

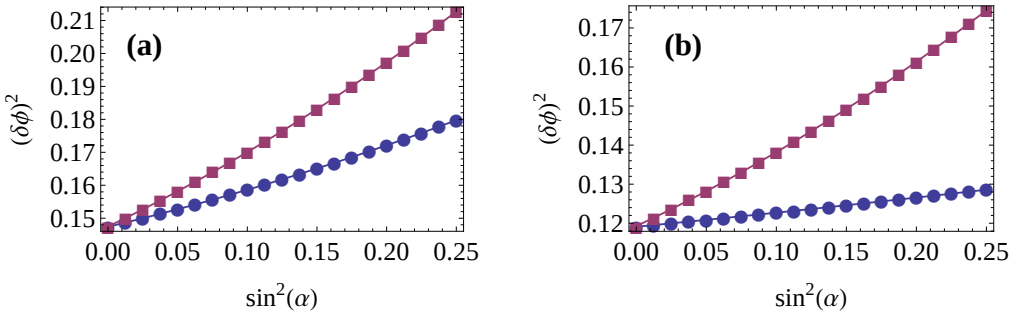

Figure 4.6: Post-measurement variance increases with photon loss rate. Squares represent a scenario where the loss rate is the same in both arms ($\beta = \alpha$), and the circles represent a scenario where loss occurs only in the upper arm ($\beta = 0$). Here the initial phase uncertainty is $\Delta = \pi$. Panels (a) and (b) show results for 4 and 5 photons, respectively. In each case, the data are well described by a power-law expansion in the loss rate $\sin^2\alpha$: $(\delta\phi)^2 \approx (\delta\phi)_0^2(1+w\sin^2\alpha+w'\sin^4\alpha)$. In panel (a), the fit parameters are $w = 0.69$, $w' = 0.78$ for $\beta = 0$ and $w = 1.38$, $w' = 1.59$ for $\beta = \alpha$; in panel (b), we have $w = 0.72$, $w' = 0.81$ for $\beta = 0$ and $w = 1.41$, $w' = 1.77$ for $\beta = \alpha$.

we have $(\delta\phi)^2 \propto N^{-\lambda}(1+\lambda\epsilon)$. Thus we may expect that the variance has a linear dependence on loss rate when the loss rate is small (the response of the optimal states to accommodate photon loss will counteract the increase in variance, but this effect is at the next order). When loss only exists in one arm, the total loss rate is halved and the variance increases half as fast. This is confirmed in Fig. 4.6, where the slope of the upper line in each panel ($\beta = \alpha$) is roughly double that of the slope of the lower line ($\beta = 0$).

The optimal states will also change with the rate of photon loss. In particular, when photon loss is present in arm 1 only, the symmetry of the optimal input state will be broken, with a greater number of photons starting out in arm 2 so as to reduce photon loss. This can can be seen for the case of $N = 4$ photons in Fig. 4.7(b), where Δ is chosen to be large so as to be in the quasi-Gaussian regime. In Fig. 4.7(a) we show the shift $\delta n = \langle n_2 - n_1\rangle = \sum_{k=0}^{N}|c_k|^2(2k-N)$, which measures the state asymmetry. At the same time, the pattern of the phases θ_k in the optimal state

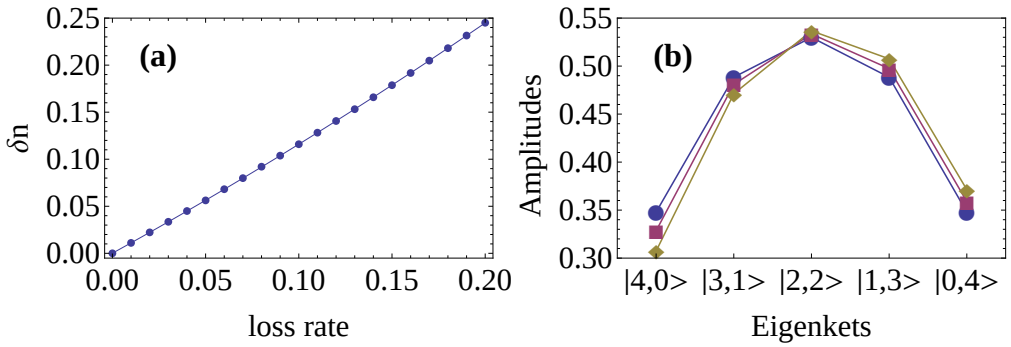

Figure 4.7: The results of input state optimization with $N = 4$ and $\Delta = \pi$ are shown, with photon loss rate $\sin^2\alpha$ in arm 1 only. Panel (a) shows that the shift $\delta n = \langle n_2 - n_1 \rangle$ increases with loss rate. The fit provides a quantitative relation, $\delta n = 1.1\sin^2\alpha + 0.66\sin^4\alpha$. Panel (b) shows the amplitudes $r_k = |c_k|$ of the optimal input state (4.1) at loss rate 0% (circles), 10% (squares), and 20% (diamonds).

(Eq. (4.20)) remains unchanged.

If the photon loss is the same in both arms, both amplitudes and phases of the optimal states will maintain the symmetric form given in Eq. (4.20), but the optimal amplitude distribution comes out to be more peaked, as compared to lossless case.

Fig. 4.7 addresses the effect of nonzero photon loss in the quasi-Gaussian regime. N00N states are also affected by photon loss, as has been studied in Ref. [71] using a classical Fisher Information approach.

4.5 Optimal states with non-flat prior phase distribution

In Secs. 4.3 and 4.4 we have focused on the case of a uniform prior distribution, $P(\phi) = 1/\Delta$ for $-\Delta/2 \leq \phi \leq \Delta/2$. However, if we want to perform a second measurement, the prior phase distribution for the second measurement is the output phase distribution from the first measurement, and this will be non-uniform even if the original prior is flat. The phase distribution after many identical measurements

will tend towards a Gaussian. Thus, it is important to understand how sensitive the optimal states are to different prior phase distributions. In this section, we consider the effect of varying the prior phase distributions, in the absence of photon loss. Several examples of prior phase distributions are shown in Fig 4.8.

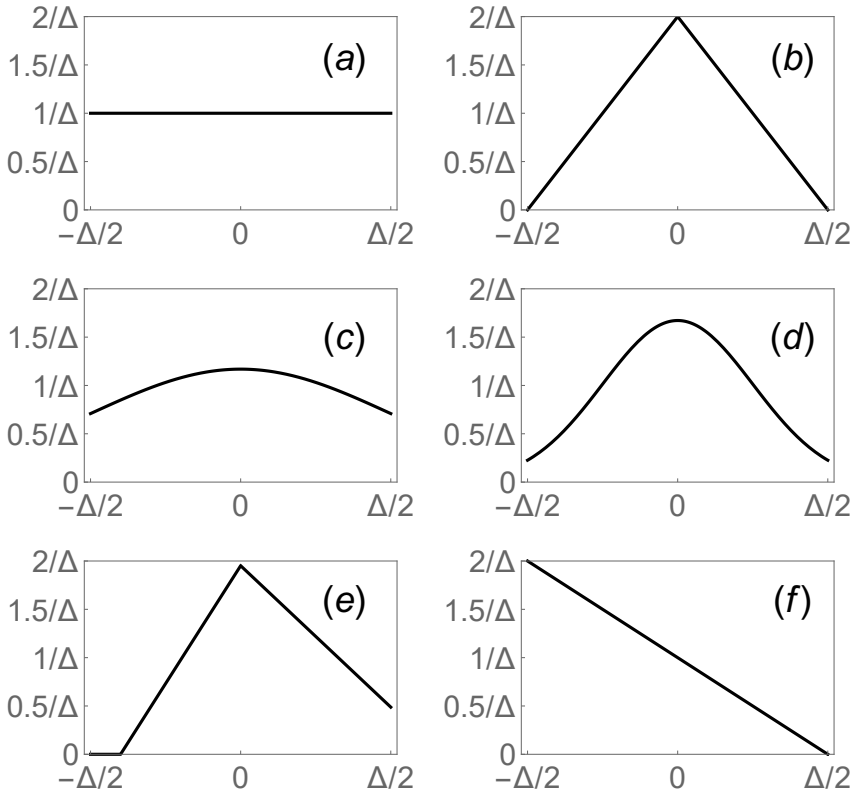

Figure 4.8: Prior phase distribution functions. (a) is a flat distribution; (b) and (e) are symmetric and asymmetric triangular distributions, respectively. (c) and (d) are Gaussian distributions with $\mu = 0, \sigma = \Delta/4$ and $\mu = 0, \sigma = \Delta/2$, respectively. The tails of Gaussian distribution are cut off outside the interval $[-\Delta/2, \Delta/2]$. (f) is a (strongly asymmetric) linear distribution function.

In Fig. 4.9, we show the results of input state optimization for $N = 4$ and $N = 5$ photons, and two different values of the prior phase variance$(\delta\phi)^2_{\text{prior}}$. In each case, the optimization is performed for all six prior distributions shown in Fig. 4.8, adjusting the parameter Δ to ensure that all six prior distributions have the same variance. We see in each case that the optimal state amplitudes are almost independent of the prior

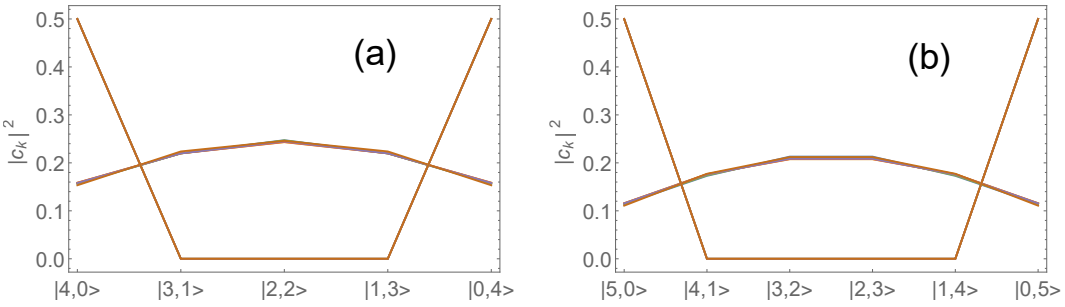

Figure 4.9: Optimal states for all six prior phase distributions depicted in Fig. 4.8. Panels (a) and (b) show results for 4 and 5 photons, respectively. In each panel, the calculation is performed for prior variance $(\delta\phi)^2_{\text{prior}} = (0.1\pi)^2/12$ (where the optimal state is the N00N state, peaked at the edges, for each prior distribution), and for prior variance $(\delta\phi)^2_{\text{prior}} = (0.7\pi)^2/12$ (where the optimal state is quasi-Gaussian, peaked in the middle, for each prior distribution). The quasi-Gaussian states seem to overlap one another totally on the scale of the figure, but they are actually slightly different for each of the six prior phase distributions.

distribution and depend only on the prior variance. In particular, for prior variance $(\delta\phi)^2_{\text{prior}} = (0.1\pi)^2/12$, the optimal input state is always a N00N state, and for prior variance $(\delta\phi)^2_{\text{prior}} = (0.7\pi)^2/12$, the optimal input state always has a quasi-Gaussian form. In the quasi-Gaussian case, the ampitudes actually do depend very slightly on the prior distribution, even after matching the prior variance, but the effect is so small as to be almost invisible on the scale of Fig. 4.9.

Additionally, the phase patterns obtained previously for a flat distribution still hold both for N00N states (Eq. (4.19)) and quasi-Gaussian states (Eq. (4.20)), except in the case of the highly asymmetric prior phase distribution shown in Fig. 4.8(f). In that case the asymmetry of the prior phase distribution breaks the symmetry in the phase pattern of the optimal input state.

The above results suggest that if phase distributions are symmetric (or only weakly asymmetric, as in Fig. 4.8(e)), the optimal input state is insensitive to the details of the prior phase distribution and depends only on the prior phase uncertainty.

In that case, results obtained for a flat prior distribution in Sec. 4.3 continue to hold, and one does not need to find a new optimal state for every different prior phase distribution.

Frequently it is the case that one wants to make multiple measurements in order to get good estimation of the phase. If we assume that the phase distribution after each measurement remains symmetric (or approximately so), we don't need to concern ourselves with the detailed structure of the evolving phase distribution, and may determine which optimal state to use for the next measurement by simply keeping track of the evolving phase uncertainty. After many measurements, we of course expect the phase distribution to approach a Gaussian form, however, for a few measurements, the assumption of a symmetric distribution may break down. In that scenario, in order to perform optimal phase measurements, the optimal input state must be obtained adaptively for each measurement. Optimization for a sequence of adaptive or non-adaptive measurements is an interesting problem that we do not address here, and leave for a future work.

4.6 Conclusions and outlook

We have studied optimal input states for a lossy Mach-Zehnder interferometer with photon counting detection, for a general prior phase uncertainty. Optimal states typically fall into one of two major groups: quasi-Gaussian states, which are optimal for large photon number or large prior uncertainty, and N00N states, which are optimal for small photon number or small prior uncertainty. An intermediate regime between these two is also explored. The characteristic behavior and asymptotic form of the quasi-Gaussian states have been presented, and the scaling of the transition between different optimal state regimes has been analyzed. We also have studied the effect of moderate photon loss and different prior phase distributions on the optimal

input states. Future work should extend the current analysis to multiple and adaptive measurements.

Appendices

Appendix A

Analytical Expression for Transfer Time τ_3 in a 3-site Chain

For a 3-site chain with arbitrary on-site energies ω_i, inter-site hopping Ω, dephasing rate γ, and site 3 coupled to the acceptor system with coupling $\Gamma_{\rm trap}$, we may solve Eq. (3.11) exactly using Wolfram Mathematica to obtain the transfer time

$$\tau_3 = \frac{X_0 + \Omega^2 X_2 + \Omega^4 X_4}{Z}\,, \tag{A.1}$$

where

$$\begin{aligned}
X_0 &= \Gamma_{\rm trap}\left[4\left(\gamma^2+(\omega_1-\omega_3)^2\right)+4\gamma\Gamma_{\rm trap}+\Gamma_{\rm trap}^2\right] && \text{(A.2)}\\
&\times \left[2\gamma\left(3\gamma^2+\omega_1^2-2\omega_1\omega_2+3\omega_2^2-4\omega_2\omega_3+2\omega_3^2\right)+\Gamma_{\rm trap}\left(5\gamma^2+(\omega_1-\omega_2)^2\right)+\gamma\Gamma_{\rm trap}^2\right]\,,\\
X_2 &= 48\gamma^2\left(\gamma^2+(\omega_1-\omega_3)^2\right)+8\gamma\Gamma_{\rm trap}\left(15\gamma^2+(\omega_1-\omega_3)(5\omega_1-\omega_2-4\omega_3)\right) && \text{(A.3)}\\
&+ 8\Gamma_{\rm trap}^2\left(11\gamma^2+(\omega_1-\omega_3)^2\right)+24\gamma\Gamma_{\rm trap}^3+2\Gamma_{\rm trap}^4\,,\\
X_4 &= 12\left(2\gamma+\Gamma_{\rm trap}\right)\left(4\gamma+\Gamma_{\rm trap}\right)\,, && \text{(A.4)}\\
Z &= 2\Omega^2\Gamma_{\rm trap}\left(2\gamma+\Gamma_{\rm trap}\right)\left[2\Omega^2\left(4\gamma+\Gamma_{\rm trap}\right)+\gamma\left(2\gamma+\Gamma_{\rm trap}\right)^2+4\gamma(\omega_1-\omega_3)^2\right]\,. && \text{(A.5)}
\end{aligned}$$

References

[1] Beenakker, C. W., "Random-matrix theory of quantum transport", *Reviews of Modern Physics* **69** (1997), no. 3, 731.

[2] Beenakker, C. and H. van Houten, "Quantum transport in semiconductor nanostructures", *Solid State Physics* **44** (1991), 1–228.

[3] May, V. and O. Kühn, *Charge and energy transfer dynamics in molecular systems*, John Wiley & Sons, 2008.

[4] Hu, X., et al., "Pigment organization and transfer of electronic excitation in the photosynthetic unit of purple bacteria", *The Journal of Physical Chemistry B* **101** (1997), no. 19, 3854–3871.

[5] Engel, G. S., et al., "Evidence for wavelike energy transfer through quantum coherence in photosynthetic systems", *Nature* **446** (2007), no. 7137, 782–786.

[6] Anderson, P. W., "Absence of diffusion in certain random lattices", *Physical Review* **109** (1958), no. 5, 1492.

[7] Moix, J. M., M. Khasin, and J. Cao, "Coherent quantum transport in disordered systems: I. the influence of dephasing on the transport properties and absorption spectra on one-dimensional systems", *New Journal of Physics* **15** (2013), no. 8, 085010.

[8] Förster, T., "Delocalized excitation and excitation transfer", Modern Quantum Chemistry Istanbul Lectures (Sinanoglu, O., ed.), vol. 3, Academic Press, New York, 1965, pp. 93–137.

[9] Celardo, G. and L. Kaplan, "Superradiance transition in one-dimensional nanostructures: An effective non-Hermitian Hamiltonian formalism", *Physical Review B* **79** (2009), no. 15, 155108.

[10] Panitchayangkoon, G., et al., "Long-lived quantum coherence in photosynthetic complexes at physiological temperature", *Proceedings of the National*

Academy of Sciences **107** (2010), no. 29, 12766–12770.

[11] Sarovar, M., et al., "Quantum entanglement in photosynthetic light-harvesting complexes", *Nature Physics* **6** (2010), no. 6, 462–467.

[12] Hossein-Nejad, H. and G. D. Scholes, "Energy transfer, entanglement and decoherence in a molecular dimer interacting with a phonon bath", *New Journal of Physics* **12** (2010), no. 6, 065045.

[13] Strumpfer, J., M. Sener, and K. Schulten, "How quantum coherence assists photosynthetic light-harvesting", *The Journal of Physical Chemistry Letters* **3** (2012), no. 4, 536–542.

[14] Fidder, H., J. Knoester, and D. A. Wiersma, "Optical properties of disordered molecular aggregates: A numerical study", *The Journal of Chemical Physics* **95** (1991), no. 11, 7880–7890.

[15] Moll, J., et al., "Optical dynamics of excitons in J aggregates of a carbocyanine dye", *The Journal of Chemical Physics* **102** (1995), no. 16, 6362–6370.

[16] Higgins, K., et al., "Superabsorption of light via quantum engineering", *Nature Communications* **5** (2014).

[17] Sarovar, M. and K. B. Whaley, "Design principles and fundamental trade-offs in biomimetic light harvesting", *New Journal of Physics* **15** (2013), no. 1, 013030.

[18] Hu, X., et al., "Architecture and mechanism of the light-harvesting apparatus of purple bacteria", *Proceedings of the National Academy of Sciences* **95** (1998), no. 11, 5935–5941.

[19] Olaya-Castro, A., et al., "Efficiency of energy transfer in a light-harvesting system under quantum coherence", *Physical Review B* **78** (2008), no. 8, 085115.

[20] Grad, J., G. Hernandez, and S. Mukamel, "Radiative decay and energy transfer in molecular aggregates: The role of intermolecular dephasing", *Physical Review A* **37** (1988), no. 10, 3835.

[21] Spano, F. C. and S. Mukamel, "Superradiance in molecular aggregates", *The Journal of Chemical Physics* **91** (1989), no. 2, 683–700.

[22] Celardo, G., et al., "Transport through nanostructures with asymmetric coupling to the leads", *Physical Review B* **82** (2010), no. 16, 165437.

[23] Giusteri, G. G., F. Mattiotti, and G. L. Celardo, "Non-Hermitian Hamiltonian approach to quantum transport in disordered networks with sinks: Validity and effectiveness", *Physical Review B* **91** (2015), no. 9, 094301.

[24] Celardo, G. L., et al., "Cooperative robustness to dephasing: Single-exciton superradiance in a nanoscale ring to model natural light-harvesting systems", *Physical Review B* **90** (2014), no. 8, 085142.

[25] Celardo, G. L., G. G. Giusteri, and F. Borgonovi, "Cooperative robustness to static disorder: Superradiance and localization in a nanoscale ring to model light-harvesting systems found in nature", *Physical Review B* **90** (2014), no. 7, 075113.

[26] Sadreev, A. F. and I. Rotter, "S-matrix theory for transmission through billiards in tight-binding approach", *Journal of Physics A: Mathematical and General* **36** (2003), no. 45, 11413.

[27] Rebentrost, P., et al., "Environment-assisted quantum transport", *New Journal of Physics* **11** (2009), no. 3, 033003.

[28] Rebentrost, P., M. Mohseni, and A. Aspuru-Guzik, "Role of quantum coherence and environmental fluctuations in chromophoric energy transport", *The Journal of Physical Chemistry B* **113** (2009), no. 29, 9942–9947.

[29] Plenio, M. B. and S. F. Huelga, "Dephasing-assisted transport: quantum networks and biomolecules", *New Journal of Physics* **10** (2008), no. 11, 113019.

[30] Lloyd, S., et al., "The quantum goldilocks effect: on the convergence of timescales in quantum transport", *arXiv preprint arXiv:1111.4982* (2011).

[31] Celardo, G. L., et al., "Superradiance transition in photosynthetic light-harvesting complexes", *The Journal of Physical Chemistry C* **116** (2012), no. 42, 22105–22111.

[32] Dicke, R. H., "Coherence in spontaneous radiation processes", *Physical Review* **93** (1954), no. 1, 99.

[33] Sokolov, V. and V. Zelevinsky, "Dynamics and statistics of unstable quantum states", *Nuclear Physics A* **504** (1989), no. 3, 562–588.

[34] ———, "On a statistical theory of overlapping resonances", *Physics Letters B* **202** (1988), no. 1, 10–14.

[35] Rotter, I., "A continuum shell model for the open quantum mechanical nuclear system", *Reports on Progress in Physics* **54** (1991), no. 4, 635.

[36] Sokolov, V. and V. Zelevinsky, "Collective dynamics of unstable quantum states", *Annals of Physics* **216** (1992), no. 2, 323–350.

[37] Scully, M. O. and A. A. Svidzinsky, "The lamb shift-yesterday, today, and tomorrow", *Science* **328** (2010), no. 5983, 1239–1241.

[38] Lloyd, S. and M. Mohseni, "Symmetry-enhanced supertransfer of delocalized quantum states", *New Journal of Physics* **12** (2010), no. 7, 075020.

[39] Scholes, G. D., "Designing light-harvesting antenna systems based on superradiant molecular aggregates", *Chemical Physics* **275** (2002), no. 1, 373–386.

[40] Monshouwer, R., et al., "Superradiance and exciton delocalization in bacterial photosynthetic light-harvesting systems", *The Journal of Physical Chemistry B* **101** (1997), no. 37, 7241–7248.

[41] Ferrari, D., et al., "Quantum biological switch based on superradiance transitions", *The Journal of Physical Chemistry C* **118** (2013), no. 1, 20–26.

[42] Heijs, D., V. Malyshev, and J. Knoester, "Decoherence of excitons in multichromophore systems: Thermal line broadening and destruction of superradiant emission", *Physical Review Letters* **95** (2005), no. 17, 177402.

[43] Celardo, G., et al., "Interplay of superradiance and disorder in the Anderson model", *Fortschritte der Physik* **61** (2013), no. 2-3, 250–260.

[44] Biella, A., et al., "Subradiant hybrid states in the open 3D Anderson-Dicke model", *EPL (Europhysics Letters)* **103** (2013), no. 5, 57009.

[45] Shahbazyan, T., M. Raikh, and Z. V. Vardeny, "Mesoscopic cooperative emission from a disordered system", *Physical Review B* **61** (2000), no. 19, 13266.

[46] Celardo, G. L., et al., "Cooperative robustness to dephasing: Single-exciton superradiance in a nanoscale ring to model natural light-harvesting systems", *Physical Review B* **90** (2014), no. 8, 085142.

[47] Wu, J., R. J. Silbey, and J. Cao, "Generic mechanism of optimal energy transfer efficiency: A scaling theory of the mean first-passage time in exciton systems", *Physical Review Letters* **110** (2013), no. 20, 200402.

[48] Caruso, F., et al., "Highly efficient energy excitation transfer in light-harvesting complexes: The fundamental role of noise-assisted transport", *The Journal of Chemical Physics* **131** (2009), no. 10, 09B612.

[49] Celardo, G., et al., "Transition from isolated to overlapping resonances in the open system of interacting fermions", *Physics Letters B* **659** (2008), no. 1, 170–175.

[50] ———, "Open system of interacting fermions: Statistical properties of cross sections and fluctuations", *Physical Review E* **76** (2007), no. 3, 031119.

[51] Sorathia, S., et al., "From closed to open one-dimensional Anderson model: Transport versus spectral statistics", *Physical Review E* **86** (2012), no. 1, 011142.

[52] Ziletti, A., et al., "Coherent transport in multibranch quantum circuits", *Physical Review B* **85** (2012), no. 5, 052201.

[53] Haken, H. and G. Strobl, "An exactly solvable model for coherent and incoherent exciton motion", *Zeitschrift für Physik A Hadrons and Nuclei* **262** (1973), no. 2, 135–148.

[54] Cao, J. and R. J. Silbey, "Optimization of exciton trapping in energy transfer processes", *Journal of Physical Chemistry A* **113** (2009), no. 50, 13825–13838.

[55] Leegwater, J. A., "Coherent versus incoherent energy transfer and trapping in photosynthetic antenna complexes", *The Journal of Physical Chemistry* **100** (1996), no. 34, 14403–14409.

[56] Chechkin, A. V., et al., "Introduction to the theory of Lévy flights", Anomalous Transport: Foundations and Applications (Klages, R., G. Radons, and I. M. Sokolov, eds.), Wiley-VCH, 2008, pp. 129–162.

[57] Zhang, Y., et al., "Opening-assisted coherent transport in the semiclassical regime", *Physical Review E* **95** (2017), 022122.

[58] Izrailev, F. M., S. Ruffo, and L. Tessieri, "Classical representation of the one-dimensional Anderson model", *Journal of Physics A: Mathematical and General* **31** (1998), no. 23, 5263.

[59] Caves, C. M., "Quantum-mechanical noise in an interferometer", *Physical Review D* **23** (1981), 1693–1708.

[60] Yurke, B., S. L. McCall, and J. R. Klauder, "SU(2) and SU(1,1) interferometers", *Physical Review A* **33** (1986), 4033–4054.

[61] Sanders, B. C. and G. J. Milburn, "Optimal quantum measurements for phase estimation", *Physical Review Letters* **75** (1995), 2944–2947.

[62] Lee, H., P. Kok, and J. P. Dowling, "A quantum Rosetta stone for interferometry", *Journal of Modern Optics* **49** (2002), no. 14-15, 2325–2338.

[63] Braunstein, S. L., "Quantum limits on precision measurements of phase", *Physical Review Letters* **69** (1992), no. 25, 3598.

[64] Pezzé, L. and A. Smerzi, "Mach-Zehnder interferometry at the Heisenberg limit with coherent and squeezed-vacuum light", *Physical Review Letters* **100** (2008), no. 7, 073601.

[65] Holland, M. J. and K. Burnett, "Interferometric detection of optical phase shifts at the Heisenberg limit", *Physical Review Letters* **71** (1993), 1355–1358.

[66] Campos, R. A., C. C. Gerry, and A. Benmoussa, "Optical interferometry at the Heisenberg limit with twin Fock states and parity measurements", *Physical Review A* **68** (2003), 023810.

[67] Motes, K. R., et al., "Linear optical quantum metrology with single photons: Exploiting spontaneously generated entanglement to beat the shot-noise limit", *Physical Review Letters* **114** (2015), 170802.

[68] Anisimov, P. M., et al., "Quantum metrology with two-mode squeezed vacuum: Parity detection beats the Heisenberg limit", *Physical Review Letters* **104** (2010), no. 10, 103602.

[69] Berry, D. and H. M. Wiseman, "Optimal states and almost optimal adaptive measurements for quantum interferometry", *Physical Review Letters* **85** (2000), no. 24, 5098.

[70] Pezzé, L. and A. Smerzi, "Phase sensitivity of a Mach-Zehnder interferometer", *Physical Review A* **73** (2006), no. 1, 011801.

[71] Lee, T.-W., et al., "Optimization of quantum interferometric metrological sensors in the presence of photon loss", *Physical Review A* **80** (2009), no. 6, 063803.

[72] Braunstein, S. L. and C. M. Caves, "Statistical distance and the geometry of quantum states", *Physical Review Letters* **72** (1994), no. 22, 3439–3443.

[73] Barndorff-Nielsen, O. and R. Gill, "Fisher information in quantum statistics", *Journal of Physics A: Mathematical and General* **33** (2000), no. 24, 4481.

[74] Braunstein, S. L., C. M. Caves, and G. J. Milburn, "Generalized uncertainty relations: Theory, examples, and Lorentz invariance", *arXiv preprint quant-ph/9507004* (1995).

[75] Wiseman, H. and R. Killip, "Adaptive single-shot phase measurements: The full quantum theory", *Physical Review A* **57** (1998), no. 3, 2169.

[76] ———, "Adaptive single-shot phase measurements: A semiclassical approach", *Physical Review A* **56** (1997), no. 1, 944.

[77] Kolodynski, J. and R. Demkowicz-Dobrzanski, "Phase estimation without a priori phase knowledge in the presence of loss", *Physical Review A* **82** (2010), no. 5, 53804.

[78] Demkowicz-Dobrzański, R., "Optimal phase estimation with arbitrary a priori knowledge", *Physical Review A* **83** (2011), no. 6, 061802.

[79] Rubin, M. A. and S. Kaushik, "Loss-induced limits to phase measurement precision with maximally entangled states", *Physical Review A* **75** (2007), no. 5, 053805.

[80] Escher, B., R. de Matos Filho, and L. Davidovich, "General framework for estimating the ultimate precision limit in noisy quantum-enhanced metrology", *Nature Physics* **7** (2011), no. 5, 406–411.

[81] Demkowicz-Dobrzanski, R., et al., "Quantum phase estimation with lossy interferometers", *Physical Review A* **80** (2009), no. 1, 013825.

[82] Gkortsilas, N., J. Cooper, and J. Dunningham, "Measuring a completely unknown phase with sub-shot-noise precision in the presence of loss", *Physical Review A* **85** (2012), no. 6, 063827.

[83] Jiang, K., et al., "Strategies for choosing path-entangled number states for optimal robust quantum-optical metrology in the presence of loss", *Physical Review A* **86** (2012), no. 1, 013826.

[84] Zhang, Y., et al., "Quantum fisher information of entangled coherent states in the presence of photon loss", *Physical Review A* **88** (2013), no. 4, 043832.

[85] Uys, H. and P. Meystre, "Quantum states for Heisenberg-limited interferometry", *Physical Review A* **76** (2007), no. 1, 013804.

[86] Durkin, G. A. and J. P. Dowling, "Local and global distinguishability in quantum interferometry", *Physical Review Letters* **99** (2007), no. 7, 070801.

[87] Dorner, U., et al., "Optimal quantum phase estimation", *Physical Review Letters* **102** (2009), no. 4, 040403.

Biography

The author received his Bachelor of Science degree in physics at Zhejiang University in China in 2011. Later that year, he attended Tulane University to begin his Ph.D. study in physics. He has since joined Dr. Lev Kaplan's Quantum Chaos and Quantum Information research group. He performed the following work during his Ph.D. study.

[1] **Y. Zhang**, G. L. Celardo, F. Borgonovi, and L. Kaplan, *"Opening-Assisted Coherent Transport in the Semiclassical Regime"*, Phys. Rev. E 95, 022122 (2017).

[2] **Y. Zhang**, G. L. Celardo, F. Borgonovi, and L. Kaplan, *"Optimal Dephasing Rate for Exciton Energy Transfer in Disordered Linear Chains"*.

[3] **Y. Zhang**, D. B. Uskov, and L. Kaplan, *"Optimization of Lossy Mach-Zehnder Interferometer with Varying Prior Phase Uncertainties Using Photon-Counting Detection"*.